Alma Mater Studiorum – Università di Bologna

DOTTORATO DI RICERCA IN

BIOLOGIA CELLULARE E MOLECOLARE

Ciclo 35

Settore Concorsuale: 05/I1 – GENETICA

Settore Scientifico Disciplinare: BIO/18 GENETICA

Harnessing the cellular and molecular complexity of high-risk neuroblastoma to investigate novel potential treatment approaches

Presentata da: Piergiuseppe De Rosa

Coordinatore Dottorato

Prof. Vincenzo Scarlato

Supervisore

Prof. Giovanni Perini

Esame finale anno 2023

ABSTRACT

Neuroblastoma (NB) is the most common type of tumor in infants and the third most common cancer in children, after leukemia and brain cancer. Current clinical practices employ a variety of strategies for NB treatment, ranging from standard chemotherapy to immunotherapy. Due to a lack of knowledge about the molecular mechanisms underlying the disease's onset, aggressive phenotype, and therapeutic resistance, these approaches are ineffective in the majority of instances. MYCN amplification is one of the most well-known genetic alterations associated with high risk in NB. The following work is divided into three sections and aims to provide new insights into the biology of NB and hypothetical new treatment strategies.

First, we identified RUNX1T1 as a key gene involved in MYCN-driven NB onset in a transgenic mouse model. Specifically, through extensive genetic screening, we identified a single-point mutation in the RUNX1T1 gene that inhibits the tumorigenic phenotype in Th-MYCN mice. RUNX1T1 is a transcriptional co-repressor that plays a role in the biology of multiple cancers, but the molecular mechanisms in which it is involved are largely unknown. Therefore, we characterized its interactome in NB cells, focusing on potential interactors that could explain the observed phenotype. We found that RUNX1T1 interacts with the transcription factor HAND2 and the transcriptional repressors HDAC1-3, LSD1, and RCOR3. Notably, HAND2 is involved in sympathetic neuron differentiation and NB's core regulatory circuitry. We observed that these proteins co-localized with RUNX1T1 on chromatin in proximity to genes involved in sympathetic neuron differentiation and that the single-point mutation in RUNX1T1 abolishes the interaction with RCOR3. These results strongly suggested that RUNX1T1 may recruit the Co-REST complex on target genes that regulate the differentiation of NB cells and that the interaction with RCOR3 is essential.

Second, we provided insights into the role of MYCN in dysregulating the CDK/RB/E2F pathway controlling the G1/S transition of the cell cycle. Here, we showed that high expression of E2F3 and MYCN correlate with poor prognosis in NB despite the RB1 levels. Through a CRISPR interference (CRISPRi) approach, we found that E2F3 is an essential gene in inducing colony formation in NB. Further, we showed that MYCN overexpression leads to RB inactivation by inducing its hyperphosphorylation in the G1 phase through cell cycle synchronization experiments. Moreover, we generated two MYCN-amplified NB cell lines conditionally Knockdown (cKD) for the RB1 gene through a CRISPRi approach. In agreement with the dispensable role of RB in regulating MYCN amplified NB's cell cycle, RB KD did not affect cell proliferation unless it was replaced with the RB unphosphorylable mutant

$RB^{\Delta CDK}$. The described genetic interaction between MYCN and RB1 provides the rationale for using cyclin/CDK complexes inhibitors in NBs carrying MYCN amplification and relatively high levels of RB1 expression.

Third, we generated an M13 bacteriophage platform to target GD2-expressing cells in NB. GD2 is a ganglioside expressed on the membrane of NB cells and is widely used as a target for immunotherapy. Here, we assayed the GD2 expression in a panel of eight NB cell lines and generated a recombinant M13 phage capable of binding GD2-expressing cells selectively ($M13_{GD2}$) by fusing a GD2-specific single chain fragment variable tho the phagic pIII protein. After the chemical conjugation of $M13_{GD2}$ with the photosensitizer ECB04 ($M13_{GD2}$-ECB04), we assessed the retargeting capability of these phages and the killing efficiency in a wide range of concentrations. Our results showed that $M13_{GD2}$-ECB04 preserves the retargeting capability, inducing cell death even at picomolar concentrations upon light irradiation. These results provided proof of concept for M13 phage employment in targeted photodynamic therapy for NB, an exciting strategy to overcome resistance to classical immunotherapy.

TABLE OF CONTENTS

INTRODUCTION

Neuroblastoma, an overview

Childhood and pediatric malignancies are among the leading causes of mortality in children during their first few years. Although researchers considered a number of risk variables that potentially predict the development of cancer in children and adolescents, their origins remain mostly unknown. Nonetheless, advancements in high-throughput sequencing methods and genome-wide analysis simplified the identification of genetic features impacting their onset and progression in many pediatric malignancies.

Neuroblastoma (NB) clearly illustrates how dysregulation of gene expression influences essential cellular functions, including proliferation, differentiation, chromosomal stability, and self-renewal (Bahmad et al. 2019). Remarkably, with 25–50 cases per million persons, NB is the most prevalent extracranial solid tumor diagnosed in infants. It is the leading cause of mortality for children aged one to five, accounting for 13% of all pediatric malignancies. Despite chemotherapy, immunotherapy, and surgery, the long-term survival rate is less than 40% (De Bernardi et al. 2003).

Based on histological features and operability, the International Neuroblastoma Staging System (INSS) has divided neuroblastoma into five stages since 1988 (G. M. Brodeur et al. 2016):

Stage 1: surgically operable localized malignant lesion and lack of metastases.

Stage 2: Small tumor mass that cannot be completely excised, with probable lymph node metastases.

Stage 3: Large tumor mass that cannot be removed entirely. Cancer has spread to distant organs.

Stage 4: Large tumor mass with widespread metastasis to the liver, skin, and bone marrow.

Stage 4S: metastatic neuroblastoma that mainly affects infants under one year, with a 90% survival rate due to spontaneous remission.

NB can be inherited in an autosomal dominant manner. Mutations of ALK and PHOX2B genes are the most correlated with familial occurrences of NB (Mossé et al. 2008; Mosse et al.

2004; Trochet et al. 2004). However, familial NB accounts for less than 2% of cases, as the vast majority are sporadic (Matthay et al. 2016). The highly heterogeneous mutation landscape makes it challenging to establish common NB mutations in sporadic cases. Several genomic abnormalities, including copy number alterations, polymorphisms, and chromosomal mutations, have been identified in sporadic NB. The amplification of the MYCN locus is one of the best-known genomic aberrations in NB; it occurs in around 20% of cases and is employed as a biomarker for risk classification (Matthay et al. 2016). In addition to the sequence encoding the transcription factor N-MYC, this locus also contains MYCNOS, which encodes the long non-coding RNA (lncRNA) N-CYM. High expression of N-CYM correlates with high-risk cases (Armstrong and Krystal 1992). In 14% of high-risk patients, gain-of-function mutations in the ALK gene were found. Moreover, due to its chromosomal association with MYCN, ALK can be co-amplified with this gene (Bresler et al. 2014). A set of polymorphisms at the LIN28B gene can cause the overexpression of the lin-28 homolog B protein, which is recognized for its potential to negatively influence the maturation of let7 pre-micro RNA (miRNA). In 10% and 25% of patients, respectively, loss-of-function mutations of the ATRX gene and rearrangements of the TERT promoter, which encode for an RNA helicase and a telomerase component, were identified (Peifer et al. 2015; Valentijn et al. 2015). Moreover, in some cases of relapse, mutations in the genes involved in the RAS- and P53-regulated pathways have been found, and it has been postulated that these mutations may be significant in the clinical course at the time of diagnosis (Ackermann et al. 2018). In addition to the amplification of MYCN, the gain of 17q and the loss of 1p were identified in NB. Gain of 1q and 2p and loss of 3p, 4p, and 14q are other chromosomal aberrations identified (Pugh et al. 2013).

Based on the mutations and the copy number alterations discovered in familial and sporadic cases of NB, a new categorization of risk has recently been established (Ackermann et al. 2018). This approach classifies cancer into three groups: extremely high risk, high risk, and low risk. NB cases with telomerase activity and abnormalities in signaling pathways mediated by RAS or p53 have been classified as extremely high-risk, whereas NB cases with telomerase activation alone are in the high-risk category. Cases of neuroblastoma that lack telomeric activity abnormalities are included in the low-risk category.

Although the primary tumor can arise from various anatomical sites, it is most commonly found in the adrenal glands or the paravertebral ganglia of the sympathetic nervous system (Garrett M. Brodeur 2003; Maris 2010). Anatomical and histological data on NB suggest that this tumor may arise from the sympathoadrenergic lineage of the neural crest. Understanding

the dynamics that determine the onset of NB requires a comprehensive understanding of the molecular mechanisms that lead to the differentiation of neural crest cells to define new therapeutic targets.

Neuroblastoma: origin and initiation

In the early stages of development, the embryo undergoes a series of morphological changes that result in the formation of embryonic structures necessary for developing the nervous system. Morphogens produced by the notochord induce the differentiation of the cells of the neural plate leading to the formation of the neural fold, which, upon closure, gives rise to the neural tube. During vertebrate neurulation, neural crest cells (NCCs) emerge from the neural fold's margins and the dorsal neural tube (Simões-Costa and Bronner 2015). NCCs are divided into four types based on their position along the anterior-posterior axis and their function: cranial, vagal and sacral, cardiac, and trunk NCCs. Each type of NCC generates distinct tissues in specific anatomical areas. Cranial NCCs differentiate into cartilage, bone, nerves, glia, and connective tissue of the head; the vagal and sacral NCCs differentiate into parasympathetic ganglia; cardiac NCCs differentiate into melanocytes, neurons, cartilage, muscle, and connective tissue of the arteries emerging from the heart; Those of the trunk differentiate into melanocytes, dorsal root ganglia, sympathetic ganglia, and the adrenal medulla (Gilbert 2000).

Based on the function and physiology of the sympathoadrenal lineage originating from the trunk NCCs, it has been hypothesized that the initiation of NB is associated with the dysregulation of the molecular pathways involved in their migration and differentiation (Marshall et al. 2014). During gastrulation, the neural plaque is induced, and its border contains a population of cells capable of giving rise to NCCs. In this context, a key role is played by the signaling pathways mediated by BMP and WNT, produced by the lateral regions of the neural plate, and the inhibitors of these pathways, produced by the medial regions. In the border region between the neural plate and the lateral regions, intermediate levels of BMP and WNT induce the expression of several transcription factors capable of activating a regulatory circuit that establishes and maintains the identity of the border cells of the neural plate (Groves and LaBonne 2014). At this stage, these cells express the border specifier genes Msx1, Msx2, Pax3, Pax7, and Zic1. Thus, border cells begin to express the neural crest specifier genes AP-2, FoxD3, Snail2, Sox9, and Sox10, allowing their migration and epithelial-mesenchymal transition (EMT). Sox9, Sox10, Cad7, ColIIa, Ngn1, Mitf, and Dct are the genes responsible for the migration of NCCs (Betters et al. 2010).

The sympathoadrenal lineage derives from the trunk NCCs. It follows the ventral migration pathway and receives signals from the neural tube, notochord, and aorta to differentiate in the adrenal medulla's chromaffin cells and the sympathetic ganglia's neurons (Huber 2006). Morphogens from the BMP family play a crucial role in the differentiation of the sympathoadrenal lineage. This signaling induces NCCs to express the transcription factor MASH1, which in turn induces the expression of PHOX2A, a transcription factor necessary for the differentiation of these cells into sympathetic neurons and chromaffin cells. PHOX2B, an independently expressed transcription factor, stimulates the expression of genes encoding for the enzymes Tyrosine hydroxylase and Dopamine -hydroxylase (TH and DBH), which are involved in the biosynthesis of neurotransmitters, as well as the transcription factors HAND2 and GATA3, which are required for the maintenance of MASH1 expression (Huber 2006). During this phase, the NCCs express high levels of MYCN, which seems to regulate their migration and growth. Thus, MYCN expression gradually decreases during sympathetic neuron differentiation (Zimmerman et al. 1986). Excess neuronal cell precursors undergo apoptosis upon the local withdrawal of nerve growth factor (NGF) (Yuan and Yankner 2000) **(Figure I)**.

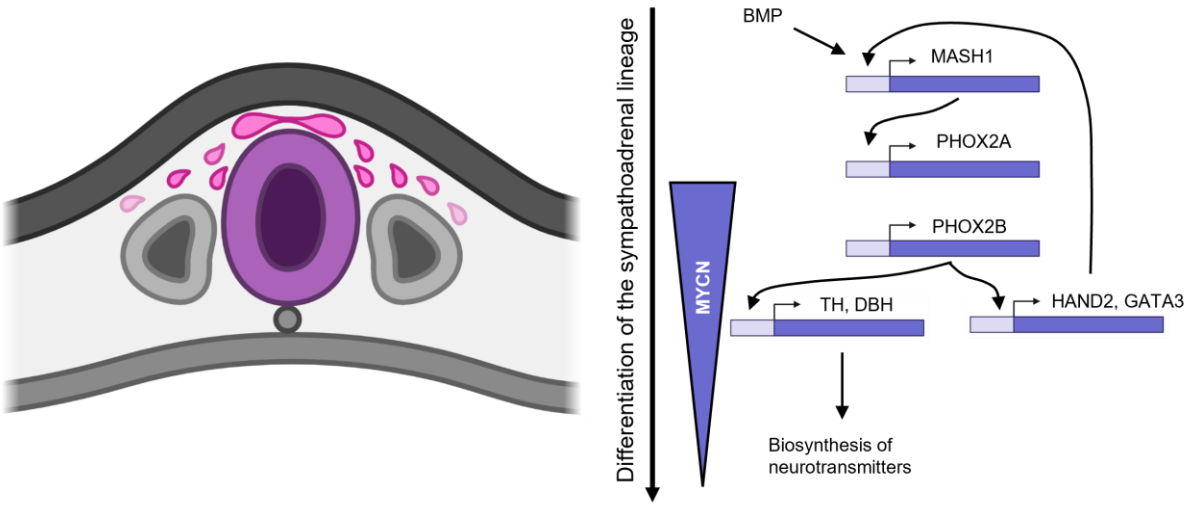

Figure I Schematic illustration of the NCCs' differentiation. Left: Diagram of transverse sections of the embryo showing the origin and migration of neural crest cells - 21 days. NCCs (pink) originate from the neural tube (purple) and follow several pathways of differentiation and migration. Right: Gene regulatory network driving differentiation of the sympathoadrenal lineage. The expression of MYCN decreases during the differentiation pathway under physiological conditions.

Generally, the pathogenesis of tumors is a multiphase process in which the cells that give rise to the neoplasm undergo a series of sequential events that might drive the tumoral transformation. Mutations and aberrations in gene expression are the events capable of fostering oncogenesis. Specifically, at least three steps in NB pathogenesis have been described (Marshall et al. 2014). First, the MYCN locus amplification reported in NB cells led to the concept that

its overexpression may play a driving role in the tumor's initiation. However, the overexpression of MYC family proteins is known to induce p53-mediated apoptosis (Murphy et al. 2008). Thus, it is plausible to hypothesize that the second event is required for neuroblasts to escape from apoptosis at this stage. In fact, the second event may be mediated by overexpression of BMI1, which functions as an E3 ubiquitin ligase for p53, or by gain-of-function mutations in the ALK gene. These aspects would explain the decreased p53 levels detected in the neuroblasts of mice carrying the MYCN transgene under lineage-specific promoter (Calao et al. 2013; Berry et al. 2012). In addition, the downregulation of the nerve growth factor receptor (NGFR) can contribute to the inhibition of neuronal development. In this setting, the overexpression of the BDNF receptor NTRK2 increases cell proliferation and resistance to programmed cell death. After birth, these precancerous cells proliferate and are resistant to apoptosis; this could result in high genomic instability, rendering them prone to definitive tumor transformation (third hit). To elucidate the role of MYCN in this setting, transgenic mice expressing this gene under the control of the Tyrosine hydroxylase (Th-MYCN) promoter have been developed. In this way, MYCN overexpression occurs at the level of sympathoadrenal NCCs during migration (Banerjee et al. 1992; Weiss et al. 1997). Thus, transgenic mice exhibited hyperplasia of neuroblasts or tumor masses with cytogenetic and histological similarities to human NB. Another mouse model has been generated based on the recent advance in cytogenetic alterations in NB. These mice carry both mutated ALK and MYCN under the control of the Th promoter (ALKF1174L/Th-MYCN). In this model, spontaneous retroperitoneal solid tumors form in the peri-renal and paraspinal regions, replicating human NB’s clinical distribution more accurately (Berry et al. 2012).

The relationship between aberrant NCCs differentiation and NB has been extensively studied in recent years. By comparing single-cell RNAseq data collected from human adrenal glands at different stages of development with human NBs, Jansky et al. revealed that NBs resembling committed neuroblasts are associated with low risk. In contrast, the undifferentiated phenotype is associated with MYCN amplification and high-risk NB, suggesting that these latter tumors arise during the early stages of development (Jansky et al. 2021). According to transcriptional and epigenetic characteristics of NB cells, recent research modelized the NB cellular phenotypes into major groups: NB cells showing sympathoadrenal signature (ADRN) and NB cells showing an undifferentiated mesenchymal phenotype (MES). The ADRN and MES phenotypes are plastic because single-cell subclones of ADRN or MES populations are able to recapitulate both transcriptional states (van Groningen et al. 2017). Besides, these two populations of cells mostly coexist in the tumoral mass, and their identity maintenance is reg-

ulated by core regulatory circuitries (CRCs) (Boeva et al. 2017; van Groningen et al. 2017). CRCs are groups of autoregulatory transcription factors associated with large euchromatin regions called super-enhancers (SEs) (Y. Chen et al. 2020). In MYCN-amplified NB, both ADRN and MES MYCN-amplified cell lines showed a CRC dependent on HAND2, ISL1, PHOX2B, GATA3, TBX2, ASCL1, and TFAP2β. Notably, most of these genes, such as HAND2, PHOX2B, and GATA3, have been described as critical regulators of sympathoadrenal lineage differentiation. A significant reduction in the aggressive phenotype was observed by silencing these genes one by one through RNAi. These findings led to the conclusion that high-risk NB cell growth is dependent on the expression of CRC transcription factors (Durbin et al. 2018a; Lu Wang et al. 2019; Durbin et al. 2022). Notably, among the genes controlled by ADRN and MES CRCs, the Cyclin D encoding gene CCND1 was significantly affected by the downregulation of CRC transcription factors (Gartlgruber et al. 2021).

NB cellular phenotype's role in therapy has emerged in recent years. New evidence indicates that the MES phenotype is significantly more resistant to standard chemotherapies. For instance, once treated with cisplatin or doxorubicin, the SK-N-SH cell line, which is characterized by the coexistence of ADRN and MES cells, displays an increase in the proportion of MES cells (Boeva et al. 2017). These data suggested two different hypotheses. First, heterogeneous tumors treated with chemotherapy might show resistance because of surviving MES cells inducing relapse; second, upon treatment, ADRN cells might change their CRC profile leading to an interconversion in MES cells (Shendy et al. 2022).

The role of MYC(N), RB, and E2F in the cell cycle and tumors

The pathway regulating proliferation is the cell cycle, divided into G1, S, G2, and M phases. G1, S, and G2 phases are called together interphase. During G1 and G2 phases, the cells receive signals from the external and internal environment that promotes or inhibits cellular division. DNA duplication occurs during the S phase, then chromosome segregation and cellular division happen during the M phase. In physiological conditions, phase-transition checkpoints are strictly held by multiple protein families, including cyclins, cyclin-dependent kinases (CDKs), and CDK inhibitors (CKIs), such as p21 and p27. Cyclins interact with CDKs activating their kinase activity, leading to the phosphorylation of multiple proteins involved in cell cycle control. On the other hand, these checkpoints are necessarily deregulated for tumor initiation and maintenance, and driver mutations in proto-oncogenes and tumor suppressor genes are responsible for malfunctioning the cell cycle (Rubin, Sage, and Skotheim 2020). Genes relevant for cell cycle progression are the proto-oncogenes MYC and E2F and the tu-

mor suppressor RB1. The following paragraphs describe the role of these genes in cell cycle progression and their role in tumorigenesis.

The MYC proto-oncogenes

MYC, one of the most-studied proto-oncogenes, plays an important role in cancer. Multiple genetic alterations impacting MYC and its paralogs MYCN and MYCL have been described in various types of malignancies. Notably, amplification of MYC and its paralogues was found in at least 28% of the tumors (Schaub et al. 2018). Additionally, other genetic alterations have been described, such as; point mutations increasing protein stability (Bahram et al. 2000; Hemann et al. 2005); amplifications or mutation of its associated enhancers (Sur et al. 2012); gain of function mutations in genes involved in cell pathways upregulating MYC genes (Herranz et al. 2014). More than 30 years ago, it was found that its overexpression was sufficient to drive tumoral transformation in mouse lymphocytes (J. M. Adams et al. 1985).

Structurally, MYC proteins are transcription factors containing a basic helix-loop-helix/leucine-zipper motif at the C-terminus and highly conserved domains known as MYC boxes (MBs) at the N-terminus. Six MBs (MB0, MBI, MBII, MBIIIa, MBIIIb, MBIV) have been described, and each interacts with several chromatin-modifying complexes, such as TRAAP, GCN5, TIP60, and TIP48 (Lourenco et al. 2021; Kalkat et al. 2018). By heterodimerization with the transcription factor MAX, MYC binds to consensus sequences called E-Boxes (CACGTG). MYC can work as a transcriptional activator and transcriptional repressor, depending on the context. By interacting with histone acetyl-transferases, MYC exerts its activator activity, while interacting with histone deacetylases, it represses gene expression (Lüscher and Vervoorts 2012).

MYC takes part in several cellular pathways, ranging from cell proliferation to immune system escape (Dhanasekaran et al. 2022). Given its role in cell proliferation, it is not surprising that MYC controls cell cycle progression by upregulating Cyclin D2 (CCND2), Cyclin E1 (CCNE1), CDK4, CDC25A, E2Fs, and by downregulating the CDK4/6 inhibitor CDKN1A (p21) (Bretones, Delgado, and León 2015). However, given its role in a wide range of cancer, most MYC family research was mainly performed on the MYC paralogue, leaving a relevant gap of evidence in MYCN and MYCL knowledge. This disparity in MYC family research is likely attributable to the frequency of MYC, MYCN, and MYCL alterations reported in various malignancies. While alterations of MYC are found in the vast majority of cancers, MYCN and MYCL alterations are detected principally in NB and specific lung cancer cases, respec-

tively (Baluapuri, Wolf, and Eilers 2020). The physiological expression of MYC genes is spatiotemporally regulated. MYC is expressed in all the proliferating adult tissues, MYCN expression is restricted in developing neuroblasts, and MYCL is expressed in the embryonic brain, kidney, and lung tissues (Brägelmann et al. 2017). Only MYC and MYCN genes knockout resulted in mice lethality, while MYCL was described as a non-essential gene (Hatton et al. 1996; Sawai et al. 1993; A. C. Davis et al. 1993). In addition, homozygous mice in which MYC was replaced with MYCN live to adulthood and are fertile (Malynn et al. 2000). Despite some intriguing differences, a recent study identified a ~70% of overlap between the interactomes of MYC and MYCN. This study was performed in lung cancer NCI-H2171 cells and in NB Kelly cells, respectively (Liyuan Wang et al. 2022). These observations led to the hypothesis that although most of the functions of MYC genes might be redundant, mechanistic differences between the family members likely exist.

As previously discussed, MYCN amplification is found in 20% of NBs and is associated with poor prognosis. MYCN is one of the essential genes involved in the proliferation of NB cells. MYCN overexpression in NB correlates with cell proliferation, as has been recognized for more than 30 years (Negroni et al. 1991; Schweigerer et al. 1990). Although several models have been proposed, molecular mechanisms leading to MYCN amplification remain mostly unknown (Aygun 2018). NB research provided multiple insights into specific MYCN's role in regulating the cell cycle. Like its ortholog MYC, N-MYC regulates several genes involved in cell cycle regulation. Microarrays performed in NB cell lines perturbing MYCN expression led to the identification of the S-phase associated kinase (SKP2) as a relevant MYCN target gene (Bell, Lunec, and Tweddle 2007; Muth et al. 2010). SKP2 is involved in the degradation of the CDK inhibitor p27, promoting the G1/S transition (Zheng et al. 2002). Recently, it was found that MYCN speeds up the G1/S transition in NB cells, inducing resistance to chemotherapy (Ryl et al. 2017). Following synchronized cells through the cell cycle, MYCN-high and MYCN-low cells moved nearly synchronously through the S, G2, and M phases, but MYCN-high cells needed a shorter time for the transition from the G1 to the S phase compared to MYCN-low cells. (Ryl et al. 2017). Moreover, MYCN is involved in the upregulation of CHK1, regulating the G2/M transition (Cole et al. 2011).

The RB1 tumor suppressor gene

The concept of the tumor suppressor gene began in 1971 when Alfred Knudson described for the first time the two-hit model for retinoblastoma tumors. Analyzing a cohort of retinoblastoma patients, he found that biallelic inactivation of the RB1 gene was sufficient to drive reti-

noblastoma. The first hit is an inherited germline mutation, while the second is a somatic mutation that occurs during development (Knudson 1971). The RB1 gene encodes for the RB protein, and its molecular mechanisms has been extensively studied, but its precise working mechanism remains an enigma (Dyson 2016).

Later, the molecular mechanisms driving RB functions have been investigated. RB inactivates E2F proteins, transcription factors binding the highly conserved sequence TTTCGCGC at the promoter of genes involved in the G1/S transition (Erik S. Knudsen and Knudsen 2008) (Rubin et al. 2005). During the G1 phase, RB mainly represses E2F target genes by interacting with E2Fs and recruiting chromatin remodeling complexes at their cis-regulatory elements. Histone modifiers complexes involved in this mechanism are Sin3, and histone deacetylase 1-3 (HDAC1-3) (Frolov and Dyson 2004).

Structurally, RB protein contains two folded domains and a substantial amount (~33% of 928 amino acids) of intrinsically disordered sequence (Rubin 2013). The structured domains are the N-terminal domain (RbN) and the pocket domain (RbP) (Hassler et al. 2007). Both these domains contain an intrinsically disordered region (RbNL and RbPL). The RbP is involved in the binding of the E2F transactivation domain and contains a LxCxE peptide involved in the interaction with other proteins (Lee et al. 2002; Xiao et al. 2003). Remarkably, the LxCxE peptide can bind the RbP leading to the lack of interaction with E2F in some specific contexts (Kim, Ahn, and Cho 2001). An interdomain linker (RbIDL) divides the structured domains RbN and RbP. Besides the RbP, RB can bind E2F and its obligate heterodimer partner DP by interacting with its RbC with their “marked box” (E2FMB-DPMB).

The current paradigm states that Cyclin-dependent kinases (CDKs) phosphorylate and inactivate RB when normal cells divide **(Figure II)**. Experiments with synchronized cells revealed that Cyclin D-dependent kinases are responsible for the initial phosphorylation of RB during the G1 phase, but Cyclin E/CDK2 is responsible for the late hyperphosphorylation of RB during the G1/S transition (Dowdy et al. 1993; Hinds et al. 1994a; 1994b; Sherr 1996).

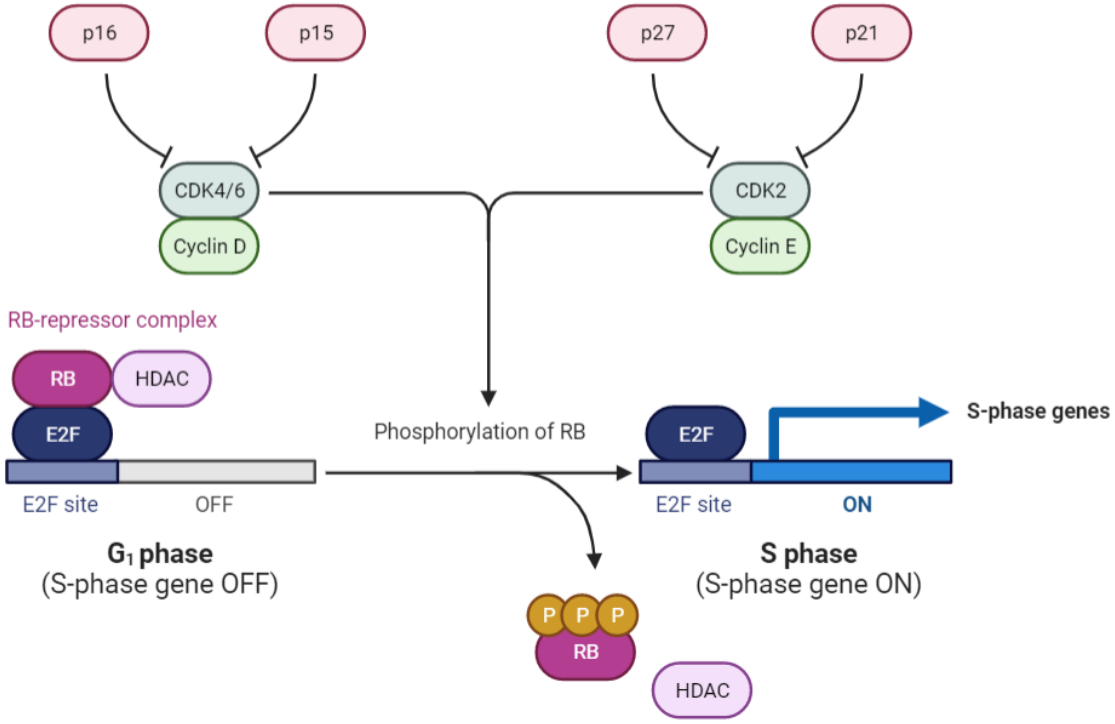

Figure II Schematization of the E2F/RB pathway.CDK4/6-Cyclin D and CKD2-Cyclin E phosphorylate RB leading to its inactivation. Inactivation of RB induces E2F activation and S-phase gene transcription. The CDK inhibitors p16, p15, p27, and p21 are involved in the inactivation of the CDK-Cyclin complexes.

The G1/S cyclin-CDK complexes CycD-CDK4/6 and CycE-CDK2 phosphorylate RB on at least 13 residues of Ser/Thr. Each phosphorylated residue is a hallmark of a specific biochemical outcome **(Table1)**. Recent findings demonstrated that the monophosphorylation of RB on each of the Ser/Thr is not capable of inactivating RB in controlling the G1/S checkpoint. In fact, the replacement of endogenous RB with monophosphorylated RB induced accumulation in the G1 phase in non-transformed hRPE1cells and significantly reduced the expression of the E2F signature (Sanidas et al. 2019). On the other hand, the same researchers found that each of the monophosphorylated forms drastically changes the RB interactome and the transcriptional output. This intricate matrix of post-translational modifications leads to the formulation of two more hypotheses on the events driving its inactivation (Rubin, Sage, and Skotheim 2020). The first states that CycD-CDK4/6 activity only prompts RB monophosphorylation, whereas RB hyperphosphorylation is observed with the CDK2 activity. When RB is monophosphorylated by CycD-CDK4/6, E2F-dependent transcriptional activation is repressed, suggesting that only CDK2 directly inactivates RB through hyperphosphorylation. This finding challenges the paradigm in which CDK4/6 inactivates RB and states that CDK2 is the inactivating kinase. However, several studies confirmed that CycD-CDK4/6 activity is crucial for cell-cycle progression and proliferation. In fact, CDK4/6-specific inhibitors like

palbociclib and ribociclib cause loss of hyperphosphorylated RB and cell-cycle block in G1. Moreover, mutation of a CDK4/6 specific docking site in RB resulted in reduced RB hyperphosphorylation and increased G1 arrest (Topacio et al. 2019). One explanation is a priming mechanism for RB hyperphosphorylation: CDK2 hyperphosphorylation would require CDK4/6 monophosphorylation or that CDK4/6 contributes to CDK2 activation by targeting other substrates. The second alternative mechanism proposed is that CDK4/6 is critical for CDK2 activity by sequestering CDK protein inhibitors like p21/p27. This model states that RB phosphorylation and its consequent inactivation depend exclusively on CDK4/6. Like the classical model, the phosphorylation by CDK4/6 precedes the CDK2 one, but according to this alternative model, the phosphorylation carried out by CDK4/6 is necessary and sufficient to inactivate RB during the G1 phase, while the activity of CDK2 is required to maintain RB phosphorylation and E2F activation only once cells are in S phase. Unlike the majority of other cell cycle regulatory proteins, RB is normally not degraded upon inactivation but rather remains until mitosis, when it is dephosphorylated by PP1 to enter the subsequent G1 phase (Kolupaeva and Janssens 2013).

Sites	Domain	Biochemical Output
S249/T252	RbN	Resistance to Inactivation by CDKs (Gubern et al. 2016)
T356	RbIDL	Reduce affinity to E2F (Lentine et al. 2012)
T373	RbIDL	Inhibits E2F and LxCxE binding to the pocket domain (Burke et al. 2010)
S608/S612	RbL	Inhibits E2FTD binding (Burke et al. 2010)
S780	RbP	Reduce affinity to E2F (Mishra, Melino, and Murphy 2007)
S788/S795	RbC	Inhibits RbC-E2F1MB binding (Rubin et al. 2005)
S807/S811	RbC	Might prime phosphorylation at other sites (E S Knudsen and Wang 1997)
T821/T826	RbC	Inhibits RbC-E2F1MB-DPMB binding and inhibits LxCxE binding to the pocket domain. (Rubin et al. 2005)

Table 1 List of the Ser/Thr residues of RB associated with phosphorylation and the associated biochemical output.

In retinoblastoma, the presence of wild-type RB1 is unexpectedly observed in 2.7% of cases (Rushlow et al. 2013a). This evidence suggests that RB1 mutations are not the only responsible driving event for retinoblastoma onset. Notably, half of the RB1 wild-type retinoblastoma cases analyzed in this study were characterized by MYCN amplification, and this latter feature was absent in the large cohort of RB1 mutated tumors (97.3% of the cases). The authors of this study concluded that in this small percentage of cases, retinoblastoma might be driven

by MYCN amplification (Rushlow et al. 2013a). Histologically, these tumors share more similarities with MYCN-amplified neuroblastomas than classical retinoblastomas, but molecular mechanisms driving its onset have only begun to be explored (Ewens et al. 2017; Singh et al. 2022). Interestingly, Singh et al. discovered that in explanted developing human retinae, N-MYC enhances the expression of CCND2 and CDK4 as MYC does in fibroblasts (C. Bouchard et al. 1999), leading to phosphorylation and inactivation of RB (Singh et al. 2022). MYCN-overexpressing retinal cells could even recapitulate MYCN-driven retinoblastoma in mouse xenografts (Singh et al. 2022).

Loss of RB by its inactivation or mutations is observed in a wide range of cancers other than retinoblastoma (Rubin, Sage, and Skotheim 2020). Intriguingly, virtually all MYCN-amplified NBs cases exhibit RB1 wild-type (Mosse et al. 2007). However, several shreds of evidence support the hypothesis that RB might be inactivated in MYCN-amplified NB. First, downregulation of its inactivator CDK2 showed synthetic lethality in MYCN-amplified cells (Molenaar et al. 2009). Second, the MYCN-amplified NB cell lines are susceptible to CDK4/6 inhibitors, CCND1 (Cyclin D1), and CDK4/6 downregulation, which was not observed in the majority of MYCN-nonamplified cell lines (Rihani et al. 2015; Julieann Rader et al. 2013). Third, pharmacologic inactivation of CDK2 in MYCN-amplified cells inhibits cell proliferation and induces cell death both in vitro and in vivo (Z. Chen et al. 2016).

The E2F family

The discovery of the adenoviral early region 2 binding factor (E2F) occurred more than 30 years ago, describing a transcription factor playing a key function in the earliest stages of adenoviral replication (Kovesdi, Reichel, and Nevins 1986). Today, E2Fs have been characterized as crucial transcriptional cell cycle regulators, but additional activities in maintaining genomic stability are just emerging. The precise mechanism through which E2Fs help regulate cellular physiology remains incompletely understood.

Historically, E2F genes are divided into three subgroups: activators (E2F1, E2F2, E2F3) expressed at high levels during the G1/S phase transition, canonical repressors (E2F4, E2F5, and E2F6) almost constitutively expressed, and atypical repressors (E2F7 and E2F8) typically expressed in the late S phase (Kent and Leone 2019). The E2Fs 1-5 activity is strictly regulated by the pocket proteins RB, p107, and p130. However, RB is the only pocket protein interacting with the activating E2F1–3, while p130 and p107 only bind to E2F4 and E2F5 (Liban et al. 2017; 2016). Genetic deletion of E2F family members in nematodes, flies, and mice has

shown to be a suitable method for dissecting the physiological activities of E2Fs. There are several clues about the redundancy of activator E2Fs. Indeed, loss of E2F1/2 is well tolerated in mice. However, loss of E2F3 leads to embryonic lethality due to problems in cell proliferation (Ciemerych and Sicinski 2005).

Structurally, E2Fs share a common helix-turn-helix DNA binding domain called "winged helix", recognizing the consensus sequence TTTCC/GCGC. By doing that, E2Fs dimerize with DP factors encoded by the TFDP1/2/3 genes (James DeGregori and Johnson 2006). E2F1-3 shares a standard structure composed of I) a nuclear localization signal; II) a cyclin A regulatory domain involved in its stabilization; III) the DNA binding domain IV) a dimerization domain involved in the interaction with DPs; V) a transactivation domain responsible for the E2F-driven transcriptional activation that can be bound RB (Kent and Leone 2019). Despite the sequence similarity between the activators E2Fs, only E2F3 has been considered a classical proto-oncogene due to its putative role in tumoral transformation in multiple types of cancer. In fact, its overexpression and its amplification were observed (Oeggerli et al. 2004; Olsson et al. 2007; Hurst et al. 2008).

E2Fs1/2 have only one reported isoform, whereas E2F3 has at least four described isoforms; the most studied are E2F3A (the longest one) and E2F3B, whereas the mitochondrial isoforms E2F3C and E2F3D were identified only recently. The only difference between E2F3A and E2F3B is the absence of the N-terminal region in E2F3B, given the presence of an alternative promoter located at ~1k downstream of the first exon of E2F3A. E2F3C and E2F3D are generated by alternative splicing and lack the DBD and the RB binding domain, and their function is mainly unknown (Araki et al. 2019). While E2F3A is considered a transcriptional activator, E2F3B works as a transcriptional repressor, mimicking the function and the expression pattern of canonical repressors (M. R. Adams et al. 2000).

Overall, E2Fs are essential for deciding when a cell will divide. Indeed, the expression of E2F targets steadily increases throughout G1 and must reach a certain level to pass a restriction point and enter in S phase. The link between this threshold of E2F activity and the restriction point has been explored through single-cell analysis. Once a threshold level of E2F activity is reached, the cell cycle progresses regardless of additional mitogen stimulation. Several factors influence the E2F threshold needed for passing the restriction point. For instance, when negative E2F regulators CDK inhibitor 1A (CDKN1A, p21), RB, or p130 are overexpressed, cells enter a deeper quiescent state, increasing this threshold. On the other hand, the expression of positive E2F regulators (MYC or CCND1) reduced the amount of mitogen stimulation re-

quired to induce cell cycle entrance. According to this evidence, quiescent cells may be encouraged to proliferate with the help of oncogenic stimulation of the E2F transcriptional pathway. (Yao et al. 2008; Kwon et al. 2017). Among the E2Fs targets, there are genes involved in G1/S transition, such as Cyclin D, Cyclin E, MYC, MYCN, and genes involved in DNA replication, such as the MCM2-7 genes and CDC6. Moreover, it is well-known that E2Fs upregulate themselves in a positive feedback loop (Bracken et al. 2004).

One of the most important genes regulated by activator E2Fs in NB is MYCN. Remarkably, E2F3 binds to the MYCN promoter and activates its transcription only in the presence of MYCN amplification (Strieder and Lutz 2003). Moreover, overexpression of E2F1 and E2F3 in NB correlates with poor prognosis, independently from MYCN amplification. Patients expressing high levels of E2F1/3 showed increased expression of genes involved in G1/S transition (H. Wang et al. 2022). Parodi et al. recently found that overexpression of E2F3 is a hallmark of impaired survival in stage 4S NBs, typically characterized by spontaneous regression (Parodi et al. 2020). However, these findings have been studied by analyzing large datasets of RNAseq, and the importance of these transcription factors in NB biology should be further validated by in vitro and in vivo experiments. Recently, the role of E2Fs in NB was further investigated. Studying the effect of the silencing and the farmaceutical inhibition of the histone demethylase KDM6B in MYCN-amplified NB cells, D'Oto et al. found a relevant reduction in cell viability and proliferation, most likely because of the downregulation of MYCN and E2F targets (D'Oto et al. 2021).

Targeted therapy for neuroblastoma

Currently, NB high-risk patients are treated with an intensive chemotherapy regimen consisting of cisplatin, vincristine, carboplatin, etoposide, and cyclophosphamide (COJEC). In specific cases, resection surgery and radiotherapy are performed (A. D. J. Pearson et al. 2008). ALK and N-MYC are under extensive investigation among the molecular targets, given their driver gain of function mutation and amplification. As established by in vitro and in vivo research (Huang and Weiss 2013), regulatory networks relying on N-MYC and ALK play a significant role in maintaining the proliferative phenotype and inhibiting differentiation pathways in brain precursors. However, although there are several ALK-specific therapies, N-Myc-specific targeting is still challenging. The N-MYC pathway can be targeted indirectly following several approaches, primarily by targeting specific downstream effectors regulating cell growth and proliferation.

Targeting MYCN-amplified NB

The N-MYC/MAX heterodimer formation inhibition is an intriguing strategy for counteracting the MYCN-activated carcinogenic regulatory network (Ferrucci et al. 2018). In the scenario, a screening of 7000 peptidomimetic compounds was performed to identify candidate peptides capable of inhibiting the dimerization of MYC and MAX. This screening found IIA6B17 and IIA4B20, two small compounds that substantially inhibit Myc–MAX dimerization and DNA binding (Berg et al. 2002). Based on these groundbreaking studies, other researchers worked in this area, discovering and optimizing new compounds such as the unique Peptomyc's Omomyc-based treatment (OMO-103). However, this peptide has been used mostly for laboratory purposes as a powerful tool to inactivate MYC and study its downstream pathway. Only recently, the potential use in clinics has started to be explored (Massó-Vallés and Soucek 2020).

N-MYC-mediated transcriptional regulation is mainly enhanced by its interaction with bromodomain and extra terminal (BET)-containing proteins, which function as chromatin readers. Indeed, BET binds to acetylated lysine residues and assists transcription. The importance of the bromodomain-containing protein 2 (BRD2), BRD3, and BRD4 in this context is relevant. Multiple investigations demonstrated that the BET inhibitor JQ1 downregulates N-MYC transcriptional signatures, reducing MYCN expression and enhancing survival in both xenograft and transgenic murine models of neuroblastoma (NB) (Puissant et al. 2013).

N-MYC positively regulates E2F expression (J. DeGregori et al. 1997; Sears, Ohtani, and Nevins 1997), and its expression positively correlate with CDK4 and Cyclin D genes (Molenaar et al. 2008). Targeting CDK, which is necessary for the transition from G0/1 into the S phase, could ideally be advantageous for putting the "brakes" on the aberrant proliferation in patients with MYCN-amplified NB (Ando and Nakagawara 2021). There are three major CDK4/6 inhibitors, palbociclib, ribociclib, and abemaciclib, all of which have shown promising results in treating other types of cancer in which The CDK/RB/E2F pathway is altered (Braal et al. 2021). The use of ribociclib in NB cellular models has only recently been examined; as expected, MYCN-amplified cell lines exhibit higher sensitivity (JulieAnn Rader et al. 2013).

MYCN-amplified NBs show deregulation of several enzymes involved in polyamine metabolisms, such as ODC1, SRM, SMS, AMD1, OAZ2, and SMOX. Notably, ODC1, a key enzyme in polyamine metabolism converting ornithine to putrescine, is a direct transcription

target of N-MYC (Hogarty et al. 2008). Polyamines are essential polycations that sustain MYCN functions through ionic and covalent activities. The decreased levels of intracellular polyamines stimulate checkpoints that limit proliferation, while enhanced polyamine synthesis supports oncogenic proliferation (Thomas* and Thomas 2001). Polyamines are involved in several biological processes, and one of the most crucial ones is spermidine. Spermidine is needed for hypusinilation of the translation elongation factor eIF5A, promoting the translation of genes containing specific aminoacidic repeats. Hypusinilated eIF5A is essential for the translation of genes encoding for proteins involved in the cytoskeletal-associated process, RNA splicing and turnover, DNA binding and transcription, and cell signaling (Casero and Marton 2007). The N-MYC target ODC1 is druggable by difluoro-methyl ornithine (DFMO), which recently completed a phase II clinical trial. DFMO treatment after completion of first-line therapy was associated with improved event-free and overall survival compared to controls treated at the same institutions of this clinical trial (Lewis et al. 2020).

Immunotherapy: Targeting GD2

Immuno-targeting MYCN-amplified NBs is challenging since N-Myc is involved in the downregulation of the major histocompatibility complex (MHC) class I antigen expression, leading to escape from cytotoxic T cells and interferon-mediated immune response. The relationship of MYCN with the tumor immune microenvironment has only begun to be explored (Blavier, Yang, and DeClerck 2020). The tumor microenvironment of MYCN-amplified NBs contains a significantly lower number of immune cells compared to the MYCN-nonamplified counterpart (Zhong et al. 2019). For these reasons, the authors of the review mentioned above describe MYCN-amplified NBs as “cold” and immune exclusive, while MYCN-nonamplified ones are referred to as significantly inflamed or “hot”. Based on this evidence, a more profound comprehension of the microenvironment’s role in NB disease could drive novel strategies for the cure of this childhood malignancy. In fact, the lack of antigen presentation due to MYCN overexpression has been successfully circumvented by developing antibodies against the targetable ganglioside GD2 (Joshi 2020).

Gangliosides are modified sphingolipids highly expressed in cancer cells. Generally, gangliosides are not considered for target therapy because they are also found in healthy tissues. Exceptionally, the ganglioside GD2 is highly expressed on the surface of NB cells, and its expression in normal tissue is limited at a relatively low level to neurons, skin melanocytes, and peripheral nerve fibers. The precise function of GD2 is unknown, although it is thought to promote tumor cell proliferation, cell adhesion mediator, motility, invasion, and migration

(Nazha, Inal, and Owonikoko 2020). Intriguingly, based on the degree of expression, therapeutic impact, immunogenicity, and antigen specificity, the U.S. national institute classified GD2 as the tenth most promising target out of 75 (Cheever et al. 2009). Moreover, GD2 is expressed in the vast majority of NBs, regardless of the grade and staging of the tumor (Z.-L. Wu et al. 1986; Schengrund 2020; Sariola et al. 1991). These characteristics make GD2 an exciting target for immunotherapy.

Several anti-GD2 antibodies (GD2 Ab) have been developed. The most studied ones are murine 3F8 and 14.G2a. Initially, these two antibodies were employed singularly or in combination with cytokines in GD2-expressing ($GD2^+$) tumors. However, significant cases of human-anti mouse (HAMA) antibody development in the host were observed, leading to a decrease in the therapeutical effect (N. K. Cheung et al. 1987). To circumvent HAMA, GD2 Ab were humanized, replacing the mouse Fc region with the human one, generating chimeric antibodies Hu3F8 (humanized 3F8) and ch14.18 (Humanized 14.G2a) (Nazha, Inal, and Owonikoko 2020). Many pathways are responsible for the efficacy of GD2 Ab, including (I) direct activation of cell death, (II) Fc receptor (FcR)–mediated antibody-dependent cell-mediated cytotoxicity (ADCC) by immune cells such as NK, macrophages, and neutrophils, and (III) complement-dependent cytotoxicity (CDC) (Morandi et al. 2021). Currently, ch14.18 produced in murine myeloma SP2/0 cell line (dinutuximab) and CHO cells (dinutuximab beta) are the only monoclonal antibodies approved by FDA and EMA for anti-GD2 immunotherapy in NB. They are used in combination with granulocyte-macrophage colony-stimulating factor (GM-CSF), interleukin-2 (IL-2), and 13-cis-retinoic acid (RA) for the treatment of high-risk NB patients who achieve at least a partial response to prior first-line therapy (Dhillon 2015).

However, several mechanisms of resistance have also been reported for his approaches, such as the development of human anti-chimeric antibody (HACA) (Yamane et al. 2009) and human anti-human antibody (HAHA) (I. Y. Cheung et al. 2017). Unfortunately, the development of antibodies anti-antibody is not the only described mechanism of resistance in anti-GD2 immunotherapy. Other limiting factors in GD2 immunotherapy are probably due to the molecular mechanisms regulating GD2 expression in NB that are not yet fully understood (Richman et al. 2018; Moghimi et al. 2021; Schumacher-Kuckelkorn et al. 2017). Recent evidence suggests that the enzymes involved in GD2 biosynthesis are controlled by another druggable target in NB: HDACs activity. Kroesen and colleagues demonstrated that expression of GD2 is enhanced by HDACi vorinostat, pan HDACi givinostat, class-I inhibitor entinostat, and an HDAC1,2-specific inhibitor. Their data highlighted that vorinostat induces higher GD2 expression, increasing GD2 synthase protein levels without altering its mRNA

levels in the NB cell line, suggesting that HDACs may act at the post-translational level of this enzyme (Kroesen et al. 2016). Moreover, the same research group found that cells that were treated with vorinostat, together with the cell-permeable sialic acid Ac5Neu5Ac, increased the expression of sialyltransferases ST3GAL5 and ST8SIA1, generating GM3 and GD3 gangliosides, the necessary precursors for GD2 synthesis (van den Bijgaart et al. 2019). The combined treatment with engineered sialic acid and HDACi may further increase the efficacy of current and future GD2-targeted immunotherapy in NB patients.

The structural characterization of the 14G2a antibody-antigen complex led to the generation of a specific single-chain variable fragment (ScFv), a useful tool for developing new biotechnological therapies (Horwacik et al. 2015). For instance, the anti-GD2 ScFv has been successfully employed to generate anti-GD2 CAR-T cells (Moghimi et al. 2021; Richman et al. 2018). ScFvs consists of a single polypeptide corresponding to the heavy and light chain of the variable fragment of antibodies. Since ScFvs can be easily expressed as recombinant proteins in bacteria, this solution appears much simpler and cheaper than the production of antibodies (Ahmad et al. 2012).

M13 bacteriophage as a platform for targeted therapy

The M13 bacteriophage is a member of the group of filamentous phages known as Ff phages (Rasched and Oberer 1986). Ff phages infect only Escherichia coli strains that express the F pilus (O'Callaghan, Bradley, and Paranchych 1973). The M13 genome is a single-stranded DNA (ssDNA) 6407 bases long, containing nine genes encoding eleven distinct proteins (van Wezenbeek, Hulsebos, and Schoenmakers 1980). Five of these proteins are coat proteins, whereas the other six are involved in phage replication and assembly **(Table 2, adapted from Ledsgaard et al., 2018)**. The virus's envelope is composed of approximately 2700 copies of the pVIII protein, while the remaining coat proteins, pIII, pVI, pVII and pIX are present in approximately five copies. The lifecycle of the M13 bacteriophage has been deeply investigated during the past decades (reviewed in Ledsgaard et al., 2018). Infection in Escherichia coli strains occurs once the pIII protein interacts with the protein on the pilus, triggering phage depolymerization and translocation of its genome inside the bacteria. Thus, the E. coli DNA replication machinery drives the synthesis of the complementary DNA, and this dsDNA is replicated by continuous rolling circle replication. In this process, pII protein plays a crucial role, and then the pV proteins cover the entire genome exposing only the packaging signal. pI, pIV, pVII, pIX, pX, and pXI are involved in the phage assembly and translocation outside the cell. pIII and pVI cooperate to release the phage from the bacteria after the phage genome has

been entirely coated with pVIII. However, if pIII or pVI are absent, additional phage genomes can be loaded, generating a significantly longer phage particle (Ledsgaard et al. 2018).

Gene	Protein	Function
I	pI	Assembly
	pXI	Assembly
II	pII	Replication
	pX	Replication
III	pIII	Coat protein Adsorption and extrusion
IV	pIV	Assembly and extrusion
V	pV	Replication
VI	pVI	Coat protein Infection and budding
VII	pVII	Coat protein Assembly and budding
VIII	pVIII	Coat protein
IX	pIX	Coat protein Assembly and budding

Table 2 List of the genes and proteins of the M13 phage with the associated function

M13 phage has been employed as a powerful tool for phage display by expressing the pIII as a fusion protein with proteins of interest. McCafferty et al. originally described antibody phage display selection by fusing a library of sequences encoding a ScFv to gene III. This method allowed for adequate antibody display on the virion, enabling the identification of antibodies with high affinity for a specific antigen (McCafferty et al. 1990). Initially, the ScFvs were cloned directly into the M13 genome. Later, the phage genome was split into two constructs: the phagemid and helper phage. The phagemid construct contains an antibiotic resistance cassette for the selection of the plasmid, the fusion gene III, and the region required for phage replication. The helper phage contains all the remaining genes and a different antibiotic resistance cassette for double selection. Bacteria co-transformed and selected with these two constructs leads to the generation of the whole recombinant phage (Hoogenboom et al. 1998). This method is particularly efficient for the production of recombinant phages on a large scale, since the fusion gene III might be driven by the LacO promoter, inducing the expression of the recombinant phage only after the induction with Isopropyl β-D-1-thiogalactopyranoside (IPTG). The M13 phage purification is an easier, unexpensive, and less time-consuming process compared to antibody purification from animal serum or cells (Klutz et al. 2016; Torres-Acosta et al. 2020). Several methods have been described, but the most largely used is the polyethylene glycol (PEG) and isoelectric precipitation of the cultured media (Passaretti et al. 2020).

The shape and proportions of the M13 phage raise the interest for application in targeted therapies for several pathologies, such as infectious and neurologic diseases (Messing 2016). In-

deed, The M13 phage shows a spaghetti-like shape, with a length of ~900 nm and a width of ~6.5 nm (Berkowitz and Day 1976). Thus, they could be retargeted and conjugated with hundreds of small molecules of interest. Moreover, they are safe, non-toxic, and well-tolerated by the host. Recently proof-of-concept for the application of retargeted phages for photodynamic therapy (PDT) for EGFR+ breast cancer has been described (Ulfo, Cantelli, et al. 2022; Bortot et al. 2022). The strategy consists of treating cancer cells with retargeted phages conjugated with photosensitizers, molecules that react with oxygen upon light irradiation, producing reactive oxygen species (ROS) capable of triggering cytotoxicity in target cells. PDT is a two-step treatment involving the administration of the PS, followed by its activation by a source of light. The primary benefit of PDT is the capacity to focus irradiation at the targeted site of action, so minimizing collateral injury to healthy tissues. Despite the benefits of photodynamic therapy (PDT), its practical applicability in cancer treatment is restricted to superficial, endoscope- or surgery-accessible areas. This is primarily attributable to light's restricted depth of tissue penetration. Thus, the quick depletion of the light dosage renders the therapy useless as the tissue becomes denser (Agostinis et al. 2011). PS might be coupled to targeting molecules that precisely bind to receptors overexpressed on tumor cells (active targeting), resulting in enhanced internalization at the location of interest and decreased off-target effects (Ulfo, Costantini, et al. 2022).

AIM

Neuroblastoma is the most prevalent type of tumor in infants and the third-most common type of cancer in children, behind leukemia and brain cancer. Despite several insights into genetic alterations and gene expression deregulation, the molecular mechanisms underlying its development and resistance to standard and tailored therapy remain elusive. This thesis aims to shed light on NB's vulnerabilities on three levels.

Aim I: According to the current state of the art, the molecular mechanisms behind the NB's onset are largely unknown, and there is an urgent need to identify critical genes involved in the malignant transformation of neural crest cells. MYCN amplification is accountable for the large majority of high-risk cases of NB, but direct targeting of N-MYC remains a challenge despite the enormous efforts of researchers in discovering MYC-specific therapies. Consequently, identifying the genes necessary for MYCN function in tumor transformation could circumvent this critical issue and lead to the discovery of new potential targetable molecular pathways. Through comprehensive genetic screening, our collaborators Michelle Haber and Murray D. Norris discovered a single-point mutation in the coding sequence of a gene capable of suppressing the tumorigenic phenotype of the mouse model Th-MYCN. Considering the lack of information about the molecular mechanisms in which this gene is involved, we aimed to characterize the interactome of the encoded protein and its chromatin-bound regions in an MYCN-amplified neuroblastoma cell line. Next, we focused on how the identified mutation might impact its interactions.

Aim II: In recent decades, the role of MYC in the cell cycle's dysregulation has been the subject of extensive research. Nonetheless, the role of its paralogue MYCN in the dysregulation of the G1/S transition checkpoint remains unclear, especially in MYCN-amplified NB. Other researchers have highlighted the hyperactivation of the CDK-RB-E2F pathway in NB, and preclinical studies on a panel of NB cell lines indicate that MYCN overexpression correlates with high sensitivity for the CDK4/6 inhibitor ribociclib. We discovered a positive correlation between the expression of MYCN and E2F factors by analyzing a large dataset of RNAseq from tumor samples. In the same dataset, we found that in the context of high expression of E2F3, the high expression of its physiological inhibitor RB1 did not improve the patient's prognosis. These results suggested that N-MYC might inhibit RB function, resulting in the uncontrolled proliferation of MYCN-amplified NB cells. To test this hypothesis, we generated NB cell lines in which the expression of E2F3 and RB1 was modulated using the CRISPRi technique and evaluated the cell behavior using cell biology assays and gene reporter genes.

Moreover, we aimed to provide additional information about the cell pathway driving the sensitivity of the NB to CDK4/6 inhibitors, asking whether the expression of RB1 might influence cellular response to the treatment.

Aim III: Targeted therapy for NB includes a wide range of approaches. Immunotherapy, one of the most recent treatments developed, showed promising results in terms of patient outcomes. Unfortunately, in some cases, resistance mechanisms render the patients' response to classical immunotherapy ineffective. Most of these mechanisms are poorly understood, but a significant portion is related to the host's immune system's inability to kill tumor cells. The ganglioside GD2 is the most employed antigen for NB immunotherapy. Conjugating anti-GD2 antibodies with chemotherapeutics and radiotherapeutics to achieve a high local concentration of the drug was one of the approaches used to circumvent immunotherapy resistance. However, given the small size of antibodies, the number of molecules that can be conjugated without impairing antibody binding is relatively low. Further, a considerable number of side effects have been reported. Thus, we aimed to produce M13 bacteriophage targeting GD2 as an alternative platform to increase the number of molecules carried to the tumor. Moreover, we tested the feasibility of using this vector for photodynamic therapy.

RESULTS (Part I)

The transcriptional co-repressor RUNX1T1 is necessary for MYCN-driven tumorigenesis in neuroblastoma

Preliminary results: A single nucleotide mutation in RUNX1T1 suppresses NB phenotype in Th-MYCN mouse

Th-MYCN mouse is a largely used rodent model to study MYCN-driven cancer. These mice carry MYCN proto-oncogene under the control of the Tyrosine-hydroxylase promoter (Th) to drive its expression in noradrenergic neurons during development. The tumoral phenotype has 100% penetrance and arises seven weeks from birth (Weiss et al. 1997).

In collaboration with Michelle Haber and Murray D. Norris laboratories of The Children Cancer Institute – Sidney, Australia, we used N-ethyl-N-nitrosourea (ENU) mutagenesis in a large-scale forward genetic screening of *Th-MYCN* mice. The primary purpose of this screening was to induce mutations capable of suppressing the tumoral phenotype, potentially identifying new genes/pathways associated with the development of MYCN-driven NB.

Of 1716 viable offspring screened, a founder mouse (1590) developed a tumor at 49 weeks of age, an unprecedented delay compared to normal tumor development. The histopathological analysis of the 1590 tumor was compatible with a teratoma rather than NB (data not shown). Following further mating, the offspring of 1590 demonstrated Mendelian inheritance, with half developing tumors typically by seven weeks of age (unsuppressed; n=11) and half displaying no tumors over the monitoring period, except for a single mouse showing delayed tumoral formation (suppressed; n=11) **(Fig.1 A, B)**.

To map the chromosomal location of the mutation responsible for this phenotype, the 1590 line, which was on a 129/SvJ background, was backcrossed to BALB/c and C57BL/6 mice bred to clonogenicity before whole-genome sequencing. From the whole genome sequencing, the critical region was specifically narrowed to the proximal end of chromosome 4 in a 9.4-43.07 Mb region. Further sequencing in this region demonstrated a single nucleotide change of thymine to cytosine in one allele of the Runx1 partner transcriptional co-repressor 1 (RUNX1T1) gene at co-ordinate chr4:13816819, resulting in an amino acid change of tyrosine to histidine (Y534H). This substitution occurred within the Nervy Homology Region 4 (NHR4), one of four highly conserved regions displaying homology to the nervy gene found in drosophila. Protein modeling showed that the tyrosine at position 534 is buried in the core of

the MYND motif. Substituting this amino acid with histidine would likely alter the nearby zinc coordination centers and be highly disruptive to the function of this domain **(Fig. 1C)**.

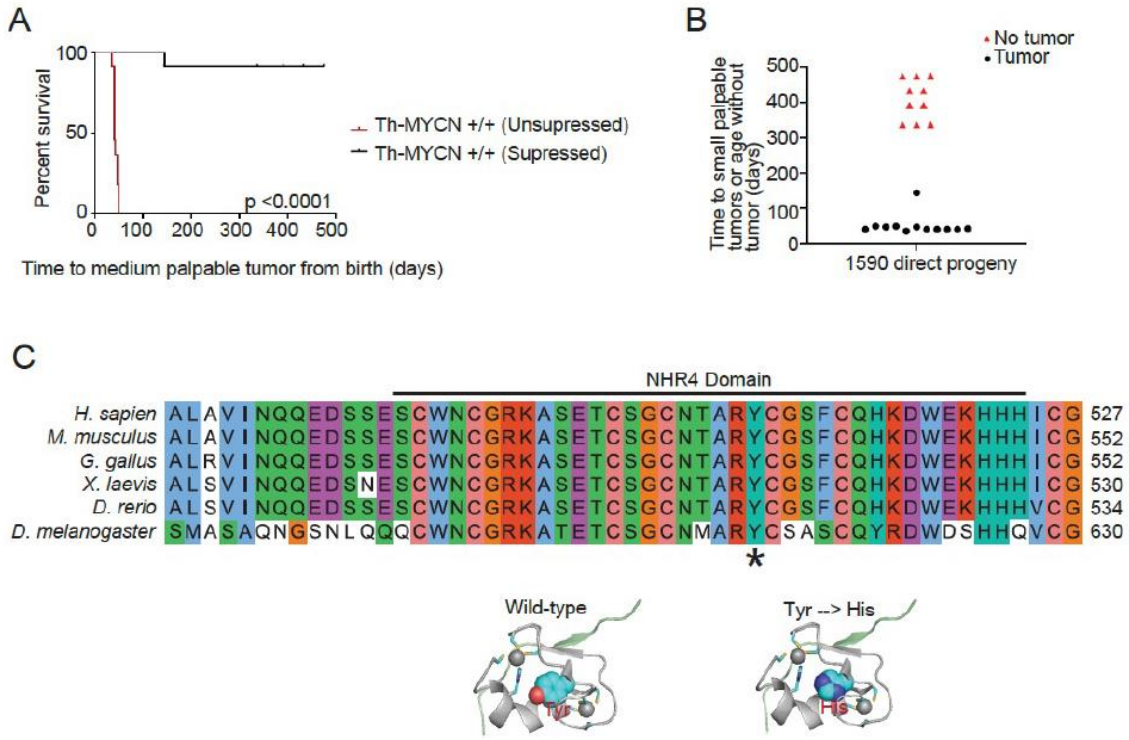

Fig. 1 Y534H mutation in RUNX1T1 suppresses the tumoral phenotype in Th-MYCN mice. **(A)** Survival curve of the 1590's offsprings (N=22), monitored for 500 days to the medium palpable tumor. The p-value by the Mann–Whitney test is indicated. **(B)** Beeswarm chart indicating time to small palpable tumors of 1590 direct progeny. The red triangles indicate offspring showing no tumors at the end of the monitoring period. **(C)** Up: Aminoacidic alignment of the RUNX1T1 orthologues' NHR4 Domains in six representative species. Asterisk indicates the Y residue involved in the mutation. Down: protein modeling of the NHR4 domain in wild-type and Y534H. Credits to Prof. Murrey D Norris and Prof. Michelle Haber.

RUNX1T1 interacts with transcriptional repressors and TFs in BE(2)C neuroblastoma cell line

The human orthologue of RUNX1T1 (hRUNX1T1), also known as Myeloid Transforming Gene chromosome 8 (MTG8) and Eight Twenty-One (ETO), belongs to the MTG protein family together with MTGR1 e MTG16, sharing with them a high degree of homology (Rossetti, Hoogeveen, and Sacchi 2004). MTG family genes encode for transcriptional co-repressors able to homo- and hetero- dimerize and tetramerize, forming large complexes involved in chromatin repression. However, little is known about the molecular mechanisms by which they exert this function (Hu et al. 2022). Given their ability to mediate multiple protein interactions with TFs and histone deacetylases, the most supported hypothesis is that they can recruit transcriptional repressors on regulatory genomic regions controlled by specific TFs (Hu et al., 2022). For instance, hRUNX1T1 is involved in 8;21 translocation in a subtype of

acute myeloid leukemia (AML), generating a fusion gene with the transcription factor AML1. The fusion protein RUNX1T1-AML1 presumably drives oncogenesis by repressing hematopoietic genes physiologically upregulated by AML1 (Rowley 1973; Downing 1999; Gelmetti et al. 1998).

To investigate the molecular mechanisms in which RUNX1T1 is involved in NB, we characterized its interactome by performing a Co-immunoprecipitation experiment coupled with mass spectrometry (Co-IP – LC-MS/MS). First, we transfected the MYCN-amplified NB cell line BE(2)C with a control construct (Empty vector, EV) or a construct encoding for 3xflag tagged RUNX1T1. Next, we performed a flag-immunoprecipitation of the nuclear extracts; we trypsinized the purified proteins and identified putative interactors by LC-MS/MS. From the list of the interactors found in RUNX1T1 Co-IP, we filtered out the non-specific interactors found in the EV condition. Given the molecular mechanisms in which RUNX1T1 is presumably involved, in the context of the characterized interactors, we only focused on proteins known to work as TFs or chromatin remodeling factors **(Fig 2A)**. Firstly, we identified some of RUNX1T1's well-known interactors, such as HDAC1-3, TCF4, and TCF12 (Rossetti, Hoogeveen, and Sacchi 2004), confirming the correctness of our approach. Interestingly, we also identified new interactors that have never been described before: KDM1A, RCOR3, SSRP1, GSE1, HAND1, HAND2, and TWIST1. Intriguingly, the lysine demethylase KDM1A, also known as LSD1, RCOR3, and HDAC1/2 are the trimeric core complex of the Co-REST, which is involved in the repression of gene expression. This complex exerts its function by de-acetylating and de-methylating, respectively, the H3K27ac and H3K4di/trimet of the histone tails of the nucleosome, achieving epigenetic transcriptional repression (Milazzo et al. 2020) (**Fig. 2B**). Among the transcription factors identified, we focused on HAND2, a well-known TF that drives differentiation of the noradrenergic lineage of the neural crest cells (Huber 2006).

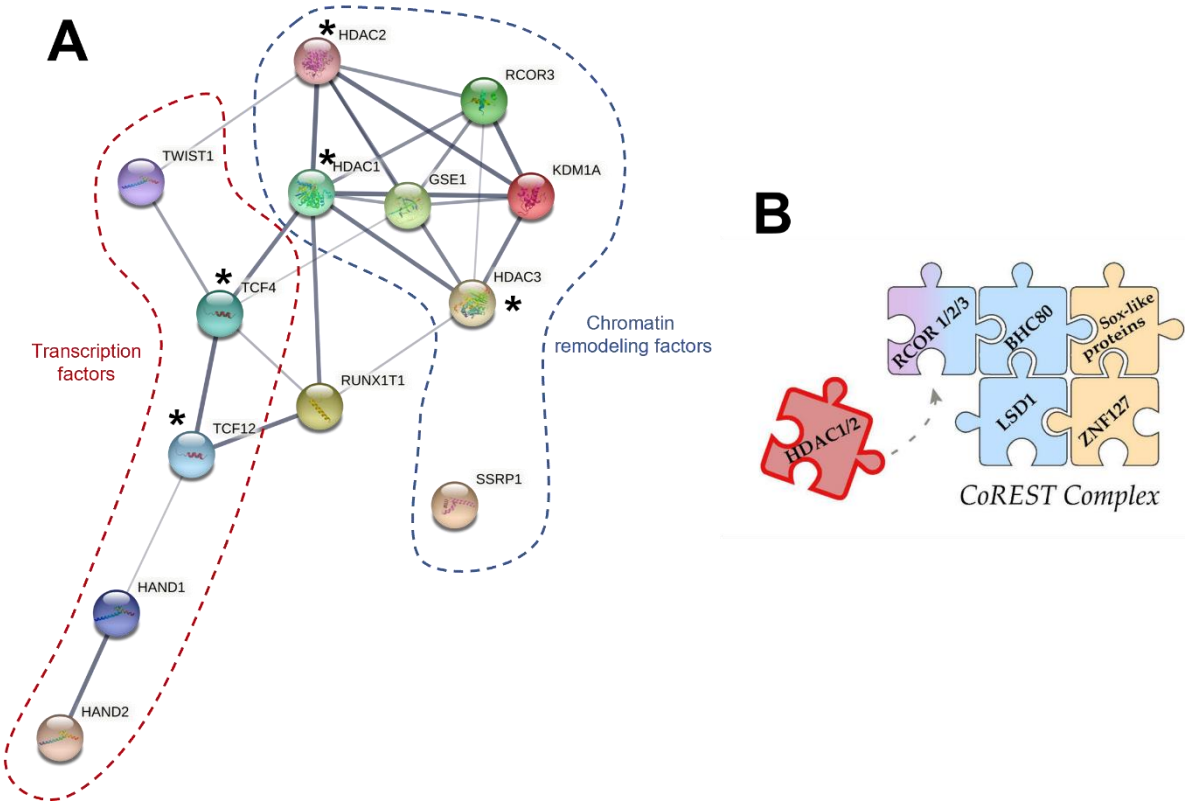

Fig. 2 RUNX1T1 interactome in BE(2)C cell line **(A)** STRING analysis of transcription factors and chromatin remodeling factors identified by Co-IP LC-MS/MS. BE(2)C were transfected with EV or 3xflag-RUNX1T1 constructs. 48h after transfection, nuclear protein extracts were immunoprecipitated with flag antibody, trypsinized, and loaded in LC-MS/MS. Proteins with at least 2-fold enrichment with $p<0.05$ were considered. The thickness of the connectors is proportional to the strength of the evidence (predicted or experimentally validated). Asterisks indicate RUNX1T1's known interactors **(B)** Schematic illustration of the Co-REST complex (Credits to Milazzo et al, 2020).

RUNX1T1, together with LSD1, HDAC1/2, RCOR3, and HAND2, binds to regulatory regions of genes involved in the autonomic system development and noradrenergic differentiation

Given the results obtained with the Co-IP-LC-MS/MS experiments, we hypothesized that RUNX1T1 might form a transcriptional repressive complex together with the Co-REST core complex (LSD1, HDAC1/2, RCOR3) and the TF HAND2. To test this hypothesis, we performed a ChIP-seq for RUNX1T1, RCOR3, and LSD1 in the MYCN amplified NB cell line Kelly and intersected the obtained peaks with the already published ChIP-seq for HAND2 performed in the same cell line (Durbin et al. 2018b).

RUNX1T1 binding was found almost exclusively within intergenic regions of the genome rather than in TSS proximity **(Fig.3A)**. From the intersection of the RUNX1T1 ChIP-seq replicates, we obtained 14062 peaks. By analyzing bound motifs through HOMER, we obtained highly significantly enriched motifs, the top-scored ones aligned with known motifs for

HAND2, PHOX2A, and TCF4 **(Fig.3 B)**. Furthermore, 36% of RUNX1T1 ChIP-seq peaks overlapped HAND2 ChIP-seq peaks previously identified in KELLY cells (Durbin et al., 2018), suggesting that HAND2 might recruit RUNX1T1 to genomic locations controlled by this transcription factor. To investigate this further, we performed additional ChIP-seq for LSD1 and RCOR3, intersecting the identified peaks with the RUNX1T1 ones. Interestingly, we observed a high level of co-localization of RUNX1T1 peaks with LSD1 and RCOR3 (41% and 43%, respectively) **(Fig.3C)**.

Strikingly, analyzing the overall intersection between the ChIP-seq results, we found that 24% of all RUNX1T1 peaks co-localized with HAND2, LSD1, and RCOR3, suggesting the existence of a unique complex composed by the identified proteins, regulating HAND2 target genes **(Fig. 3D)**. Next, to identify the biological relevance of these data, we performed a Gene Ontology analysis for the genes found in the nearby of the common peaks. Interestingly, highly significant associations were observed with neuronal differentiation and development, including autonomic nervous system development, sympathetic nervous system development, noradrenergic neuron differentiation, nerve development, and neural crest cell migration **(Fig. 3E)**.

Overall, these findings suggested that RUNX1T1 and the Co-REST complex proteins might be involved in the repression of genes involved in neuroblast differentiation. This latter pathway is thought to be altered virtually in all NBs, driving its undifferentiated phenotype (Shendy et al. 2022).

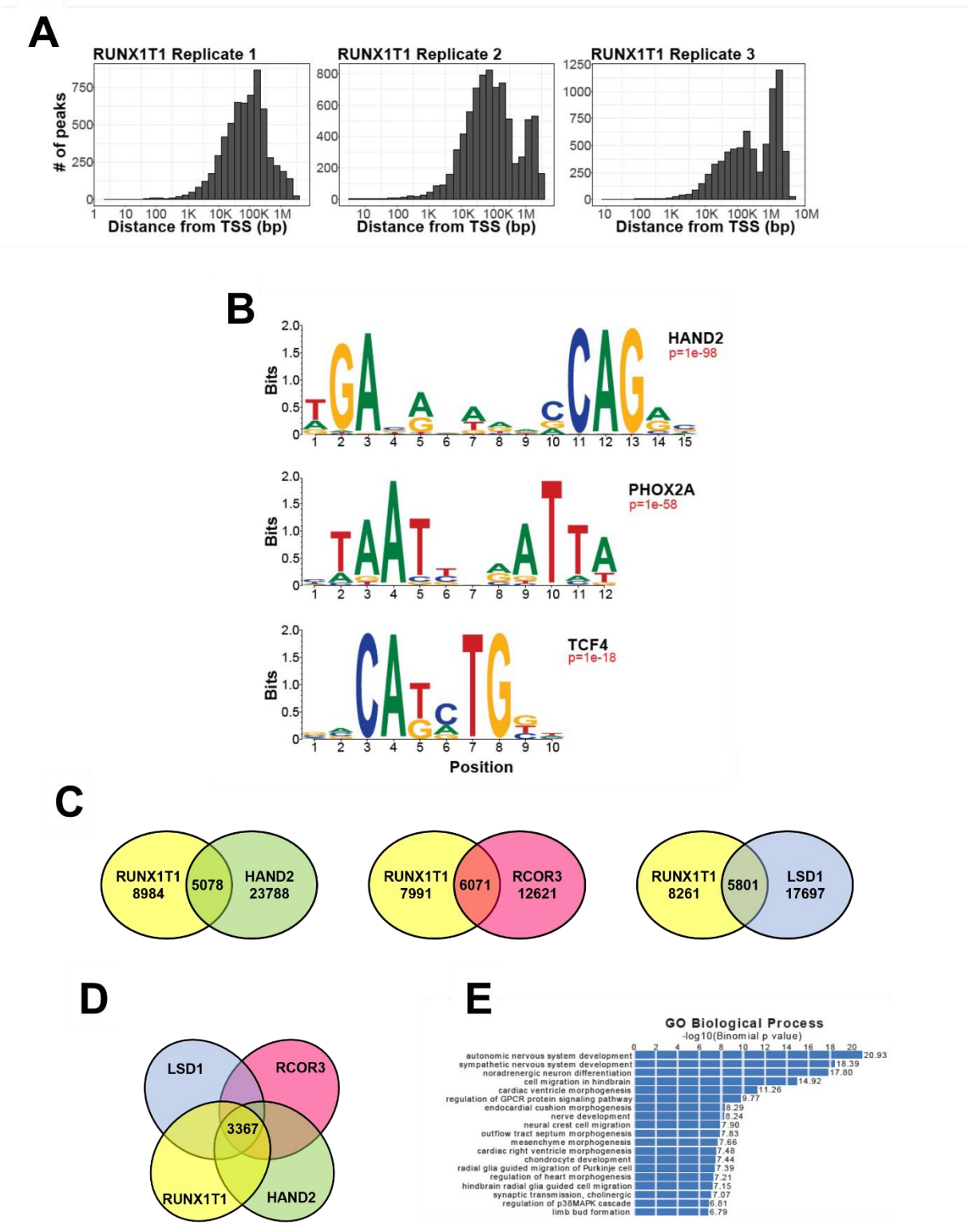

Fig. 3 RUNX1T1, LSD1, RCOR3, and HAND2 bind to chromatin regions associated with neuronal differentiation. **(A)** Distribution of RUNX1T1 peaks carried out from ChIP-seq performed in KELLY cell line. Results are shown as the number of peaks identified in each independent replicate as a function of the distance from the genes' transcriptional start site (TSS). **(B)** HOMER motif-enrichment analysis of regions bound by RUNX1T1. P-value is indicated in red. **(C)** Venn diagrams illustrating overlapping peaks between RUNX1T1 and HAND2, RUNX1T1 and RCOR3, RUNX1T1 and LSD1. **(D)** Venn diagram illustrating overlapping peaks between LSD1, RCOR3, HAND2, and RUNX1T1. 3367 peaks correspond to 24% of RUNX1T1 peaks. **(E)** Gene Ontology on the 3367 overlapping regions performed by Genomic Regions Enrichment of Annotations Tool (GREAT).

The tumor-suppressor single-point mutation in RUNX1T1 abolishes the interaction with RCOR3

Once we identified the candidate interactors of RUNX1T1 and the chromatin-bound regions, we validated the protein-protein interactions of this putative complex by performing Co-IP experiments with RUNX1T1. Due to the high degree of overlapping genomic regions bound by these interactors with RUNX1T1 ChIPseq peaks, we decided to validate LSD1, RCOR3, HAND2, and HDAC1/2/3 as RUNX1T1 interactors. Moreover, we asked if the single point mutation in RUNX1T1 capable of suppressing tumoral phenotype in Th-MYCN mice could perturb these interactions. To address this question, we transfected HEK 293-T cells with the EV control, 3xflag-RUNX1T1^{wt,} or 3xflag-RUNX1T1^{mut} plasmids together with the plasmid encoding for one of the candidate interactors tagged with the HA epitope. Next, we immunoprecipitated RUNX1T1^{wt} or RUNX1T1^{mut} using the anti-flag antibody in the nuclear protein extracts and assayed the co-immunoprecipitation of the HA-tagged proteins by western blot.

As expected, all the candidate interactors were correctly recovered with RUNX1T1^{wt}, observing the co-immunoprecipitated protein in the RUNX1T1^{wt} IP lane and no bands in the EV control IP lane. In the context of the Co-IPs between RUNX1T1^{mut} and the candidate interactors, we observed interaction with HAND2, LSD1, and HDAC1/2 **(Fig. 4A, B, D, E)**. Of note, introducing the single point mutation in RUNX1T1 (RUNX1T1^{mut}), we observed a slight decrease in the co-immunoprecipitated proteins HAND2, HDAC2, and HDAC3 **(Fig.4A, E, F)**. Interestingly, RUNX1T1^{mut} completely abolished the interaction with RCOR3 **(Fig. 4C)**. This latter finding suggested a crucial role of the interaction between RUNX1T1 and RCOR3 for MYCN-driven NB onset.

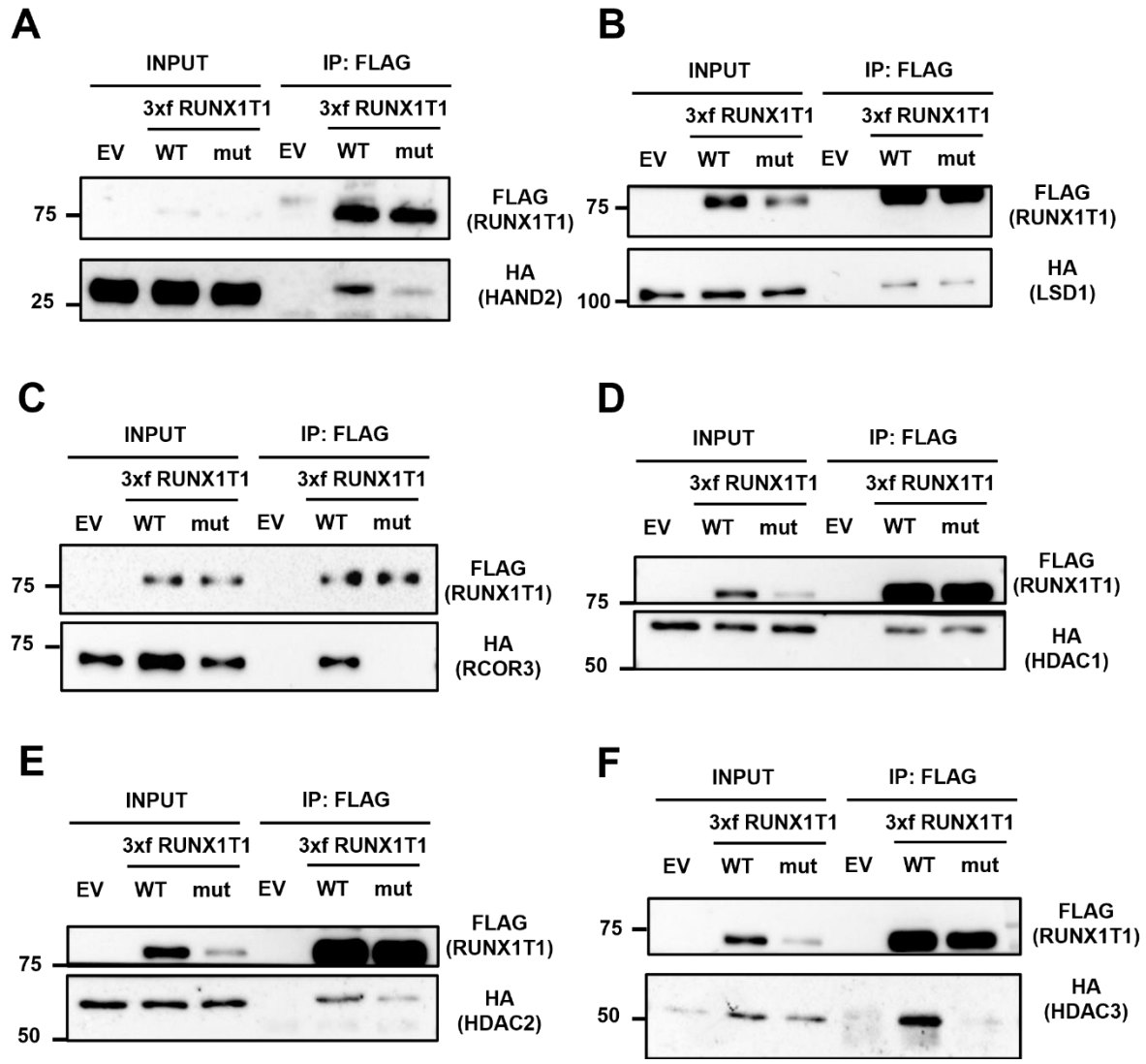

Fig. 4 Western blots of the exogenous Co-Immunoprecipitations (Co-IPs) in the HEK-293T cell line. Cells were co-transfected with empty vector (EV), 3xflag tagged RUNX1T1^{wt} or RUNX1T1^{mut} plasmids together with the HA-tagged putative interactor encoding plasmid. 24h after transfection, an anti-flag IP was performed on the nuclear protein extracts. Input refers to the 5% of the protein extract used for the Co-IP. IP: FLAG refers to the anti-flag immunoprecipitated sample. Co-IP were performed transfecting **(A)** HAND2; **(B)** LSD1; **(C)** RCOR3; **(D)** HDAC1; **(E)** HDAC2; **(F)** HDAC3. Figures A-F are representative of three independent experiments.

RUNX1T1's Nervy Homology Regions (NHRs) 2 and 4 are necessary for the interaction with the Co-REST complex

RUNX1T1 contains four evolutionarily conserved domains called Nervy Homology Region (NHR) 1-4 (J. N. Davis, McGhee, and Meyers 2003). NHR1 shares similarity with drosophila's TBP-associated factor 130 (hTAF 130), hTAF 105, and TAF 110. The small NHR2 domain contains a repeat of seven hydrophobic amino acids and is necessary for RUNX1T1 to form homodimers and heterodimers with other proteins of the MTG family. Remarkably, it has been demonstrated that the NHR2 domain is necessary to form homodimers and homotetramers (Liu et al. 2006). The NHR3 and NHR4 domains interact with transcriptional re-

pression complexes by recruiting N-CoR / SMRT and histone deacetylases (HDACs) (J. N. Davis, McGhee, and Meyers 2003). NHR4 contains two zinc-finger motifs, one of type CxxC 7x CxxC and another of type CxxC 7x HxxC, highly conserved from nematodes to humans.

To better characterize the interactions between RUNX1T1 and the Co-REST core complex, we wondered which of the highly conserved Nervy Homology Regions (NHRs) 1 to 4 are necessary for interacting with HDAC1, HDAC2, LSD1, and RCOR3. To address this question, we generated RUNX1T1 mutants by singularly deleting the NHRs domains in the RUNX1T1^{wt} encoding plasmid by whole plasmid PCR **(Fig. 5A)**.

Then, we co-transfected the HEK-293T cell line with the EV control, 3xflag RUNX1T1^{wt}, RUNX1T1^{mut}, or RUNX1T1$^{\Delta NHR1-4}$ plasmids, along with a construct encoding the HA-tagged Co-REST complex's proteins, and performed an anti-flag Co-IP. Interestingly, deleting the NHR1 domain decreased the interaction with HDAC1 compared to the wild-type interaction. The recovery of HDAC1 in the other samples suggested the dispensable role of the other NHR domains for protein complex formation **(Fig. 5B)**. Although we observed the preservation of the interaction between RUNX1T1$^{\Delta NHR2}$ and HDAC1, this mutant showed a decrease in HDAC2 recovery **(Fig. 5C)**. For what concerns the Co-IP between the RUNX1T1 mutants and LSD1, we observed the complete lack of the interaction with the RUNX1T1$^{\Delta NHR2}$ mutant. However, LSD1 was wholly co-immunoprecipitated with the other mutants **(Fig. 5D)**. Mapping the domains needed for the interaction with RCOR3 confirmed that RUNX1T1's NHR4 domain was necessary for this interaction. As expected, we observed a lack of interaction with RUNX1T1^{mut}, and we obtained the same result in the Co-IP with RUNX1T1$^{\Delta NHR4}$. Interestingly, we also found that as RUNX1T1 needed the NHR2 domain for the interaction with LSD1, the same domain was necessary for the interaction with RCOR3 **(Fig. 5E)**.

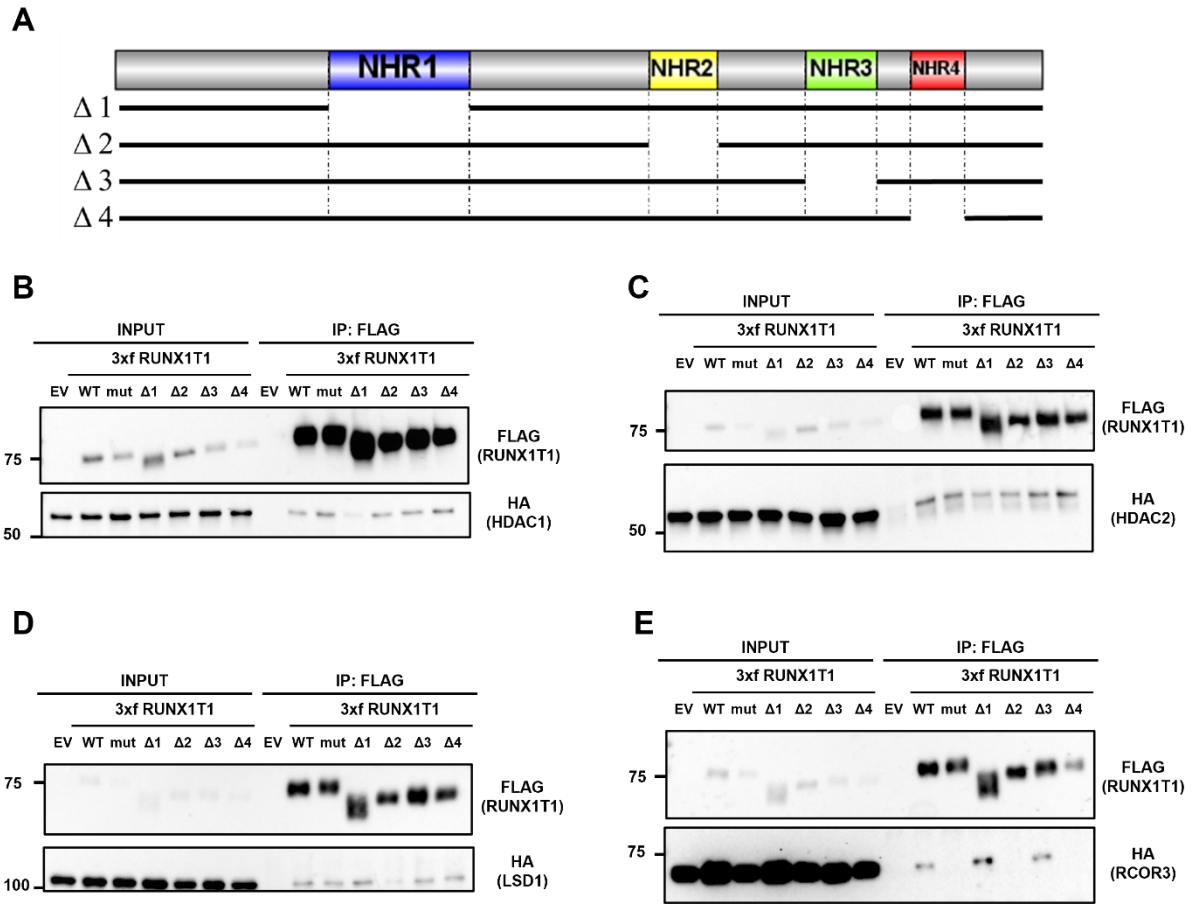

Fig. 5 Mapping the RUNX1T1's necessary domains for interacting with the Co-REST complex. **(A)** Top: schematic representation of the RUNX1T1's NHR domains. Bottom: schematic illustration of the interstitial deletions generated in the RUNX1T1^{wt} plasmid used for the Co-IP experiments. **(B-E)** Western blots of the co-immunoprecipitations (Co-IP) between 3xflag-RUNX1T1 wt or mutants and the HA-tagged Co-REST complex's proteins. Empty vector (EV) control plasmid, RUNX1T1wt, RUNX1T1^{mut,} or RUNX1T1$^{\Delta NHRs\ 1\text{-}4}$ were singularly co-transfected in HEK-293T cells together with HA-tagged **(B)** HDAC1 **(C)** HDAC2 **(D)** LSD1 **(E)** RCOR3. The anti-flag IP was performed on the nuclear protein extracts. Inputs refers to the 5% of the protein extract used for the Co-IP. IP: FLAG refers to the anti-flag immunoprecipitated extract. Absence of co-immunoprecipitation in the IP: FLAG EV lane confirms the specificity of the interaction. Figures B-E are representative of two independent experiments.

The Proline-rich domain of RCOR3 is necessary for the interaction with RUNX1T1

To identify the RCOR3 region involved in the interaction with RUNX1T1, we searched for information about features in common between RCOR3 and other interactors with whom RUNX1T1's NHR4 domain interacts. Interestingly we found that RUNX1T1's NHR4 domain forms a complex with NCoR and SMRT co-repressors by interacting directly with their proline-rich motifs 'PPPLI' (Liu et al. 2007).

RCOR3 contains five evolutionarily conserved domains: ELM2, SANT1, coiled-coil, SANT2, and Proline-rich. Strikingly, we identified three motifs within the proline-rich do-

main of RCOR3 with high homology to the NCOR2/SMRT's motifs known to bind to the NHR4 domain **(Fig. 6A)**. Therefore, we hypothesized that RCOR3 might interact with the same proline-rich motifs with RUNX1T1. Thus, we generated two HA-tagged RCOR3 encoding constructs, one lacking an amino acid sequence from 471 to 515 (Δ1), including the three 'PPPL' regions, and another lacking just the 'PPPLI' motif identical to NCOR2/SMRT (510-515, Δ2) **(Fig. 6B)**. These two constructs were co-transfected with 3xflag-RUNX1T1 into HEK-293-T cells, and their interaction was evaluated using anti-flag Co-IP on nuclear extracts. The results showed that, unlike wild-type RCOR3 and Δ1 RCOR3, the mutant protein Δ2 no longer interacts with RUNX1T1 **(Fig. 6C)**. However, we observed a slight decrease in Δ1 RCOR3 recovery compared to the wild-type, suggesting the importance of this motif in the stability of the interaction. Overall, these findings provide conclusive evidence that RUNX1T1 and RCOR3 interact directly via their NHR4 and Proline-rich domains, respectively.

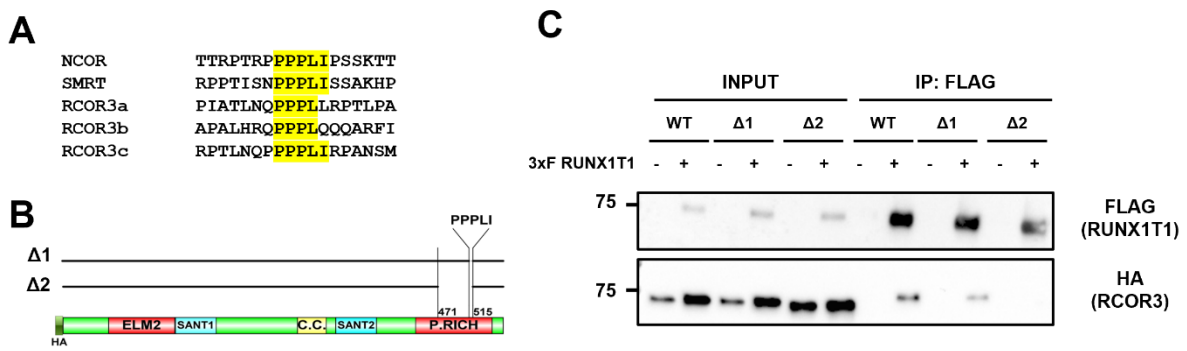

Fig. 6 RUNX1T1 and RCOR3 directly interact through their NHR4 and Proline-rich domains, respectively. **A)** Aminoacidic alignment between SMRT, N-CoR, and RCOR3. Three PPPL motifs found in the RCOR3 Proline-rich domain are reported. PPPL motifs are highlighted in yellow. **B)** Bottom: schematic illustration of HA-RCOR3 protein. Hemagglutinin tag (HA); Coiled-coil domain (C.C). Top: schematic illustration of the two deleted proteins lacking a.a sequence 510-515 (Δ1) and 471-515 (Δ2). **C)** Western blot of the flag Co-IP between RUNX1T1 and RCOR3. HEK293T cells were transfected with empty vector control (EV) or 3xflag RUNX1T1 together with HA_RCOR3^{wt}, HA_RCOR3$^{\Delta 1}$, or HA_RCOR3$^{\Delta 2}$. 24h after transfection, nuclear protein extract was immunoprecipitated with the anti-flag antibody. Input refers to 5% of the extract before the Co-Immunoprecipitation.

RUNX1T1 is required for RCOR3 recruitment on the chromatin

To better elucidate the role of RUNX1T1 in the Co-REST complex assembly on the target genes, we evaluated the binding of RCOR3 to the chromatin as function of RUNX1T1. Thus, we employed the KELLY cell line expressing doxycycline-inducible shRNA anti-RUNX1T1 and assessed the RCOR3 binding to the chromatin by dual-step ChIP, analyzing four genomic regions identified by the intersection of RUNX1T1, LSD1, RCOR3, and HAND2 ChIPseq. This cell line was transfected with HA-RCOR3 construct and cultured in the presence or ab-

sence of doxycycline. As sown in figure 7A, RUNX1T1 was correctly downregulated in the presence of doxycycline. Performing an anti-HA dual-step ChIP for RCOR3, we found that the four analyzed regions were bound by RCOR3 (~5-fold enrichment) only in the absence of doxycycline, while non-significant enrichment was observed in the presence of doxycycline (RUNX1T1 KD) (Fig. 7B). This result confirmed the crucial role of RUNX1T1 in the recruitment of RCOR3 to the identified genomic regions.

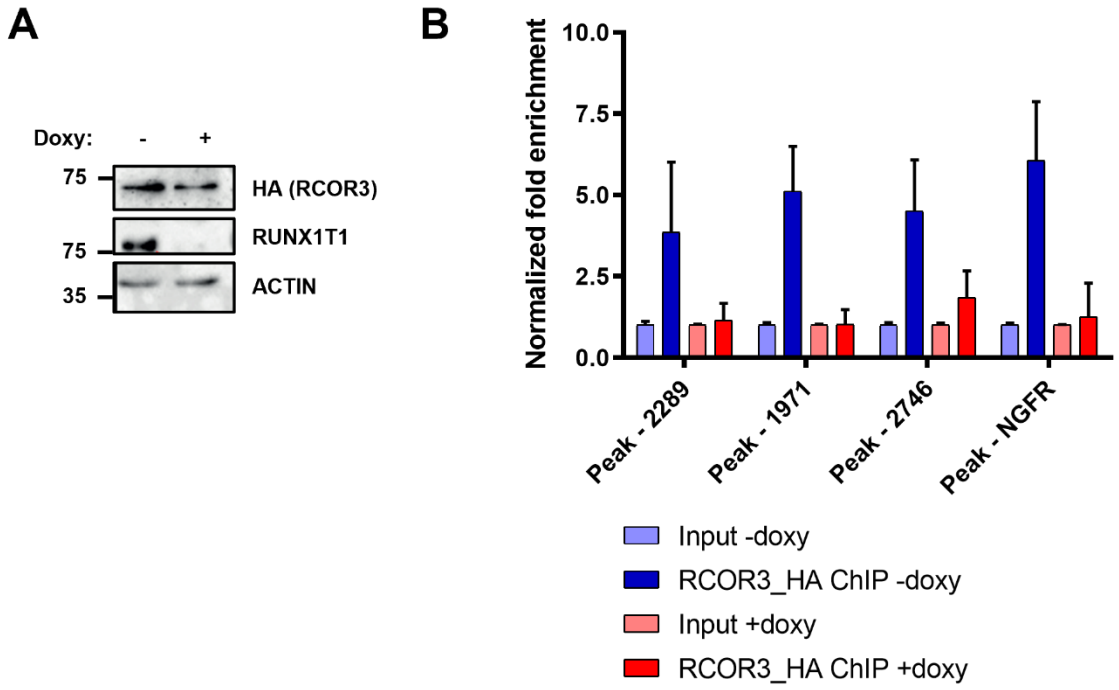

Fig. 7 RUNX1T1 is required for RCOR3 binding to the chromatin. Kelly cell line expressing doxycycline-inducible shRNA anti-RUNX1T1 were transfected with HA-RCOR3 construct and treated 48h in the presence or absence of doxycycline. **(A)** Western blot confirming the downregulation of RUNX1T1 and the expression of exogenous RCOR3. **(B)** Dual-step ChIP coupled with qPCR on HA-RCOR3. Four randomly chosen sequences were analyzed for RCOR3 binding. Results are plotted as normalized fold enrichment relative to a control region. Bars represent the mean ± SD of two (N=2) independent experiments.

DISCUSSION (Part I)

Our discovery that Y534H mutation in RUNX1T1 suppresses the tumoral phenotype in Th-MYCN animals is attributable to a lack of function of this nuclear co-repressor, given its ability to disrupt the NHR4 domain. Two alternative spliced variants encoding long and short murine RUNX1T1 isoforms were identified in preadipocyte cells (Zhao et al. 2014). In murine 3T3-L1 preadipocyte cells, the overexpression of the short isoform of RUNX1T1 promotes adipogenesis, while the overexpression of the long isoform inhibits differentiation (Merkestein et al. 2015; Zhao et al. 2014). The identification of Y534H point mutation in the carboxy-terminal NHR4 domain of the long isoform implies that the full-length protein isoform is required for tumorigenesis and might help maintain a de-differentiated phenotype in Th-MYCN mice.

Previous research revealed the existence of core regulatory circuitries (CRCs) in high-risk NB cells that involve a limited group of master transcription factor genes associated with super-enhancers participating in cell state maintenance (Boeva et al. 2017; Durbin et al. 2018b). Although we could find no evidence from ChIPseq data indicating binding of RUNX1T1 to super-enhancer regions (data not shown), we found a high level of overlap of RUNX1T1 ChIP-seq peaks with previously reported HAND2 ChIP-seq peaks (Durbin et al. 2018b). HAND2 is a critical component of sympathoadrenal and mesenchymal CRCs, and plays an essential role in neurogenesis and neural crest cell specification, particularly neural crest-derived noradrenergic sympathetic neuron development (Hendershot et al. 2008). Here, we showed that RUNX1T1 interacts with HAND2 and the Co-REST repressor complex involving the histone demethylase LSD1, RCOR3, and histone deacetylases HDAC1/2. It was demonstrated that LSD1 plays a crucial role in neuronal differentiation and that its high expression is associated with a poor outcome. Importantly, its high expression was associated with poorly differentiated NB tumors (Schulte et al. 2009). There are three known RCOR proteins, all of which interact with LSD1 and are needed for its correct functioning (Milazzo et al. 2020). However, according to our Co-IP LC-MS/MS data, only RCOR3 was found to bind RUNX1T1. Remarkably, among the tested proteins, the interaction between RUNX1T1 and RCOR3 was the only one lost following mutation of the NHR4 domain. Based on this evidence, we speculated that RUNX1T1 might drive the repression of genes involved in neuronal differentiation by recruiting the Co-REST complex on those genes.

Furthermore, Co-IP experiments revealed that other than the RUNX1T1's NHR4 domain, the NHR2 domain was also necessary for the interaction with RCOR3. Interestingly, the NHR4

domain was dispensable for the interaction with LSD1, while the NHR2 domain was necessary. Given the NHR2 domain's potential to drive RUNX1T1 homodimerization (Liu et al. 2006), we hypothesized that dimerization of RUNX1T1 would facilitate the interaction with the Co-REST complex. In this way, $RUNX1T1^{wt}$/$RUNX1T1^{mut}$ dimers might form a non-functional repressive complex in the absence of RCOR3. This latter hypothesis might explain why the RUNX1T1 mutation acts in a dominant-negative way, suppressing the tumoral phenotype even in heterozygosis. Going deeper into the interaction between RUNX1T1 and RCOR3, we found that their interaction is dependent on the Proline-rich domain of RCOR3. If the role of this interaction in the initiation of the tumor phenotype is validated, our findings will be helpful for further structural investigations to discover potential inhibitors of this interaction.

RESULTS (Part II)

MYCN overexpression overcomes RB function leading to unconditional hyperactivation of E2F in high-risk neuroblastoma

High expression of E2F3 correlates with poor prognosis despite RB1 levels in NB patients

Recent studies showed that E2F proteins cooperate with N-Myc to drive the oncogenic phenotype (Kalkat et al. 2018; Strieder and Lutz 2003; H. Wang et al. 2022). Moreover, our recent observations suggest that N-MYC and E2F transcriptional activators might establish a functional axis relevant for cancer initiation/progression in NB diseases carrying MYCN amplification (Ciaccio et al., unpublished data). The E2F gene family encodes for eight transcription factors (E2F1-8), playing a crucial role in cell cycle progression. However, only E2F1, E2F2, and E2F3 are formal transcriptional activators, and their principal role is to drive the transition from G1 to the S phase of the cell cycle. In fact, E2F1-3 activity is deregulated in most cancers, mainly by their overexpression or RB1 mutations (Kent and Leone 2019).

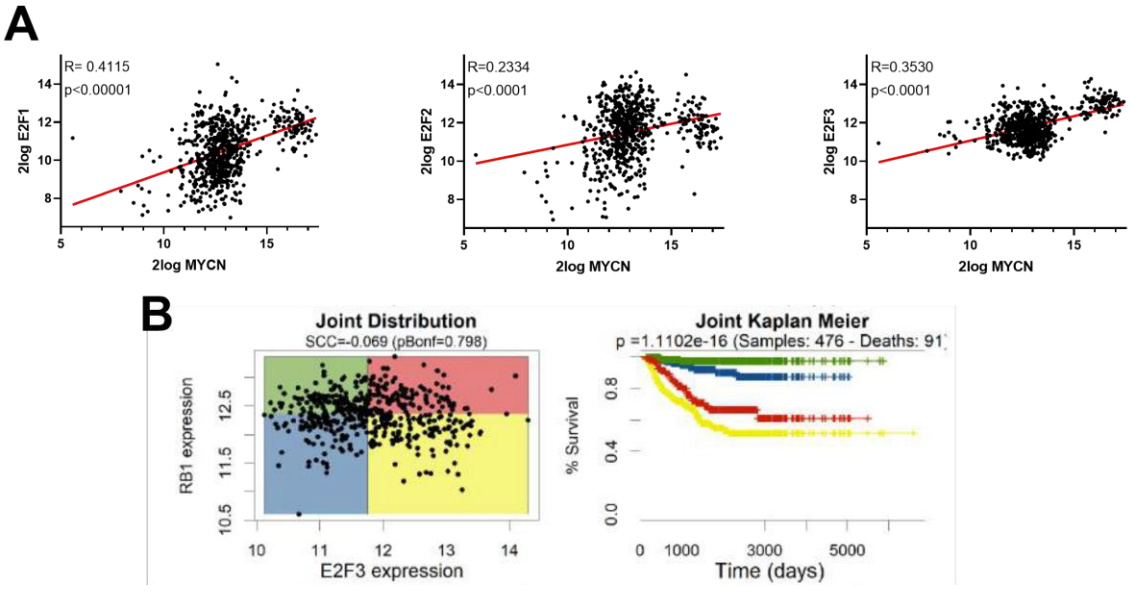

Fig. 8 High expression of E2F correlates with poor prognosis despite the RB1 levels. **A)** Spearman correlation between MYCN and E2F1-3 in a cohort of 649 NB patients. The p-value by the Mann–Whitney test is indicated. **B)** Survival analysis of the Kocak NB dataset as function of E2F3 and RB1 expression. E2F3 and RB1 expression were evaluated through Cox model analysis and separated into four quadrants according to median expression levels of RB1 and E2F3. The colors of Kaplan Meier curves match the colors of the quadrants. The p-value by the Cox model test is indicated.

To shed light on the functional interaction between E2F and MYCN, we first analyzed the mRNA expression correlation between E2F1-3 and MYCN in a cohort of 649 NB patients (Kocak et al. 2013). As expected, E2F activators' expression correlates with MYCN expression with high statistical significance **(Fig. 8A)**. In the context of E2F activators, E2F3 showed the highest correlation with poor prognosis (Parodi et al. 2020; H. Wang et al. 2022). Moreover, we recently found that the E2F3A isoform, not the E2F3B one, correlates with poor prognosis (Ciaccio et al., unpublished data). Given the importance of E2F3 in NB prognosis, we asked if the high expression of the E2Fs' physiologic inhibitor RB1 was able to rescue the prognosis of the patients expressing high levels of E2F3. Surprisingly, we did not observe any relevant improvement in the survival rate, comparing the overall survival curve of the high-E2F and high-RB1 expressing tumors with the high-E2F3 and low-RB1 expressing patients **(Fig. 8B)**.

E2F3A KD by doxycycline-inducible CRISPRi reduced colony formation of CHP-134 cell line

To verify the pro-tumorigenic activity of E2F3 in the MYCN-amplified NB cell lines, we analyzed the colony formation ability of the MYCN-amplified CHP-134 cell line following the conditional Knock-Down (cKD) of E2F3. Nevertheless, considering the prognostic value of the E2F3A isoform, we needed to repress E2F3A selectively. Because of the high similarity between the E2F3A and E2F3B mRNA sequences **(Fig. 9A)**, we decided to KD E2F3A using a CRISPR interference approach (CRISPRi) rather than RNAi. CRISPRi works with a nuclease-deficient spCAS9 (dead-Cas9, dCas9) expressed as a fusion protein with the transcriptional repression domains KRAB and MeCP2. When the dCas9 is co-expressed with a single-guide RNA (sgRNA) targeting the cis- regulating region of a specific gene, it triggers the KD of the target gene with high efficiency (Yeo et al. 2018).

In this way, we engineered the CHP-134 cell line to express a doxycycline-inducible HA-tagged dCas9-KRAB-MeCP2 with a sgRNA targeting the TSS of E2F3A (CHP-134 E2F3 cKD). This latter element was driven by a constitutive promoter **(Fig. 9B)**. Next, we checked by western blot the expression of the dCas9 and E2F3A with or without the doxycycline addition, confirming its repression **(Fig. 9C)**. Thus, we confirmed that the repression of E2F3A did not perturb the expression of the other E2F activators by qRT-PCR. However, we observed a significative upregulation of E2F3B **(Fig. 9D)**. Lastly, CHP-134 E2F3 cKD cells

were tested for colony formation. Interestingly, the KD of E2F3A induced a relevant reduction in colony formation **(Fig. 9E)**.

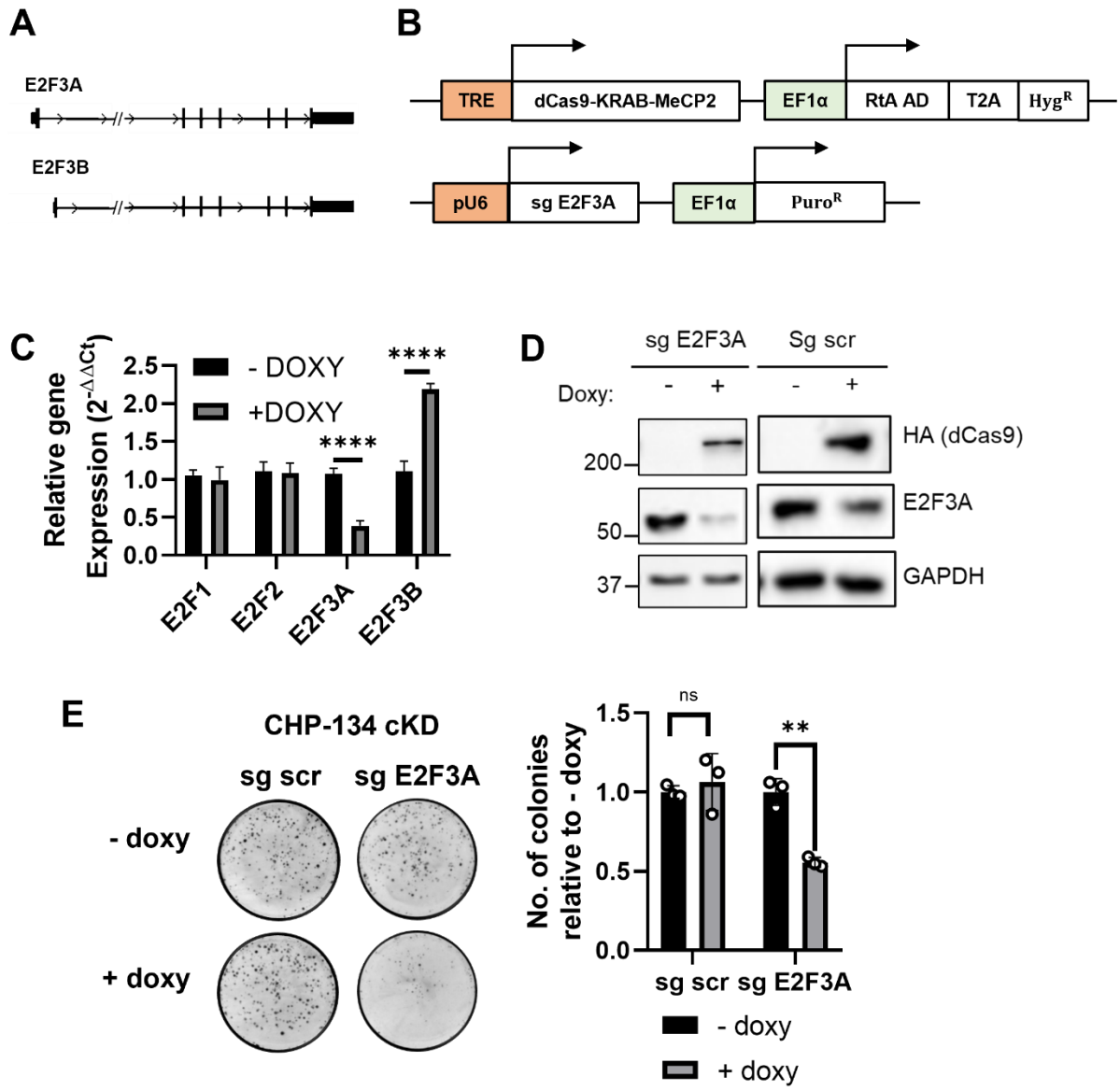

Fig. 9 E2F3A influences CHP-134 clonogenicity activity. **(A)** Schematic representation of the E2F3 isoforms. E2F3A and E2F3B show different transcriptional start sites. **(B)** Schematic representation of the dCas9-KRAB-MeCP2 inducible system. The PiggyBac transposon plasmid PB-TRE_dCas9-KRAB-MecP2 contains the dCas9-KRAB-MeCP2 expression cassette under the control of the TRE3G promoter, containing seven repetitions of the TET-responsive element (TetO). A constitutive promoter drives the expression of the trans-activator (rTtA)-T2A-Hygro^R cassette. The pLENTIsgRNA lentiviral construct contains the single-guide RNA (sgRNA) under the control of a constitutive promoter (p-U6). A second constitutive promoter (pEF1-α) drives the expression of the Puro^R cassette. In the presence of doxycycline, the complete dCas9-KRAB-MeCP2-sgRNA complex is reconstituted. **(C)** qRT-PCR on CHP-134 cKD cells after 72 hours of ± doxycycline treatment. Data were normalized using the GUSB housekeeping gene. The experiments were performed in triplicate (N=3) and plotted with the respective standard deviations. Data are shown as the mean ± SD of three independent experiments. Statistical analyses were performed using t-test. Error bars represented SD. *, **, *** indicated P < 0.05, 0.01, 0.001, and 0.0001, respectively. **(D)** Western blots of CHP-134 cKD scrambled (sg scr) or cKD E2F3A (sgE2F3A). Cells were incubated 72h with or without doxycycline. GAPDH was used as loading control. **(E)** Colony formation assay of CHP-134 cKD scrambled or E2F3A. 250 cells were seeded in a 6-well dish, and a picture was taken after 14 days. Left: representative pictures of the colony formation assay. Right: quantitative analysis of the

colony formation assay. Data are shown as average normalized on the -doxy condition ± SD of three (N=3) independent experiments.

MYCN overexpression overcomes RB repressive activity

Several studies in rodent models showed cooperation between MYCN and loss of RB1 in accelerating retinoblastoma formation (N. Wu et al. 2017). Strikingly, that effect can also be observed in tumors carrying MYCN amplification in which RB1 is not mutated. For instance, a small but significant percentage of retinoblastoma cases are genetically marked by MYCN amplification in a wild-type RB1 background (Rushlow et al. 2013a; Zugbi et al. 2020). This last evidence, together with the correlation between E2F3 expression and the poor outcome in NB patients despite RB1 levels, lets us hypothesize that a high dosage of MYCN in the cell may overcome RB function to promote an E2F-driven transcriptional activation.

To test this hypothesis, we evaluated the activity of the regulatory region of CDC6, a well-known E2F-driven promoter (Bracken et al. 2004), depending on the RB and MYCN expression **(Fig. 10A)**. Therefore, we engineered the MYCN non-amplified NB cell line SK-N-AS to KD RB1 with the doxycycline-inducible CRISPRi system (SK-N-AS cKD RB1). Next, we assessed the activity of the CDC6 promoter in the presence or absence of MYCN by dual-luciferase assay. As expected, the CDC6 promoter was significantly upregulated (~50% increase) when doxycycline was added to the media (RB1 KD) in the absence of MYCN ($P<0.001$). Notably, when MYCN was transfected, we observed roughly the same increase in luciferase activity compared to the EV - doxycycline condition ($P<0.0001$). On the other hand, unlike the EV condition, no significant effect on the CDC6 promoter was observed with the repression of RB **(Fig. 10B)**.

In a complementary experiment, we assessed the repressive activity of RB in the presence or absence of MYCN. Thus, we used the TET21, a widely employed cell line for studying molecular mechanisms dependent on MYCN. TET21N is a NB cell line derived from the MYCN-nonamplified cell line SHEP, carrying the MYCN transgene under the control of a doxycycline-repressive promoter (TET-OFF) (Bell, Lunec, and Tweddle 2007; L. Chen et al. 2010; Gamble et al. 2012). TET21N cells were transfected with pGL3b control, the CDC6 luciferase construct (pGL3_CDC6), and E2F3A or E2F3A + RB^{wt}. Furthermore, we also evaluated E2F3A activity co-transfecting an RB's hyperactive mutant ($RB^{\Delta CDK}$), lacking the 15 Ser/Thr residues substrate of the cyclin/CDK kinases activity leading to RB hyperactivation (Narasimha et al. 2014) **(Fig. 10C)**. Analyzing the -doxy and the +doxy condition separately, the transfection of the CDC6 promoter together with E2F3A induced a strong upregulation of

the promoter activity compared to the condition of the CDC6 promoter alone. Introducing RB^{wt}, we observed the repression of E2F3A activity, and this effect was even stronger with $RB^{\Delta CDK}$. Comparing the E2F3 + RB^{wt} samples in the ± doxy experimental conditions, we observed a significant decrease in E2F3-driven activity in the absence of MYCN ($P<0.01$). Taken together, these findings strongly suggested that MYCN is involved in RB inactivation, leading to its ineffectiveness in blocking the E2F3A function.

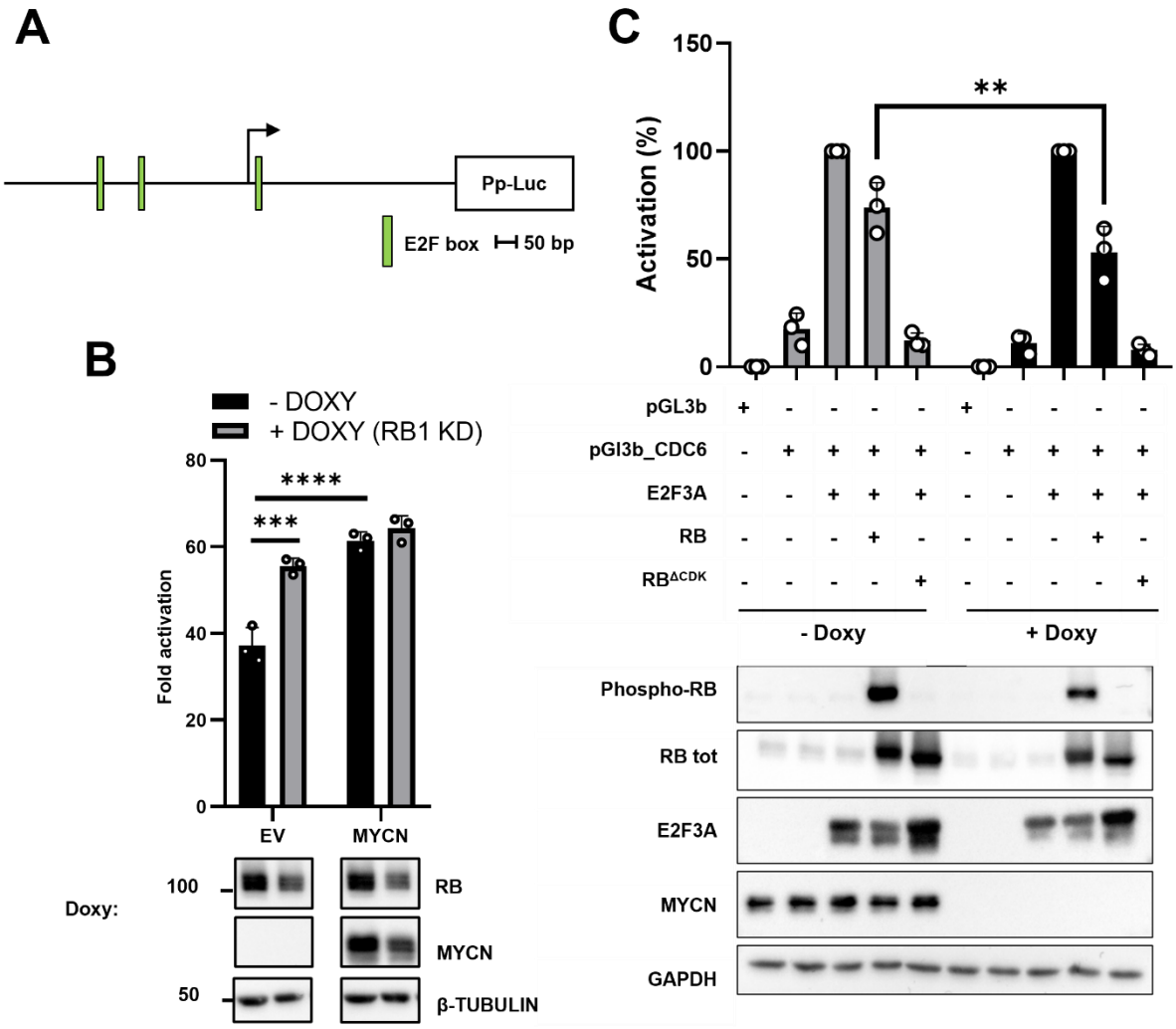

Fig. 10 MYCN overcomes RB function in SK-N-AS and TET21N cell lines. **(A)** Schematic illustration of the CDC6 regulatory region. E2F consensus boxes are highlighted in green. **(B)** Up: dual luciferase assay in SK-N-AS cKD RB1 cell line. Cells were incubated with or without doxycycline for 48 hours to induce RB1 downregulation, then were transfected with pGL3b, pGL3b_CDC6 + EV or pGL3b + MYCN. Constitutive promoter-driven Rr luciferase was used as internal control. Fold activation values represent Pp/Rr luciferase activity relative to the pGL3b alone condition. Down: western blot of the same cells transfected with the indicated construct. β-Tubulin was used as loading control **(C)** Up: dual luciferase assay in the TET21N cell line. Cells were incubated with or without doxycycline for 48 hours to induce MYCN downregulation, then were transfected as shown. Constitutive promoter-driven Rr luciferase was used as internal control. Activation (%) values represent Pp/Rr luciferase activity relative to pGL3b_CDC6 + E2F3A sample. Down: western blot of the same cells transfected as indicated. GAPDH was used as loading control. Luciferase experiments results were shown as an average of three (N=3) independent experiments ±SD. *, **, ***, **** indicated $P < 0.05$, 0.01, 0.001, and 0.0001, respectively. Statistical analyses were performed with Two-way ANOVA.

MYCN overcomes RB function by upregulating and downregulating CCNE1/2 and CDKN1A, respectively

Understanding how MYCN overcomes RB function might lead to new molecular targets for high-risk NB. Groundbreaking studies on MYC, the MYCN paralogue, shed light on its relevant role in cell cycle progression by upregulating cyclin genes and downregulating CDK inhibitors (García-Gutiérrez, Delgado, and León 2019; Ohtani, DeGregori, and Nevins 1995; Ohtsubo et al. 1995). However, little is known about the role of MYCN in this context, and further investigations are needed for NB.

In this scenario, we hypothesized that MYCN might abolish the RB1 function by indirectly modulating its phosphorylation status. Thus, we analyzed the expression correlation between MYCN and several genes involved in the Cyclin/CDK pathway during the G1/S transition in the NB patients' RNAseq database (Kocak et al. 2013). Interestingly, we found that cyclins E (CCNE1/2) positively correlate with MYCN expression in the context of the analyzed genes ($R=0.4023$ and 0.2497, respectively. $p<0.0001$). On the other hand, the CDKN1A gene encoding for Cyclin/CDK inhibitor p21 negatively correlates with MYCN ($R=-0.3195$, $p<0.0001$) **(Fig. 11A)**. This latter finding was consistent with previous results showing that MYCN directly represses CDKN1A expression in NB cells (Amente et al. 2015).

Thus, we hypothesized that RB phosphorylation status might be affected by MYCN presence by the aberrant upregulation of CCNE1/2 and downregulation of CDKN1A. For this purpose, we analyzed the phosphorylation status of RB in TET21 cells in the presence or absence of MYCN. Considering that in physiological conditions, RB is phosphorylated during the G1/S transition and remains in this state for the rest of the cell cycle, we also assayed the RB phosphorylation status in cells synchronized in the G1 phase by serum withdrawal. We decided to check the RB phosphorylation status by western blot using an antibody recognizing Thr 821 and Thr 826 dually phosphorylated, associated with its inactivated status (Rubin 2013; Sm et al. 2005). As shown in **Fig. 11B**, TET21 cells were correctly synchronized by 18 hours of serum starvation both in the presence and absence of doxycycline, and RB is phosphorylated only in the absence of doxycycline. However, the MYCN-dependent phosphorylation of RB is not evident in asynchronous cells (-FBS). Coherently with Pearson's correlation analysis, G1 synchronized cells showed a significant upregulation and downregulation of CCNE1/2 and CDKN1A, respectively **(Fig. 11C)**.

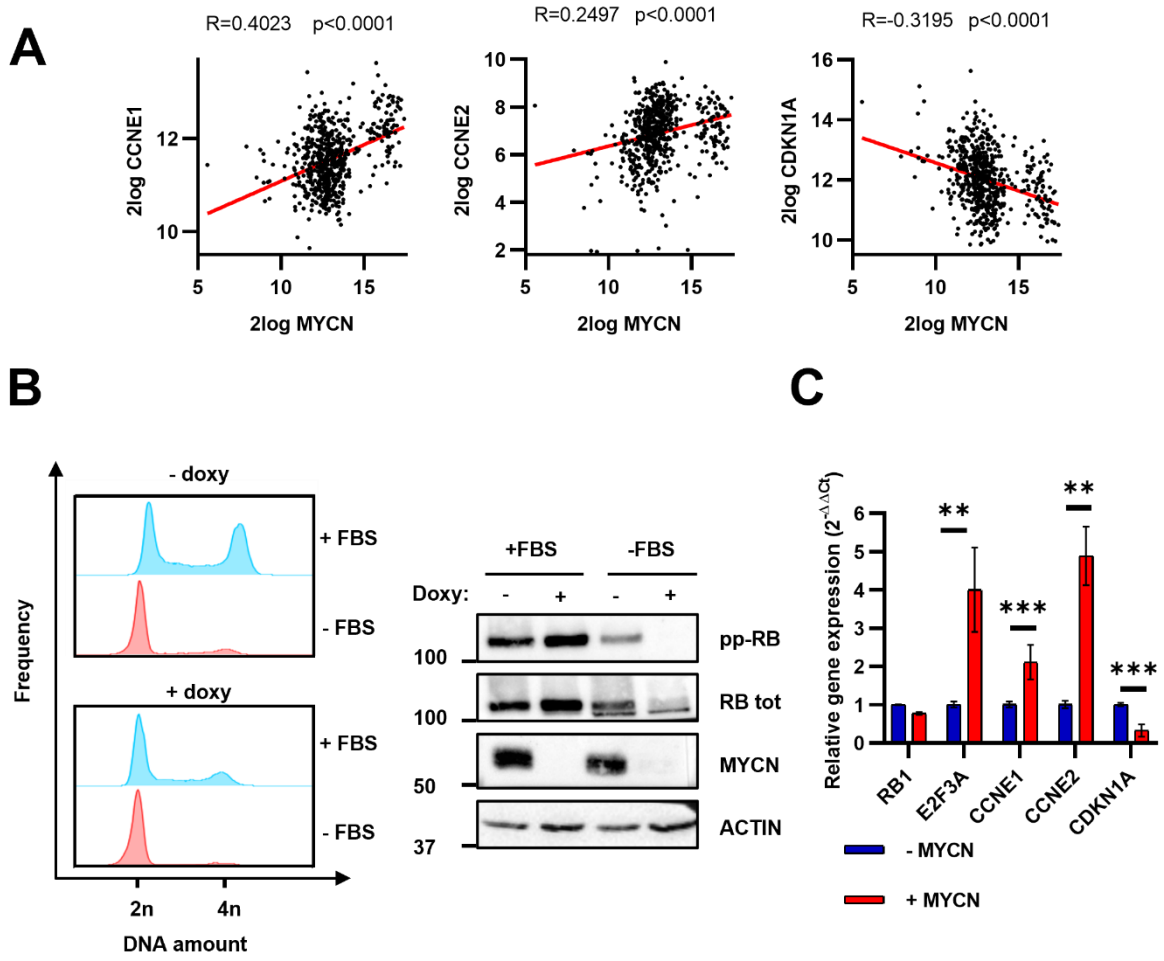

Fig. 11 MYCN induces RB phosphorylation in the G1 phase. **(A)** Pearson's correlation between MYCN and CCNE1/2 or CDKN1A in a cohort of 649 NB patients. The p-value by the Mann–Whitney test is indicated. **(B)** TET21 cells were incubated with 1µg/mL of doxycycline for 48 hours to induce MYCN KD and seeded at low density in the presence or absence of fetal bovine serum (FBS) for G1 synchronization. Left: After 18 hours, cells were harvested and stained with propidium iodide for cell cycle analysis in flow cytometry. 2n and 4n indicate the relative amount of DNA. Right: Western blot of TET21N cells treated as described. Results are representative of two (N=2) independent experiments **(C)** qRT-PCR on G1 synchronized TET21 cells in the presence (-MYCN) or absence (+MYCN) of doxycycline. Data were normalized using the TBP housekeeping gene. The experiment was performed in duplicate (N=3) and plotted with the respective standard deviations. Data are shown as the mean ± SD of two independent experiments. Statistical analyses were performed using Two-way ANOVA. Error bars represented SD. *, **, *** indicated P < 0.05, 0.01, 0.001, and 0.0001, respectively.

Endogenous RB replacement with RB$^{\Delta CDK}$ triggers proliferation arrest and differentiation in MYCN-amplified NB cell lines

To confirm the crucial role of MYCN in inducing RB phosphorylation and its subsequent inactivation leading to aggressive NB phenotype, we assessed the cell proliferation phenotype of MYCN-amplified cells where endogenous RB was replaced with its hyperactive mutant (RB$^{\Delta CDK}$). For this purpose, we engineered CHP-134 and KELLY cell lines to cKD RB1 by CRISPRi. Therefore, we transduced these cell lines with a third construct carrying the tetra-

cycline response element (TRE) upstream of RB^{wt} or $RB^{\Delta CDK}$. A third cell line was produced by transducing a construct containing only the TRE as control to study the cell behavior in the only absence of RB (EV) **(Fig.12A)**. With this approach, we were able to downregulate endogenous RB1 and upregulate exogenous RB^{wt} or $RB^{\Delta CDK}$ by adding doxycycline to the media. Next, we measured the cell growth for 72 hours by taking pictures every 2 hours by live imaging. Analyzing the growth curves, we observed that knocking down RB, as well as reintroducing it in its wild-type form, does not affect cell proliferation, consistent with the observation that RB is not functional in both cell lines carrying MYCN amplification. However, when we replaced endogenous RB with its ΔCDK mutant, we observed a drastic decrease in cell ratios (+doxy/-doxy) in 72 hours **(Fig. 12 B, C)**. Moreover, observing the microphotographs of the cells after 72hours from the addition of doxycycline, we noticed that CHP-134 $RB^{\Delta CDK}$ expressing cells showed a strongly neuronal-differentiated phenotype compared to the not treated control and the other experimental conditions **(Fig. 12D)**. However, despite the observed decrease in proliferation for KELLY $RB^{\Delta CDK}$ expressing cells, we were not able to see the same differentiated phenotype **(Fig. 12E)**.

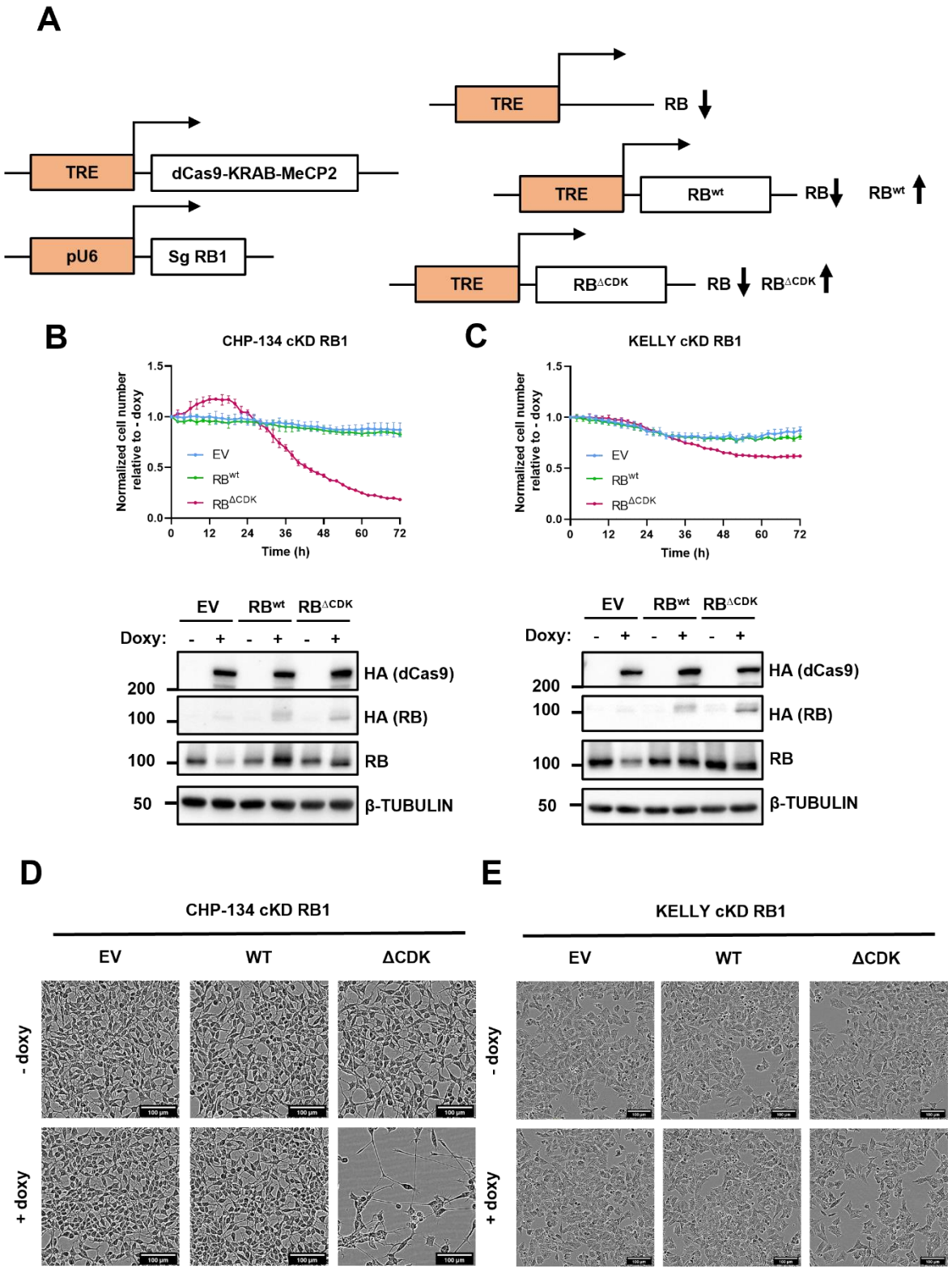

Fig. 12 Endogenous RB replacement with RBΔCDK induces a drastic effect on cell proliferation in MYCN-amplified cell lines. **(A)** Schematic illustration of the system. dCas9-KRAB-MeCP2 and $RB^{wt/\Delta CDK}$ are under the control of a tetracycline response element (TRE) responsive to the trans-activator rTtA. Constitutive pU6 promoter drives the expression of the sgRNA targeting the RB1 promoter (sgRNA RB1). In the presence of doxycycline RB1 is repressed, and exogenous $RB^{wt/\Delta CDK}$ is upregulated depending on the transduced construct. **(B, C)** Up: CHP-134 and KELLY cKD RB1 EV, WT or ΔCDK cell lines were seeded in 96 well in the presence or absence of doxycycline. Microphotography pictures were taken every two hours, and cells were counted by Incucyte2020C software. Results were plotted as the number of cells normalized on 0h of the +doxy sample divided by -doxy

sample (Normalized cell number relative to -doxy). Down: Western blot ensuring the proper working of the system. **(D, E)** Phase-contrast microphotographs of the cells employed for the assay after 72 hours from the doxycycline addition.

RB expression influences MYCN-amplified cell line sensitivity to CDK4/6 inhibitors

CDK4/6 inhibition is a widely used cancer therapy for breast cancer subtypes (Goel et al., 2018). To our knowledge, the only clinical trial performed for NB included a small patient cohort without any eligibility criteria regarding cytogenetic features of the tumor, leading to acceptable safety but unsatisfactory results in progression-free survival (B et al. 2017). However, previous preclinical results on a panel of NB cell lines treated with CDK4/6 inhibitor ribociclib, showed that MYCN-amplified cell lines were several magnitudes more susceptible to this drug compared to the MYCN-nonamplified cell line (Julieann Rader et al. 2013).

Given our results underlining the influence of MYCN on the RB inactivation promoting its phosphorylation, we speculated that this effect might depend on RB1 expression. To prove this hypothesis, we employed the CDK4/6 inhibitors palbociclib and ribociclib on CHP-134 and KELLY cell lines cKD for RB1, expecting to trigger their resistance by the downregulation of RB1. Thus, we treated these cell lines with ribociclib and palbociclib ranging from 15nM to 10μM concentrations, assessing the cell viability through MTS assay after 72h treatment in the presence or absence of doxycycline. Notably, CHP-134 acquired resistance to both ribociclib and palbociclib when RB1 is downregulated **(Fig. 13A)**. Moreover, the same resistant phenotype was observed performing the assay with Kelly cKD RB1 in the presence of doxycycline **(Fig. 13B)**.

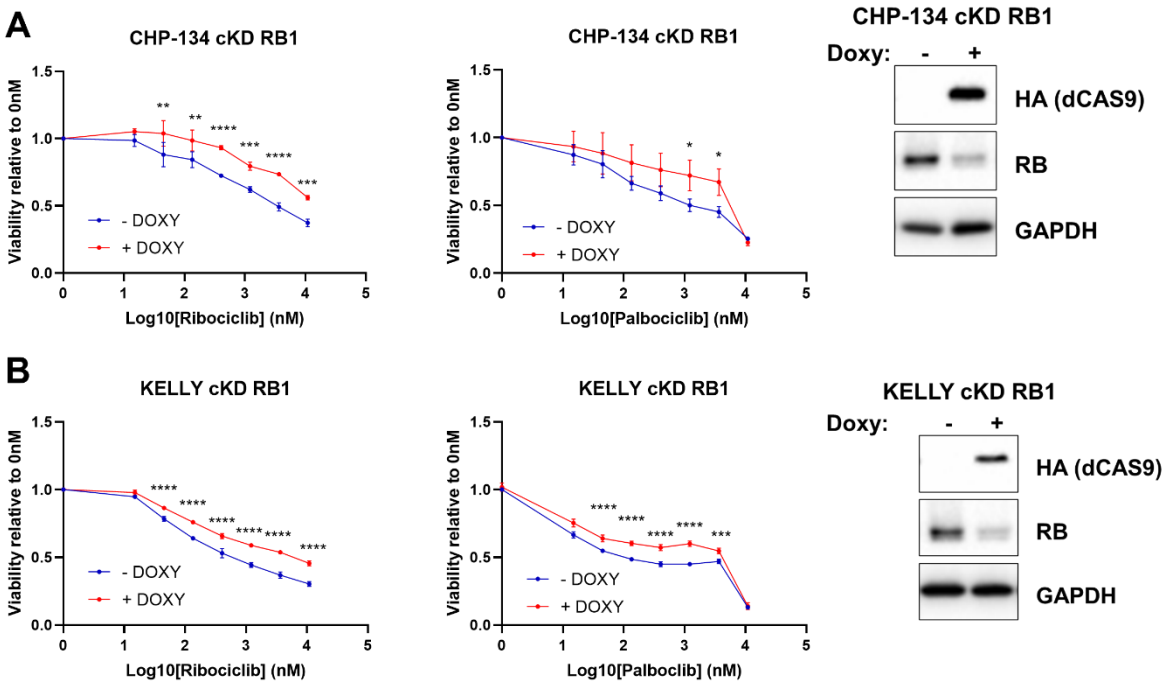

Fig. 13 RB1 downregulation induces resistance to CDK4/6 inhibitors ribociclib and palbociclib. CHP-124 and KELLY cKD RB1 cells were seeded at low confluence in 96-well plate and treated with ribociclib and palbociclib for 72 hours in the presence or absence of doxycycline. **(A)** Left: MTS results of CHP-134 cKD RB1. Right: western blot confirming the correct downregulation of RB1. **(B)** Left: MTS results of KELLY cKD RB1. Right: western blot confirming the correct downregulation of RB1. Data are plotted as absorbances normalized on the 0nM sample as averages of three (N=3) independent experiments. Statistical analysis was performed by Two-way ANOVA between -doxy and + doxy samples per each concentration. Error bars represented SD. *, **, ***, **** indicated P < 0.05, 0.01, 0.001, and 0.0001, respectively.

DISCUSSION (Part II)

Despite the recent advances in understanding NB biology and new insights into NB vulnerabilities, there is still a substantial unmet medical need for high-risk cases. According to international guidelines, high-risk patients are treated with a rigorous chemotherapy regimen of cisplatin, vincristine, carboplatin, etoposide, and cyclophosphamide (COJEC). When possible, resection surgery is performed with myeloablative therapy, hematopoietic stem cell reinfusion, and local radiation therapy (A. D. Pearson et al. 2008). However, where these medications are unsuccessful, the rapid development of precision and personalized medicine raises the opportunity to treat high-risk patients according to the molecular features of their tumors. The primary limit in following this approach is NB's extreme genetic and epigenetic heterogeneity, leading to an intricate matrix of possible approaches (Ciaccio et al. 2021).

This work aimed to shed light on how MYCN influences the proper working of the cell cycle machinery, particularly in the G1/S transition, to find molecular targets specific for MYCN-amplified NBs. MYCN amplification is a widely recognized negative prognostic factor for NB high-risk cases, leading to advanced tumor stage, high aggressiveness, and poor outcome (Matthay et al. 2016). We found that MYCN expression correlates with all the canonical E2F activators in a cohort of 649 NB patients and that patients expressing high levels of E2F3 showed a poorer prognosis compared to the low-expressing ones. Furthermore, we verified the crucial role of E2F3A isoform in maintaining the NB aggressive phenotype by selectively repressing its expression in the MYCN amplified cell line CHP-134 by CRISPRi. When E2F3 was knocked down, the colony formation ability was drastically decreased.

Next, given the ability of RB to repress E2F-mediated transcriptional activation, in the context of the patients showing high expression of E2F3, we compared the overall survival of the RB1 high-expressing patients with the low expressing ones, expecting a rescue in overall survival. Surprisingly, the comparison showed no significant differences between these two cohorts. These findings, together with previous insights showing that RB1 mutations are tendentially mutually exclusive with MYCN amplifications in retinoblastoma (Rushlow et al. 2013b), let us hypothesize that MYCN might overcome RB function leading to unconditional hyperactivity of E2F transcription factors. To prove that, we analyzed the activity of a well-known E2F responsive promoter perturbing RB1 expression by CRISPRi and forcing the expression of MYCN in the MYCN non-amplified cell line SK-N-AS. Our results showed that MYCN overexpression somewhat mimics the RB1 downregulation and that the downregulation of RB1 had no effect when MYCN was transfected. Moreover, by modulating MYCN

expression in the TET21N cell line, we observed a significant increase in RB repressing activity in the absence of MYCN, suggesting that MYCN negatively influences RB function, as hypothesized.

Next, we investigated the mechanism driving this phenomenon by analyzing the expression of G1/S transition genes as function of MYCN. Other researchers underlined the role of MYCN in the NB cell cycle, demonstrating that N-MYC influences cell proliferation by upregulating genes involved in G1/S phase progression, such as cyclin D2, E2Fs, CDK4/6, and CDC2 (Bell, Lunec, and Tweddle 2007; Caroline Bouchard et al. 2001; Woo et al. 2008). Cdk4/6-Cyclin D, and later in G1 Cdk2-CycE, are responsible for RB phosphorylation and its subsequent inactivation. In fact, at the end of the G1 phase, E2F proteins are fully activated and free to promote the expression of S genes and the progression of the cell cycle (Rubin 2013). In agreement with this extensive literature, we found that MYCN upregulates the activity of cyclin/CDK complexes by positively regulating the expression of cyclins E1/2 and negatively regulating the CDK inhibitor CDKN1A (p21). In addition, we found that this MYCN-driven effect is particularly efficient in cells artificially blocked in the G1 phase, leading to the aberrant phosphorylation of RB. Our results suggested that although RB1 is correctly expressed in its wild-type form, its function seems to be abrogated by MYCN expression. The dispensable role of RB in regulating cell proliferation in MYCN amplified cells is further sustained by the observation that the RB1 repression by CRISPRi in CHP-134 and KELLY cell lines did not substantially affect their growth curves. Additionally, the critical inactivation of RB by its phosphorylation came out when we replaced the expression of endogenous RB1 with its non-inactivable variant $RB^{\Delta CDK}$. Introducing this RB mutant, MYCN amplified cells showed a drastic decrease in cell proliferation, while reintroducing its wild-type form has no relevant effect on cell proliferation. Besides, CHP-134 cells showed a substantial increase in neurite length, which corresponded to a highly differentiated phenotype.

Thus, we wondered: how might RB1 function be rescued in RB1-expressing MYCN amplified cells? The most logical answer to this question is to compensate for the MYCN's positive effect on cyclin/CDK complexes by treating NB cells with cyclin/CDK inhibitors. Preclinical studies have already demonstrated the promising effects of CDK4/6 inhibitors on MYCN-amplified NB, without going deeper into the possible mechanisms behind this observation (Julieann Rader et al. 2013). In this work, we gave a possible explanation for this phenomenon, and we demonstrated that the effect of CDK inhibitors palbociclib and ribociclib is proportional to RB1 expression. Altogether, these findings encourage the employment of these

drugs in NB patients without any other therapeutical alternatives, expressing both high levels of MYCN and RB1.

RESULTS (Part III)

Retargeting M13 bacteriophage for drug delivery in GD2-expressing neuroblastoma

Characterization of GD2 expression in a panel of NB cell lines

Given the literature ambiguity for GD2 expression in NB cellular models, we analyzed a panel of NB cell lines for the expression of crucial genes encoding for enzymes involved in GD2 biosynthesis. The pathway for GD2 biosynthesis requires four enzymes, B4GALT6, ST3GAL5, ST8SIA1, and B4GALNT1, which converts GlcCer into LacCer, LacCer into GM3, GM3 into GD3 and GD3 into GD2, respectively. Among these enzymes, ST8SIA1 and B4GALNT1 are directly involved in catalyzing GD2 synthesis **(Fig. 14A)**.

According to RNAseq on the NB cell lines database provided by Maris et al. (Harenza et al. 2017), B4GALT6, ST3GAL5 and B4GALNT1 were expressed in all cell lines. However, the gene ST8SIA1, encoding for the enzyme involved in GM3 into GD2 conversion, was poorly expressed in SK-N-AS, SK-N-SH, and SK-N-BE (2)C compared with the other cell lines. These findings let us hypothesize that the latter cell lines could be GD2 negative ($GD2^-$). To test this hypothesis, we performed both GD2 immunofluorescence (IF) experiments to obtain a qualitative evaluation of GD2 expression. As expected, GD2 IF showed that LAN-5, CHP-134, IMR32, Kelly, and SH-SY5Y were $GD2^+$, while SK-N-AS, SK-N-SH, and BE(2)C were $GD2^-$ **(Fig. 14B)**.

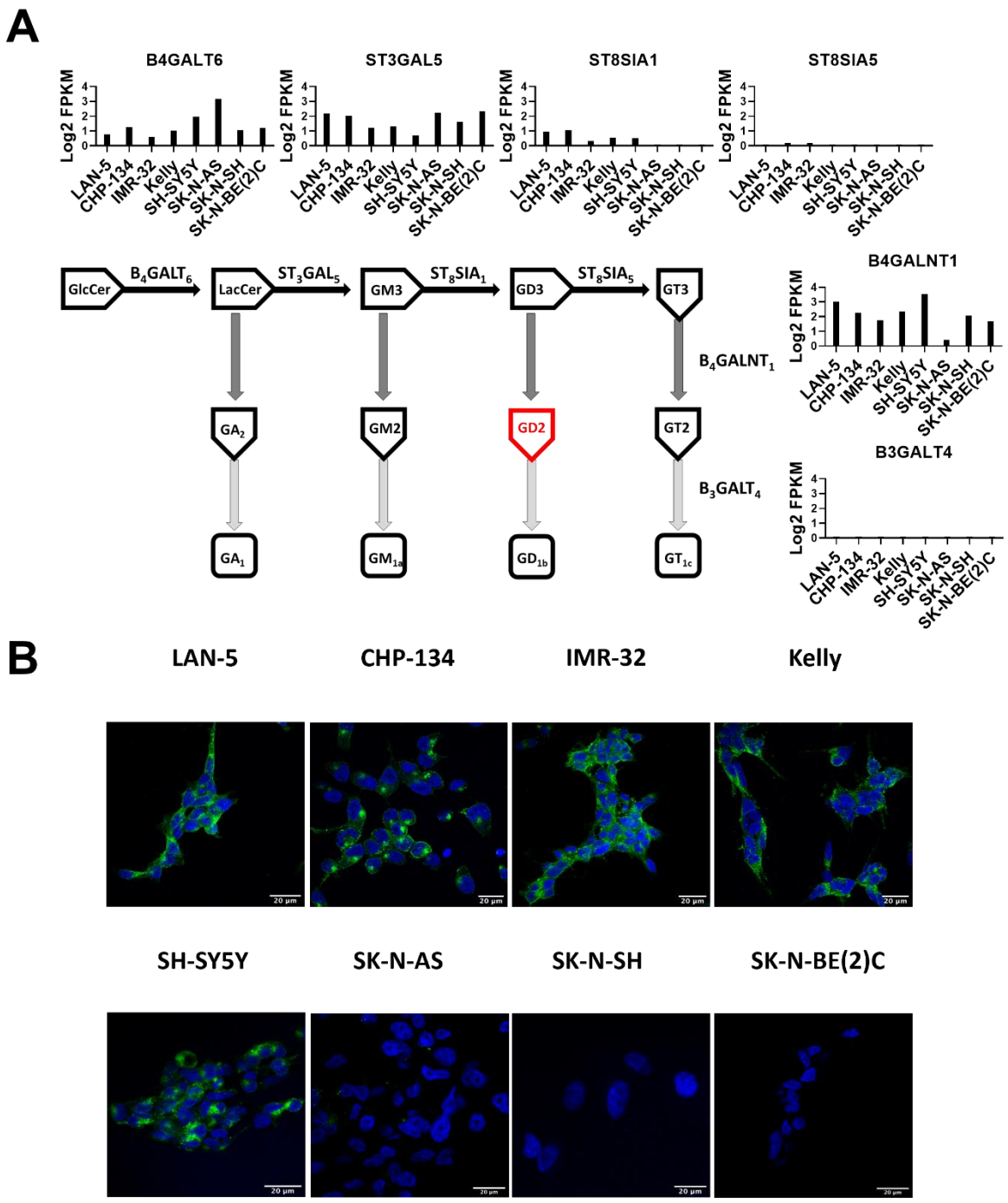

Fig. 14 Expression of GD2 in a panel of NB cell lines. **(A)** Expression analysis of the genes involved in GD2 biosynthesis, based on published available RNAseq database (Harenza et al. 2017). **(B)** IF for GD2 in eight NB cell lines.

$M13_{GD2}$ specifically binds to $GD2^+$ cells

To deliver M13 bacteriophages on $GD2^+$ cells, we genetically modified it by fusing the pIII protein to a single chain fragment variable (ScFv) anti-GD2 ($M13_{GD2}$). The sequence of the ScFv chosen for the M13GD2 production corresponds with the heavy and light chain's variable region of the 14.G2a antibody. We chose the 14.G2a antibody since it is an FDA-approved antibody that has been extensively used for GD2 targeting immunotherapy (Dhillon

2015). For M13GD2 production, we co-transformed the DH5α E. coli strain with two plasmids. First, M13ΔpIII helper: encoding all the minor and major structural proteins necessary for M13 bacteriophage assembly except pIII protein. Second, Phagmid: pIII-ScFv anti-GD2: encoding the pIII protein fused with ScFV retargeting GD2 **(Fig. 15A)**. The correct expression of the recombinant pIII protein fused with scFv was checked by western blot, observing a band of the expected molecular weight recognized by anti-M13 pIII antibody **(Fig.15B)**.

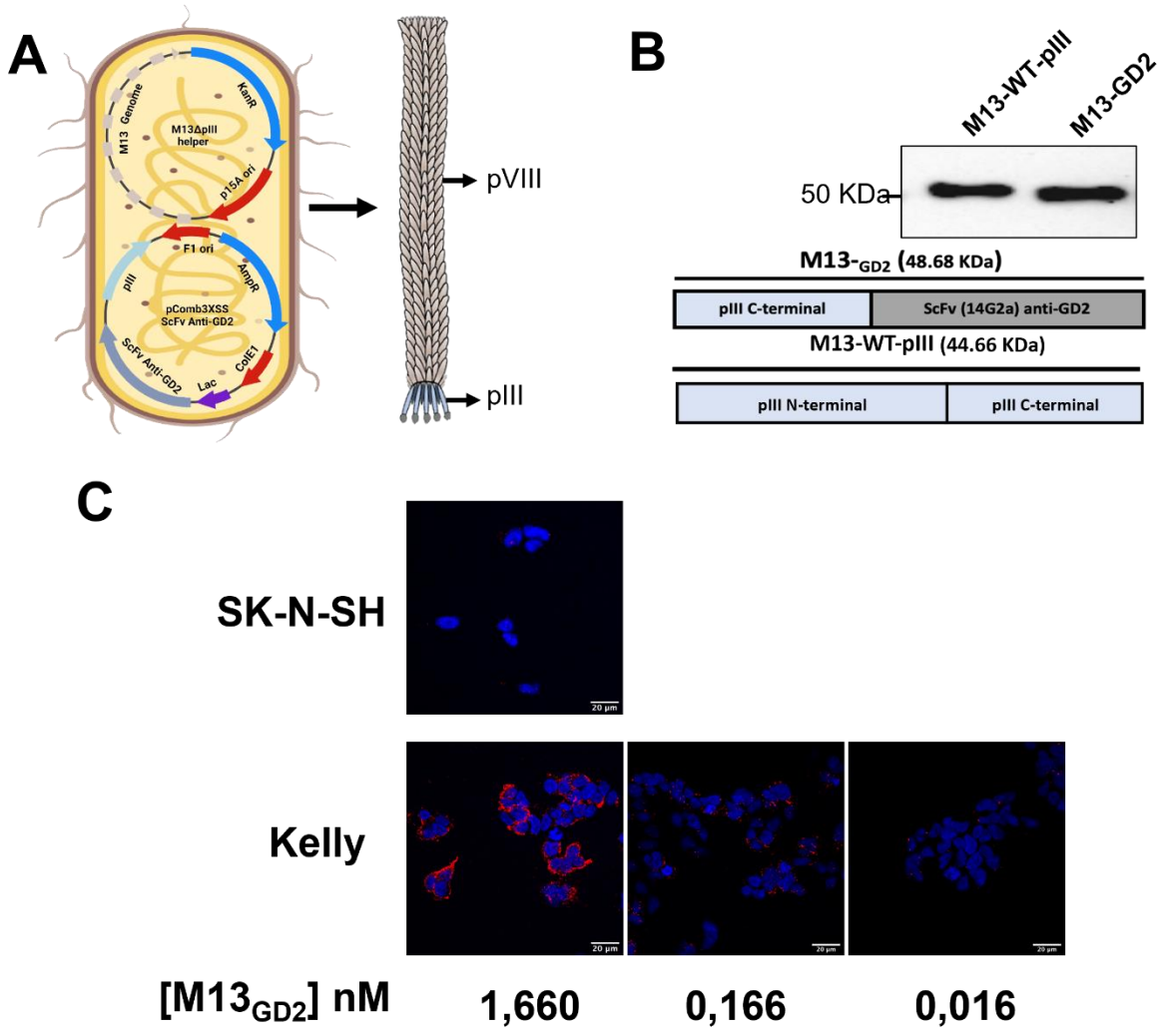

Fig. 15 $M13_{GD2}$ binds to $GD2^+$ cells selectively. **(A)** Schematic illustration of the M13 bacteriophage production **(B)** Western blot on the purified phages. Phages were produced as described in the material and methods section. Next phages were loaded in an acrylamide gel and blotted for the pIII protein. M13 wt phage was used as control. **(C)** IF staining for the pIII protein of SK-N-SH and Kelly cells. Cells were seeded at low confluence and incubated with indicated concentration of $M13_{GD2}$ phages. Unbound phages were washed away, then IF on phagic pIII protein was performed.

To determine the retargeting of $M13_{GD2}$ of NB cell lines, we incubated different concentrations (1.660 nM to 0.016 nM) of M13GD2 with $GD2^+$ cell line Kelly and $GD2^-$ cell line SK-N-SH and tracked the phage with anti-pVIII antibody in IF. Our results showed that $M13_{GD2}$ is bound to $GD2^+$ cells at all the tested concentrations. Strikingly, we also found that $M13_{GD2}$

bound only the $GD2^+$ cells with extreme specificity, whereas it does not bind to $GD2^-$ cells even with the highest concentration of the phage **(Fig. 15C)**. These results demonstrated that our $M13_{GD2}$ is a perfect platform for drug delivery on NB cells, potentially having no off-target effects on $GD2^-$ cells.

$M13_{GD2}$-ECB04 , selectively binds and induces $GD2^+$ cell death

Given the rising interest in photodynamic therapy (PDT) efficacy and the recently developed M13-associated PDT targeting $Her2^+$ cancers (Ulfo, Cantelli, et al. 2022), we decided to test $M13_{GD2}$ application in this context. For this reason, we chemically conjugated M13GD2 with the recently developed PS ECB04 ($M13_{GD2}$-ECB04) (Cantelli et al. 2021). After the chemical conjugation of M13GD2 with ECB04, we analyzed its UV-vis absorption spectrum to provide an accurate quantification for subsequent downstream experiments. As expected, the $M13_{GD2}$ absorption profile was drastically affected after the conjugation with ECB04 **(Fig. 16A)**.

The conjugation reaction involves **ε**-amino functionalization of M13GD2 proteins. This profound modification of M13GD2 molecules may lead to a loss of binding capacity to $GD2^+$ cell lines. To check the retargeting of M13GD2-ECB04 on NB cells, we performed an IF on cells treated with the engineered phages using an antibody against PVIII protein. The staining results indicated that $M13_{GD2}$-ECB04 firmly maintained its specificity for $GD2^+$ cells and no binding to GD^- cells **(Fig 16B)**. Once the $M13_{GD2}$-ECB04 targeting moiety was confirmed, we investigated the photodynamic activity of $M13_{GD2}$-ECB04 and its killing potential on the $GD2^+$ cell line Kelly and $GD2^-$ cell line SK-N-SH. We incubate the aforementioned cell lines with various concentrations of $M13_{GD2}$-ECB04 (nM: 1.6, 0.8, 0.4, 0.2, 0.1). After washing away the free phages, the cells were irradiated with white light, and controls were kept in the dark. The survival rate was measured after 24 hours by MTT assay. Significant cell death has been observed in irradiated cells in a dose-dependent manner, even with picomolar concentration of M13GD2-ECB04 compared with the dark condition. Remarkably, no killing has been observed in $GD2^-$ cells upon irradiation, even with the highest concentration of $M13_{GD2}$-ECB04 **(Fig. 16 C)**. Altogether, these findings demonstrated that $M13_{GD2}$-ECB04 is highly efficient in killing $GD2^+$ cells with extreme specificity.

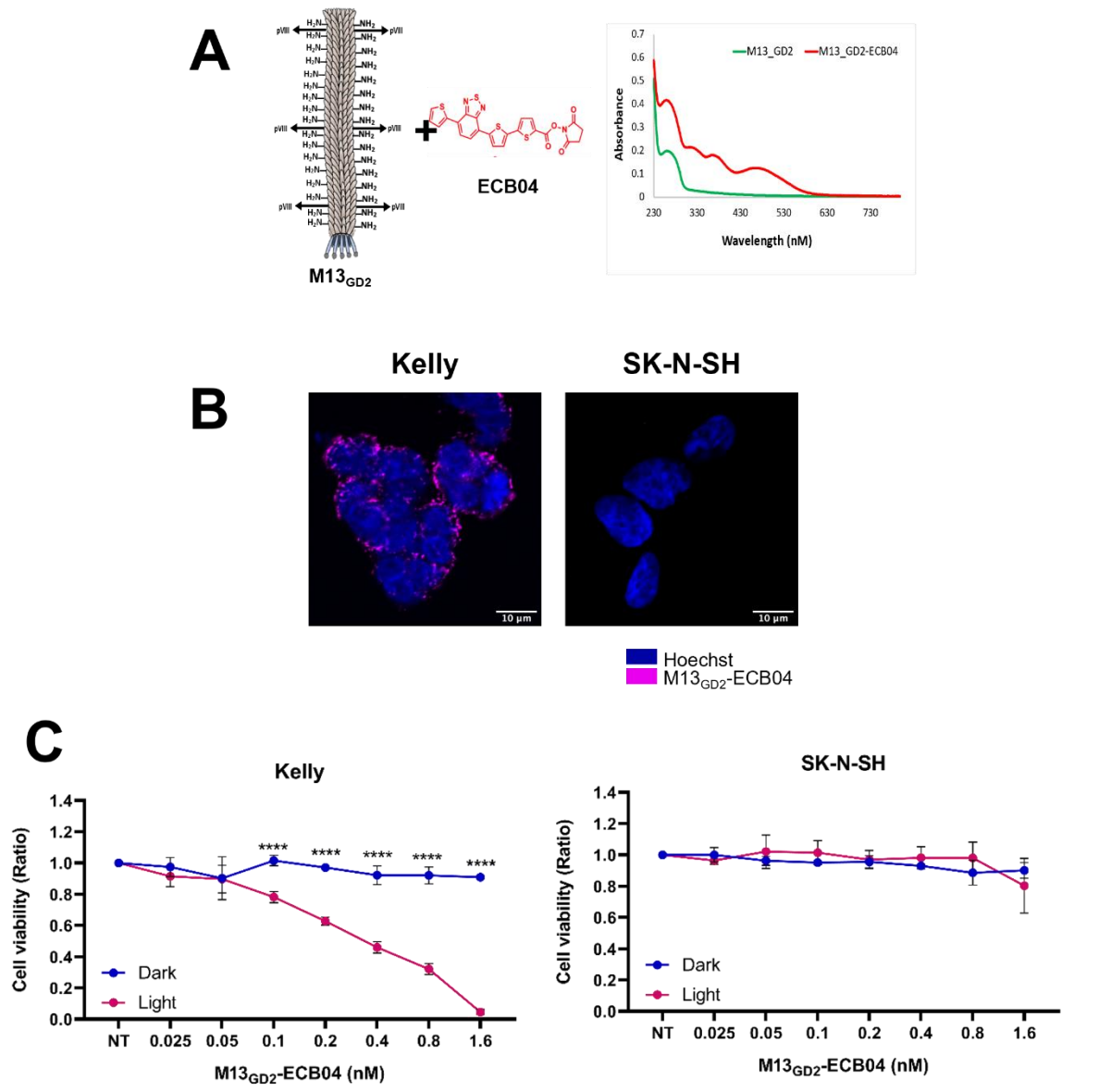

Fig. 16 $M13_{GD2}$-ECB04 phages selectively bind and kill $GD2^+$ cells. **(A)** Left: schematic illustration of the conjugation reaction. Right: Absorption spectrum of the nude phages (green) and conjugated phages (red). **(B)** IF staining for the pIII protein of SK-N-SH and Kelly cells. Cells were seeded at low confluence and incubated with $M13_{GD2}$-ECB04 phages (1.66 nM). Unbound phages were washed away, then IF on phagic pIII protein was performed. **(C)** Viability assay on cells treated with different concentrations of $M13_{GD2}$-ECB04 in the presence (red) or absence (blue) of light. Cells were seeded in 96-well and treated with the indicated concentration of $M13_{GD2}$-ECB04. Next, cells were exposed to light and were assayed for cell viability through MTT assay after 24 hours. Cell viability values are shown as absorbances normalized on the not treated (NT) sample of each condition. An average of three (N=3) independent experiments was plotted. Statistical analysis was performed by Two-way ANOVA, comparing the cell viability between light and dark samples per each concentration. Error bars represented SD. *, **, ***, **** indicated $P < 0.05$, 0.01, 0.001, and 0.0001, respectively.

DISCUSSION (Part III)

Gangliosides are carbohydrate-containing sphingolipids expressed by a wide range of tumors. However, since they are ubiquitously expressed in both tumoral and healthy cells, they are generally not considered a strategic target for tumoral therapy (Krengel and Bousquet 2014). On the other hand, the disialoganglioside GD2 shows unique features in terms of tumoral expression specificity, and it is widely considered a tumor-associated antigen (Cheever et al. 2009). Indeed, GD2 is typically expressed only on the cell surface of fetal tissues and can be barely detected in adult tissues. GD2 is expressed in the developing brains, particularly in the cerebellum as well as peripheral nerve cells (Lammie et al. 1993). Several tumors express GD2 on their cell membranes, such as NB, small cells lung cancer, Ewing sarcoma, melanoma, osteosarcoma, and breast cancer (Nazha, Inal, and Owonikoko 2020). However, GD2 expression is not a hallmark of all NBs. Thus, to study the effectiveness of anti-GD2 therapies in vitro, there is a profound need to characterize NB cellular models showing this feature.

Firstly, our findings shed light on the expression of GD2 in a group of eight NB cell lines. By doing so, we analyzed data on the expression of genes encoding enzymes involved in the GD2 pathway biosynthesis and performed IF for GD2. Among the cell lines tested, we found that LAN-5, CHP-134, IMR32, Kelly, and SH-SY5Y were $GD2^{+}$, while SK-N-AS, SK-N-SH, and BE(2)C were $GD2^{-}$. This finding was coherent with the gene expression analysis showing that the last three cell lines lack the expression of ST8SIA1, crucial for the biosynthesis of the GD2 precursor, GD3.

Currently approved therapies for GD2-expressing tumors consist of administering a combination of the humanized anti-GD2 14.G2a (dinutuximab) antibodies and the immune-response stimulators granulocyte-macrophage colony-stimulating factor (GM-CSF), interleukin (IL-2), and retinoic acid (RA) (Dhillon 2015). The anti-neoplastic activity of dinutuximab is driven by its cooperation with natural killer (NK) cells. Indeed, NK cells kill antibody-bound NB cells via antibody-dependent cellular cytotoxicity (ADCC). However, this immune system-related response could be circumvented by several mechanisms (reviewed in Keyel and Reynolds, 2018). Thus, several strategies for targeting GD2 with host immune system-independent mechanisms were developed, such as anti-GD2 CAR-T cells and the conjugation of dinutuximab with anti-cancer drugs. However, given their ability to cross the blood-brain barrier, CAR-T had considerable side effects in preclinical rodent models, and antibody conjugation with anti-cancer drugs leads to only ~ 4 molecules/antibody (Richman et al. 2018; Kalinovsky et al. 2022). Compared with antibody production, M13 phage production in bacte-

ria is an attractive non-expensive alternative for drug delivery to cancer cells (Klutz et al. 2016; Torres-Acosta et al. 2020). Additionally, the M13 bacteriophage dimensions allow the conjugation of hundreds of molecules per particle, drastically increasing the local concentration of the drug. Thus, we correctly engineered the M13 filamentous phage to express the ScFv 14.G2a against GD2 as a fusion protein with the pIII. Our data demonstrated that the $M13_{GD2}$ phage binds specifically to $GD2^+$ cells and that this specificity was not lost even after the conjugation with the PS ECB04. Regarding its carrying capability, our results showed that our phage platform could carry an average of ~ 450 molecules without impairing its retargeting specificity. Our phage-based drug delivery platform was correctly validated by incubating $M13_{GD2}$-ECB04 with a $GD2^+$ and a $GD2^-$ cell lines, showing specificity in killing in a dose-dependent manner. Although M13 bacteriophage can cross the blood-brain barrier (Staquicini et al., 2020), potential side-effects might be overcome by the dual spatial specificity of our proposed approach. Indeed, our results demonstrated that the selective killing of $GD2^+$ cells elicited by $M13_{GD2}$-ECB04 is also light-dependent: no killing in cells kept in the dark was observed.

Overall, we developed a promising anti-NB therapy with high killing activity and specificity. However, further in vivo studies are needed to demonstrate its feasibility in clinical application.

THESIS CONCLUSIONS

Neuroblastoma is a neoplastic disease associated with poor survival in infants and children. Despite the recent advances in understanding the molecular mechanisms driving its onset, progression, and resistance to classical therapies, a consistent percentage of patients are still receiving non-resolutive treatment. This work provided data about i) the role of an essential gene involved in MYCN-driven NB onset; ii) the involvement of MYCN in the dysregulation of the NB cell cycle iii) the generation of a new potential biotechnological drug capable of selectively targeting NB cells.

Our results showed that RUNX1T1 is an essential gene involved in MYCN-driven NB's onset. RUNX1T1 exerts its function by interacting with the transcription factor HAND2 and recruiting the proteins belonging to the Co-REST complex at its target genes. Moreover, we mapped the interaction with the proteins of the Co-REST complex, providing structural insights into the surface of interaction between RUNX1T1 and RCOR3. This latter interaction might be necessary for NB onset and could be targeted by specific molecules in the future.

By studying the MYCN/RB1/E2F axis in NB, we found that E2F3 is an essential gene regulating colony formation and that N-MYC overcomes the physiological function of RB to inhibit E2F-driven transcriptional activation. During the G1 phase, MYCN overexpression drives the upregulation and the downregulation of Cyclin E1/2 and CDKN1A, respectively. These events lead to the hyperphosphorylation of RB. Coherently, its replacement with a non-phosphorylatable mutant drastically decreases cell proliferation, inducing differentiation in MYCN-amplified NB cell lines. The employment of CDK inhibitors in MYCN amplified NB has only begun to be explored, and the data presented in this thesis provided the rationale for their administration to patients carrying MYCN-amplified tumors expressing relatively high levels of RB1. In fact, the downregulation of RB1 increases the resistance of NB cells to these drugs.

Lastly, we designed a new phagic platform to deliver photosensitizers to NB cells expressing the disialoganglioside GD2. By fusing the ScFv generated from the FDA- and EMA-approved dinutuximab to the phagic pIII protein, we obtained an M13 phage binding selectively to $GD2^+$ cells. It is known that immune system inefficacy drives NB resistance to standard immunotherapies in a large cohort of patients, and this new tool might be helpful in circumventing this issue.

MATERIALS AND METHODS

Cell culture

Neuroblastoma SK-N-BE(2)C, LAN5, IMR32, SH-SY5Y, SK-N-AS, TE21/N and HEK-293T cells were cultured in Dulbecco's modified Eagle's medium (DMEM) supplied with 10% FBS and 2 mM of glutamine and antibiotics (penicillin, 100 U/ml; streptomycin, 100 μg/ml). Kelly, CHP-134, and SK-N-SH cells were cultured in Roswell Park Memorial Institute Medium (RPMI) 1640 supplemented with 10% FBS and 1% L-glutamine and 2 mM of glutamine and antibiotics (penicillin, 100 U/ml; streptomycin, 100 μg/ml). All cell lines were cultured in a humidified incubator Mycoplasma-free at 37 °C and 5% CO2. TET21/N, and RB1 or E2F3A cKD cells were treated with doxycycline from Sigma-Aldrich (final concentration: 1 μg/mL) for the indicated time reported in the results paragraph.

Plasmids

Relative to Results (Part I):

RUNX1T1 was amplified from mouse cDNA using RUNX1T1_Fw: TTTAAGCTT-GCGGCCGCAATATCTGTCA and RUNX1T1_Rv: ACGACGCCTCGCTAGTTTCTAGA, digested with NotI – XbaI and cloned into the pCM10 plasmid (Sigma Aldrich). RUNX1T1 and RCOR3 mutants plasmid were generated by whole-plasmid PCR on the pCMV10_RUNX1T1 plasmid using the following divergent primers:

RUNX1T1mut_FW: 5'-CACTGTGGCTCTTTTTGCCAGCAT-3'

RUNX1T1mut_RV: 5'-CGGCTGTAACACGGCCCGA-3'

ΔNHR1_FW: 5'-CAGCTGCTTCTGGATGCCA-3'

ΔNHR1_RV: 5'-ACCACAGGCTGGGGGC-3'

ΔNHR2_FW: 5'-GCGGACCGGGAAGAACTG-3'

ΔNHR2_RV:5'-ACGTGTGCCATGTAACCCC-3'

ΔNHR3_FW: 5'-GCGAAGAGGCAGGCAGCAGAAGATGC-3'

ΔNHR3_RV: 5'-CGGCACGTATCCAGACGCAGGCCTG-3'

ΔNHR4_FW: 5'-ATCTGTGGACAGACCCTGCAG-3'

ΔNHR4_RV: 5'-CTGCTGGTTGATGACTGCTAGAG-3'

Δ2_RCOR3_RV: 5'-CTGGTTCAGAGTGGCAATAGGGG-3'

Δ1/2_RCOR3_FW: 5'-CGCCCTGCTAATTCCATGCCA-3'

Δ1_RCOR3_RV: 5'-AGGCTGATTTAAAGTTGGCCGGG-3'

PCR products were thus ligated using T4-DNA ligase (NEB) and transformed in DH5α E. Coli strains (NEB).

Relative to Results (Part II):

For the generation of the constructs encoding the sgRNA, two complementary oligonucleotides were annealed, phosphorylated, and cloned into the pLenti-sgRNA plasmid. The sequences used are reported below:

RB1sg1_fw: caccgCTGAGCGCCGCGTCCAACCG

RB1sg1_Rv: aaacCGGTTGGACGCGGCGCTCAGc

sg_scrambled_Fw: caccgGCTTAGTTACGCGTGGACGA

sg_scrambled_Rv: aaacTCGTCCACGCGTAACTAAGCc

E2F3Asg1_Fw: caccgGAAATCCGAGTTTCGCGGGG

E2F3Asg1_Rv: aaacCCCGCGAAACTCGGATTTCc

For the generation of the TET-ON stable cell line expressing RB^{wt} or $RB^{\Delta CDK}$, the sequences to clone were amplified from pCMV HA hRB-wt and pCMV HA hRb delta CDK using the following primers: BamHI_Rb_Fw: CGAGGATCCATGTACCCATACGATGTTCCA; and NotI_Rb_Rv: CCCGCGGCCGCGGTACCTCATTTC. Then, the PCR product was digested using BamHI and NotI and cloned into the pLVX-TRE3G (Takara Bio, Cat n. 631193) plasmid in which the puromycine resistance cassette was replaced with a Geneticine resistant cassette.

pCMV HA hRb delta CDK was a gift from Steven Dowdy (Addgene plasmid # 58906 ; http://n2t.net/addgene:58906 ; RRID:Addgene_58906). pCMV HA hRB-wt was a gift from Steven Dowdy (Addgene plasmid # 58905 ; http://n2t.net/addgene:58905 ; RRID:Addgene_58905). PB-TRE-dCas9-KRAB-MeCP2 was a gift from Andrea Califano (Addgene plasmid # 122267 ; http://n2t.net/addgene:122267 ; RRID:Addgene_122267). pLenti-sgRNA was a gift from Eric Lander & David Sabatini (Addgene plasmid # 71409 ; http://n2t.net/addgene:71409 ; RRID:Addgene_71409).

Relative to Results (Part III):

Optimized sequence for E. Coli expression encoding for the ScFv of the 14.G2a antibody (Horwacik et al. 2015) was generated with NovoPro tool (https://www.novoprolabs.com/tools/codon-optimization) and synthesized by Doulix Srl. The sequence was amplified using 14.G2a_Fw: GTTTTTGAGCTCGAAGTTCAGCTGC and 14.G2a_Rv: GTTTTTACTAGTTTTCAGTTCCAGTTTAGTACC primers by PCR. The PCR product was cloned in pCOMB plasmid (Ulfo, Cantelli, et al. 2022) using NcoI / BamHI restriction enzymes.

All the plasmids were sequenced by Sanger method before proceeding with the experiments.

Lentiviral production and transduction

Relative to Results (Part II):

Lentiviruses for sgRNA were produced in HEK-293 packaging cells by co-transfection of pLenti-sgRNA (Addgene plasmid #71409) and helper plasmids psPAX2 (Addgene plasmid #12260) and pMD2.G (Addgene plasmid #12259) After 72 h, viral media were collected and used to transduce P.B. TRE dCas9-KRAB MeCP2 cell lines with a MOI of 0.5. The transduction agent used was Polybrene (Santa Cruz Biotechnology) as 10.000X. Positive cells were selected with Puromycin (Sigma-Aldrich) at 1 µg/mL for 7 days. The same protocol was used to produce stable cell lines for pLVX-TRE3G (Takara Bio) constructs (EV, RB^{wt}, $RB^{\Delta CDK}$). After transduction, positive cells were selected with Geneticin (Gibco) 800 µg/mL until complete death was observed in a non-transduced control plate.

Stable cell lines generation

Relative to Results (Part II):

For the generation of the stable cell lines expressing doxycycline-inducible dCas9-KRAB-MeCP2, we transfected CHP-134, Kelly and SK-N-AS cell lines with 0.4µg PB-TRE-dCas9-KRAB-MeCP2 plasmid together with 80 ng of the Super PiggyBac Transposase Expression Vector (SBI, cat. PB210PA-1) using Effectene (Qiagen) as transfection agent in a 10mm dish. Next, we transduced lentivirus generated with pLENTI-sgRNA plasmid with a MOI of 0.5. Cells were selected with puromycin (Thermofisher) at 1µg/mL, Hygromycyne (Thermofisher) at 600 µg/mL. For the growth curve experiment, Kelly and CHP-134 cKD RB1 cells were

transduced with pLVX_G418_RB$^{wt/\Delta CDK}$ and selected with G418 (Thermofisher) at 800 µg/mL.

Transfections

Relative to Results (Part I):

The HEK-293T and SK-N-BE (2) C cell lines were transfected with the agent polyethyleneimine (PEI). Cells were grown in a 10 cm diameter Petri dish until a confluence of about 70% was reached (transfection point). The next day, two solutions were prepared for each transfection point, in which the first (DNA mix) contained 18 µg of plasmid DNA in 300 µL of 150mM NaCl and the second (PEI mix) contained 5.4 µL of PEI (0.3 µL of PEI per 1µg of DNA) in 300µl of 150mM NaCl. The solutions were incubated for 15 minutes at room temperature. Subsequently, the solutions were combined in a single tube and incubated for another 30 ’at room temperature (transfection mix). The transfection mix was then brought to a volume of 5 mL with DMEM medium with L-glutamine to complete the transfection medium. The cells, previously washed with PBS, were treated with the transfection medium and incubated for 4 hours. At the end of the incubation, the transfection medium was removed, and complete culture medium was added.

Relative to Results (Part II):

SK-N-AS and TET21N were transfected with an equimolar ratio of the indicated plasmids with Lipofectamine 3000 reagent (Thermofisher) I a 24-well plate following manufacturer instructions. pCMV10 EV was used to reach 1.5 µg of total plasmid per each transfection.

Co-IP

Relative to Results (Part I):

Three million HEK-293T cells were transfected with the indicated plasmids in equimolar ratio. 24h after transfection, the cells were scraped and collected in tubes for nuclei isolation. Samples were incubated with 500 µL of hypotonic buffer (HEPES 10 mM, NaCl 50mM, sodium pyrophosphate 1 mM, sodium orthovanadate 1 mM, sodium fluoride 1 mM) supplied with Phenylmethanesulfonyl fluoride (Sigma) and Complete protease inhibitor (Roche) for 15 minutes at 4°C and next, NP40 was added up to 0,2% w/v final concentration and incubated for 15 minutes. Nuclear pellets were obtained through 10 minutes centrifugation at 750g and,

lysed in 100 µL of TNT buffer (Tris HCl pH 8.00 50 mM, NaCl 250 mM, sodium pyrophosphate 1 mM, sodium orthovanadate 1 mM, sodium fluoride 1 mM, Triton 1% w/v) supplied with Phenylmethanesulfonyl fluoride (Sigma Aldrich) and Complete protease inhibitor (Roche) for 30 minutes. Nuclear lysates were centrifugated at 20000g for 20 minutes to discard insoluble material, and supernatants (nuclear protein fractions) were collected and quantified with BCA method (Thermofisher) following manufactural instructions. Next, 220 µg (1µg/µL) of lysate was added to 450µg of dried pre-equilibrated Dynabeads protein G (Thermo Fisher Scientific) for 1h pre-clearing in rotation at 4°C. 20 µL of pre-cleared lysate was collected as INPUT sample and the remaining 200µL were incubated with 1.5 µg of Anti-flag antibody (#F3165 Sigma) for 1h immunoprecipitation at 4°C in rotation. Samples were added to 450µg of dried pre-equilibrated Dynabeads protein G and were incubated in rotation at 4°C for 1h for pull-down. The beads were washed 5 times in 200µL TNT buffer, eluted in 1xNuPAGE buffer (Thermo) 70°C for 10 min and stored at –80°C until immunoblot analysis.

LC-MS/MS

Relative to Results (Part I):

The co-immunoprecipitated proteins were incubated with four volumes of acetone overnight at -20 ° C for precipitation. The protein pellet was washed with 1 mL of acetone at -20 ° C. The sample was centrifuged and resuspended in 30µl of MS resuspension solution (6 M urea, 100 mM ammonium bicarbonate). 3 µL reduction solution (ammonium bicarbonate 10 mM; DTT 0.15 mg / mL) were subsequently added for incubation at 56 ° C for 30 min. At the end of the incubation, 1 µL of MS alkylation solution (Iodoacetamide 5.5 mM; ammonium bicarbonate 10 mM) was added to the samples for further incubation of 20 min in darkness. 0.6 µL of inactivation solution (DTT 50 mM; ammonium bicarbonate 10 mM) was added to the sample. The sample was brought to 500 µL with 10mM AmBiC to dilute the urea to a final concentration of 0.36 M and left to pass through a 3K column previously washed with 400 µL of H2O. The sample was centrifuged for 10,000 g for 20 min until reaching a volume of about 250 µL. 250 µL of 10 mM AmBiC were added in order to bring the urea to a final concentration of about 0.24 M. The sample was centrifuged at 10000 g for 45 min to obtain a protein sample of about 30-50 µL. The concentrated proteins were collected in a new tube and added with 3 µL of trypsin (Sigma-Aldrich) [0.4 µg / µL] and incubated at 37 ° C for 20h. 1/10 of the volume of 5% formic acid was added to the trypsinized proteins, and the proteins were lyophilized in SpeedVAC set to Dry-rate MEDIUM. The samples thus prepared were sent to the Interdepartmental Center for Large Instruments (C.I.G.S) of the University of Modena e Reg-

gio Emilia, which performed the LC-MS / MS mass spectrometry analyses providing a list of identified peptides.

Dual-step ChIP

Relative to Results (Part I):

20 million cells were harvested and resuspended in PBS at a concentration of 1 million cells/ mL. Thus, disuccinimidyl glutarate (DSG, SantaCruz Biotechnologies) was added to reach 2mM final concentration starting from a freshly prepared 500mM stock in DMSO. Samples were incubated at RT for 45 min, protected from light. Cells were washed three times in PBS, formaldehyde was added to a final concentration of 1% and incubated 10 min at RT on a wheel. To stop the cross-linking reaction, 0.5 mL of 2.5 M Glycine was added and the samples were incubated 5 min at RT on wheel at 12 rpm. Thus, samples were centrifuged 5 min at 1500rpm (350 x g) at 4 ° C and the pellet was washed three times in 10 mL of ice-cold PBS. Next, the pellet was resuspended in 500 µl of ice-cold Cell Lysis Buffer for nuclei release (Pipes pH8 5mM, KCl 85mM, NP40 0.5%, PMSF 1mM, Complete 1X, MilliQ Water) and kept in ice for 10 min. Afterwards, the samples were centrifuged at 1700 g for 10min at 4 ° C, the supernatant was discarded and 200 µl of RIPA Sonic-Buffer (NaCl 150mM, NP40 1%, PMSF 1mM, Complete 1X, SDS 0.5%, Tris HCl 50mM, MilliQ Water) was added for a further incubation of 20 min. Nuclei were sonicated with 5X 10 cycles: 30 'ON - 45' OFF; High Power. Add Ripa sonic buffer without SDS was added to each sample to bring SDS to a final concentration of 0.18%, and BSA-coated protein Aor G sepharose beads (Thermofisher) were added for 30 min pre-clearing. 1/10 of the sample was kept as input. The pre-cleared lysate was incubated with 2 to 10 µg of antibody to each sample overnight. At this step, we used the following antibodies depending on the target protein: RUNX1T1 (Cat. No. C15310197 diagenode); LSD1 (C15410067 diagenode); Anti-CoREST3 / RCOR3 antibody (ab76921 Abcam); HA-Tag (C29F4) Rabbit mAb#3724 - Cell Signaling Technology. The next day, 40 µl of coated beads were added to the complexes and incubated in constant rotation for 1 hour at RT. Next, complexes were washed five times with RIPA buffer; once with LiCl Wash Buffer (NaDoc 1%, NP40 1%, 500mM LiCl, 100mM Tris HCl, MilliQ Water.); and twice with TE buffer. Beads were resuspended in 70µL of TE buffer plus 10 µl (10µg/µL) of RNAse A (Sigma-Aldrich). reaction was incubated for 45 'at 37. DNA was released in the solution by adding 20 µL of Proteinase K Buffer 5X and 6µL of Proteinase K (19 mg / mL) and by incubating overnight at 65 ° C. The purified DNA was extracted by adding 1 volume of a Phenol / Chloroform method.

ChIPseq analysis

Relative to Results (Part I):

ChIP-seq samples were sequenced using the NextSeq 500 platform, with reads 75bp single-end and encoded in FASTQ files. The quality of the files was evaluated using the FASTQC program, which did not reveal problems related to duplication of reads, presence of Illumina adapters within the reads, over-representation of sequences at 5'. The alignment was performed using Human_hg38 as the reference genome using Hisat2 software (https://www.ncbi.nlm.nih.gov/pmc/articles/PMC4655817/). The alignment allowed to convert FASTQ files into BAM aligned on the hg38 genome. Identification of the ChIP peaks for each factor was conducted using MACS software (https://genomebiology.biomedcentral.com/articles/10.1186/gb-2008-9-9-r137), comparing the ChIP signals with those of the "Input" sample. These files have been encoded in the BED format, and the location with respect to the TSS of each peak and its distance, expressed in kb, was analyzed through the ChIPpeakAnno pipeline on R software (https://bmcbioinformatics.biomedcentral.com/articles/10.1186/1471-2105-11-237). These analyzes were conducted in collaboration with Prof. Federico Giorgi.

Peak intersection was performed by the BedSect tool (https://imgsb.org/bedsect/). 50bp overlapping was considered as a co-peak. GO was performed by GREAT (http://great.stanford.edu/public/html/) using as input data the BED file relating to the intersection of the genomic regions considered.

Colony formation assay

Relative to Results (Part II):

CHP-134 cKD E2F3A cells or scrambled were seeded in 6-well plates at a concentration of 500 cells/well and later treated with DMSO (vehicle treatment control) or Doxycycline (0.2 µg/ml). After ten days, colonies were washed twice with PBS, fixed and stained with crystal violet solution (0.5% crystal violet, 50% methanol) for 30 min, washed with water and let dry for three days. Pictures of the wells were taken via the ChemiDoc MP system (BioRad). The total number of colonies was determined using ImageJ software. Colonies smaller than 50 cells were excluded from the analysis. Three replicates of the experiment were performed.

Gene reporter assays

Relative to Results (Part II):

Luciferase reporter activity was measured using the Dual Luciferase Assay System (Promega, E1980). Chemiluminescence values for Firefly (Photinus pyralis, Pp) and Renilla (Renilla reniformis, Rr) luciferases were measured using a GloMax 20/20 instrument (Promega).

TET21N and SK-N-AS RB1 cKD were treated for 48 h with 1µg/mL doxycycline. 50.000 TET21N and 100.000 SK-N-AS were seeded in a 24-well plate, both – and + doxycycline. The following day the cells were transfected in duplicate through Lipofectamine 3000 (Invitrogen) following manufacturer instructions. 24 h after transfection, the cells were washed with PBS, Passive Lysis Buffer 1X (PLB) (E194A) was added to each well, in constant agitation for 20 minutes. 15 µL of cells lysate was collected in a 1.5 ml tube and 35 µl of Luciferase Assay Reagent II (LAR II) were added, then Firefly luciferase activity was read. Afterward, 35 µL of Stop & Glo were dispensed in the tube, and the Renilla Luciferase activity was read. Data were represented as ratio of Pp/Rr activities and normalized on pGL3b ratio, relative to the correspondent – or + doxycycline condition.

Flow cytometry

Relative to Results (Part II):

For cell cycle synchronization, after 72h of treatment with 1µg/ml doxycycline, or not, 4 million TET21N cells were seeded in a 10 cm dish in DMEM serum free media, for 18 h.

Thus, 1 million cells were resuspended in 1mL of PBS. Next, 2.5 mL of ethanol 100% was added under continuous agitation to allow the fixation without forming cell clumps. Cells were incubated overnight at -20 °C. Afterward, the cells were centrifuged for 5' at 300 g, washed by PBS, and then resuspended in 500 µl of PBS and RNAse A 1 µg/mL (Sigma-Aldrich). Cells were incubated for 30' at 37 °C and then kept on ice. DNA staining was performed by adding 25 µL of Propidium Iodide 1 mg/mL (Sigma-Aldrich). Fluorescence-activated cell sorting (FACS) analysis was performed on a CytoFLEX (Beckman Coulter), and the data were analyzed with FlowJo software. Cells singlet were gated as PE Area vs. PE Width and histograms were generated as frequency we PE A.

Growth curves

Relative to Results (Part II):

3.000 CHP-134 cells and 10.000 Kelly cells (stable cell lines for pLVX TRE3G EV, RB^{wt}, $RB^{\Delta CDK}$) were seeded in triplicate in a 96 well plate. Directly before the beginning of the analysis, doxycycline 1µg/ml was added or not to the wells. The cells were incubated at 37°C and 5% CO_2 in the Incucyte® S3 (Sartorius). Each well was analyzed every two hours for 72 h, taking two images at a 10x magnification on the phase contrast channel. Cell numbers were counted by the Incucyte® analysis software, which determined the object count per mm^2 per image, normalized on t0.

Western Blot

Total protein extract was obtained by adding to the cells RIPA buffer supplemented with protease inhibitor (PMSF, Sigma-Aldrich and cOmplete, Roche) and phosphatase inhibitor (PhosSTOP, Roche). Protein concentrations were measured by BCA Protein Assay kit (Pierce Biochemicals) following manufacturer instructions, and 50 µg of protein extract was electrophoresed on an 8% polyacrylamide gel and transferred on a nitrocellulose membrane (GE Healthcare). Membranes were incubated with Clarity Western ECL (BIO-RAD) and then scanned with ChemiDoc (BIO-RAD).

Relative to Results (Part I):

Primary antibodies: Flag (Sigma-Aldrich, F1804), HA (Cell Signaling, #3724). Secondary antibodies: rabbit anti-mouse and goat anti-rabbit light-chain specific HRP (Jackson, 115-035-174, 211-032-171).

Relative to Results (Part II):

Primary antibodies: RB (Abcam, ab181616), Phospho-RB (SantaCruz, sc-271930), E2F3A (SantaCruz, sc-56665), MYCN (SantaCruz, sc-53993), HA (Cell Signaling, #3724), GAPDH (ProteinTech, 10494-1-AP), β-tubulin (ProteinTech 66240-1-IG), β-actin (Sigma-Aldrich, A2228). Secondary antibodies: rabbit anti-mouse and goat anti-rabbit HRP (Jackson, 115-035-003, 111-035-144).

Relative to Results (Part III):

Primary Anti-m13 pIII monoclonal antibody (NEB, E8033S). Secondary antibody: rabbit anti-mouse HRP (Jackson, 115-035-003).

qRT PCR

Total RNA was extracted with TRI Reagent (Sigma-Aldrich), 500 µl were added to a 1 cm dish. Chloroform was added (0,2 ml/mL TRI Reagent), and after phase separation, the supernatant was mixed 1:1 with isopropanol. RNA was precipitated by salting out, and the pellet was resuspended in 50 µl of Molecular Biology Grade water (Sigma-Aldrich). 5µg of RNA was treated with DNA-free Removal kit (Invitrogen). 1 µg of RNA DNA-free undergo retrotranscription into cDNA with iSCript reverse transcription supermix kit (BIO-RAD). Quantitative Real Time PCR was performed using SSOAdvanced Universal SYBR green supermix (BIO-RAD) on 5 µg of cDNA.

Relative to Results (Part II):

Primer sequences: RB1: Fw: ACTCCGTTTTCATGCAGAGACTAA, Rv: GAGGAATGTGAGGTATTGGTGACA, E2F3A: Fw: ACTGCTAGCCAGCCCCG, Rv: GGACTATCTGGACTTCGTAGTGCAGC; CCNE1: Fw: CAGACCCACAGAGA-CAGCTTG; Rv: GCTCTGCTTCTTACCGCTCT , CCNE2: Fw: CGAGCGG-TAGCTGGTCTGG; Rv: GGGCTGCTGCTTAGCTTGTA , CDKN1A: Fw: CAGACCAG-CATGACAGATTTCTAC; Rv: TGTAGAGCGGGCCTTTGAGG. TBP: Fw: CCGCCGGCTGTTTAACTTC, Rv: AGAAACAGTGATGCTGGGTCA.

M13 phage production

Relative to Results (Part III):

Bacteria carrying 14G2a phagemid (pCOMB) and helper phage (m13ko7) were grown at 32°C overnight in culture containing ampicillin-kanamycin resistance and 0.4mM IPTG, reaching an OD of 2.0. Expression of phagemid was induced under P lac promotor resulting in a fusion of ScFv with pIII. The culture was centrifuged 10000g for 20min at 4°C to pellet bacteria. The supernatant was transferred to fresh bottles, and additional centrifugation was carried out for 5 min to pellet the remaining bacteria, and the supernatant containing M13GD2 was carefully transferred to fresh bottles. Next, final concentration NaCl 4% and PEG 8000 3% were added to the supernatant and incubated for 90 minutes at 4°C for phage precipitation. Supernatant containing M13GD2 /PEG 8000/ NaCl were centrifuged at 10000g

for 20 minutes at 4°C. Pelleted phages were resuspended in PBS followed by lowering the pH to 4.2 with HCL 0.5M to reach phages isoelectric point (IEP), and centrifuged with 14000g for 15 min at 4°C followed by gentle resuspension of pellet in PBS. Phage concentrations were checked by UV-Vis Spectrophotometer at 269nm, using an extinction coefficient of ε = 3.84 μM.

Immunofluorescence

Relative to Results (Part III):

Glass coverslips were placed in 6 wells plate and coated with collagen-containing 0.02% acetic acid, leaving for one hour at Room Temperature (RT). Thus, the coverslips were washed with Phosphate Buffer Saline (PBS) twice, followed by cells (LAN-5, CHP-134, IMR-32, Kelly, SH-SY5Y, SK-N-AS, SK-N-SH, SK-N-BE(2)C) seeding at 80% confluency. Only for the phage retargeting test, 1.66nM of M13GD2 phages were resuspended in DMEM and incubated for 45 minutes at RT followed by twice washes with washing buffer (PBS+0.05% tween 20). The day after, Culture media were aspirated and washed with PBS. Next, cells were fixed with 4% Paraformaldehyde in PBS (Sigma-Aldrich) at RT for 15 minutes. Afterward, cells were briefly washed with PBS-0.05% Tween 20 and blocked with normal donkey serum (NDS) 4% for 45 min at RT and followed by primary antibody anti-GD2 14G2a overnight incubation at 4°C. The next day, cells were incubated with secondary antibody conjugated with FITC (Jackson, 115-095-003) for one hour at RT, nuclear staining was carried out with Hoechst 1ug/ml for 10 minutes, and coverslips were mounted in mounting media. Images were acquired by 40X, NIKON Eclipse Ti2 confocal microscope, and ImageJ were used for analysis.

M13 phage conjugation

Relative to Results (Part III):

Bioconjugation of ECB04 to M13 phages was performed via a cross-coupling reaction between the reactive NHS ester of the ECB04 and the amino acid amine groups present on the surface of the M13 capsid. An ECB04 5mM solution was prepared in DMF. 50 μL of the ECB04 solution were added in a dropwise manner to 1 mL solution of M13 2.4·1013 virions/ml (40 nM) in sodium carbonate/bicarbonate buffer 100 mM (pH 9). The reaction was incubated in the dark overnight at 25 °C under constant shaking at 700 rpm (ThermoMixer

HC, S8012-0000; STARLAB, Hamburg, Germany) and then it was centrifuged for ten minutes at 14000 g and 15 °C to remove the insoluble excess of nonconjugated ECB04. The product was dialyzed versus PBS (pH 7.4) in regenerated cellulose membrane (14 kDa cut-off) to change buffer, remove DMF and reaction byproducts and then it was centrifuged once again with the same parameters as before to remove the remaining unreacted ECB04. The absorption spectrum of the purified Phage−ECB04 bioconjugate showed a red-shift in the absorption maximum, compared to the starting ECB04. This modification in the absorption spectra confirms the attachment of the dye to the phage. Considering the initial phage concentration and a molar extinction coefficient of 26875 M-1cm-1 the ECB04, approximately 400 molecules of ECB04 were conjugated per phage.

Viability assays

Relative to Results (Part II):

After 72 h of pre-treatment with doxycycline 1µg/ml, 5.000 CHP-134 and 10.000 Kelly (both RB1 cKD) were seeded in triplicate in a 96 well plate. Ribociclib (LEE001) and Palbociclib (PD-0332991) (MedChemExpress) were resuspended in DMSO and added to the cells at different concentrations (10.935 µM, 3.645 µM, 1.215 µM, 405 nM, 135 nM, 45 nM, 15 nM, 0 nM), equivalent amounts of DMSO were added to each point to avoid DMSO cytotoxicity artifacts. After 72 h of drug treatment, cell viability was evaluated through MTS assay (Promega) following the manufacturer's instructions. Absorbances were detected by Victor microplate reader at 490 nm. Three independent experiments were performed for each cell line.

Relative to Results (Part III):

For PDT, we Kelly SK-N-SH cells were seeded for cell viability assay at density of 50000/well in 96 well plate and incubated in humidified incubator containing 5% CO2 at 37°C. After 24 hours, the medium was aspirated and washed with PBS. Subsequently, cells were incubated with $M13_{GD2}$-ECB04 starting from a concentration of 1.66 nM with two-folds serial dilution down to 0.026 nM in DMEM supplemented with 10% FBS, penicillin-streptomycin 1% (100 U/ml) for 90 minutes. Following incubation, the cells were washed three times with DMEM without red phenol (Sigma-Aldrich cat no. 21063029) to eliminate unbound M13GD2-ECB04. Further, the cells were irradiated with white light from a 30cm distance for 15 min, and in the irradiation step, the cells were maintained in DMEM without

red phenol to allow the light to flow through readily. Immediately after irradiation, the medium was changed and placed in the incubator for 24 hours. Control experiments were conducted under the same conditions keeping cells in the dark.

Cell viability was determined using the 3-[4,5-dimethylthiazole-2-yl]-2,5-diphenyltetrazolium bromide (MTT) assays after 24 hours of post-PDT. The medium was aspirated from the 96-well plate, and the freshly added medium contained a final concentration of MTT 0.5 mg/ mL. Cells were placed for 90 minutes incubation in humidified incubation containing 5% CO2 at 37 ° C. After incubation, the insoluble product formazan produced by the reduction of MTT by NADPH dependant oxidoreductases expressed in the live cell was solubilized in dimethyl sulfoxide at RT and protected from light. The absorbance was then assessed at the wavelength of 570 and 690 nm by the EnSpire Multimode plate reader (Perkin, Inspire, USA).

Statistical analysis

Experiments for statistical analysis were performed at least three times. Data analysis was performed using Graphpad Prism 8 software and showed a mean ± standard error or standard deviation. Differences were examined for significance with a two-sided unpaired t-test for two groups or ANOVA among groups. Expression correlations between MYCN, E2F1-3, CDKN1A, and CCNE1/2 in human neuroblastoma tissues were tested using a two-sided Pearson’s correlation. According to Kaplan and Meier's method, survival was established from diagnosis until death or until the last observation if the patient did not die. Survival analyses were performed using GraphPad Prism 8.0 software, and comparisons of survival curves were performed using two-sided log-rank tests. A P-value of 0.05 or less was considered statistically significant. All statistical tests were two-sided.

ACKNOWLEDGMENTS

The work presented in this thesis would not have been possible without the guidance of Prof. Giovanni Perini. His effort in teaching and supervising was crucial for my growth path during my PhD, and his brilliant attitude to research mentored me. Also other professors contributed to this work: Prof. Federico Giorgi was a landmark for bioinformatic analysis shown in this thesis. Moreover, a special acknowledgment goes to Prof. Alberto Danielli and Prof. Matteo Calvaresi. The M13 phage project I had the honor of working on also resulted from their inspiring ideas.

During this exciting research experience, many people were on my side, and I learned how to face hitches with them. Among them all, dr. Giorgio Milazzo played a fundamental role. I spent long days with him in the laboratory, elaborating hypotheses, exchanging ideas, and planning experiments. Despite some divergence, he will be sincerely an example of a work attitude for the rest of my life. Dr. Roberto Ciaccio, and Suleman Khan Zadran have been more than colleagues for me. They were friends on my side in personal and working issues during the whole period. Master students made a fundamental contribution to my growth path. I taught them, and at the same time, they also taught me more than they thought. A special acknowledgment goes to Federica Severi, one of the smartest students I have ever met. Lastly, I have to thank other people with whom I shared this experience: Dr. Roberto Bernardoni, Dr. Simone Di Giacomo, Sara Aloisi, Alberto Rigamonti, Emanuel Forciniti, Sophia Marrero, and Martina Santulli.

Outside of the working environment, I have been supported by several people. I would never endure the hardships of the PhD path without them. My parents were by my side from the beginning of this experience. They gave me the motivation to go on studying to pursue my life goals. Unfortunately, this period was profoundly marked by my father’s disease. Despite the difficulties and the fear of losing each other, we took the opportunity to get closer. I would like to thank the brothers I have never had: my friends. Giulio and Mario were wonderfully supportive, as always. Finally, there are not enough pages to thank my life partner Irene. She provided me the emotional strength to keep going. Her brilliant ideas intellectually stimulated me.

REFERENCES

1. Ackermann, Sandra, Maria Cartolano, Barbara Hero, Anne Welte, Yvonne Kahlert, Andrea Roderwieser, Christoph Bartenhagen, et al. 2018. “A Mechanistic Classification of Clinical Phenotypes in Neuroblastoma.” *Science* 362 (6419): 1165–70. https://doi.org/10.1126/science.aat6768.

2. Adams, J. M., A. W. Harris, C. A. Pinkert, L. M. Corcoran, W. S. Alexander, S. Cory, R. D. Palmiter, and R. L. Brinster. 1985. “The C-Myc Oncogene Driven by Immunoglobulin Enhancers Induces Lymphoid Malignancy in Transgenic Mice.” *Nature* 318 (6046): 533–38. https://doi.org/10.1038/318533a0.

3. Adams, M. R., R. Sears, F. Nuckolls, G. Leone, and J. R. Nevins. 2000. “Complex Transcriptional Regulatory Mechanisms Control Expression of the E2F3 Locus.” *Molecular and Cellular Biology* 20 (10): 3633–39. https://doi.org/10.1128/MCB.20.10.3633-3639.2000.

4. Agostinis, Patrizia, Kristian Berg, Keith A. Cengel, Thomas H. Foster, Albert W. Girotti, Sandra O. Gollnick, Stephen M. Hahn, et al. 2011. “Photodynamic Therapy of Cancer: An Update.” *CA: A Cancer Journal for Clinicians* 61 (4): 250–81. https://doi.org/10.3322/caac.20114.

5. Ahmad, Zuhaida Asra, Swee Keong Yeap, Abdul Manaf Ali, Wan Yong Ho, Noorjahan Banu Mohamed Alitheen, and Muhajir Hamid. 2012. “ScFv Antibody: Principles and Clinical Application.” *Clinical and Developmental Immunology* 2012: 980250. https://doi.org/10.1155/2012/980250.

6. Amente, Stefano, Giorgio Milazzo, Maria Cristina Sorrentino, Susanna Ambrosio, Giacomo Di Palo, Luigi Lania, Giovanni Perini, and Barbara Majello. 2015. “Lysine-Specific Demethylase (LSD1/KDM1A) and MYCN Cooperatively Repress Tumor Suppressor Genes in Neuroblastoma.” *Oncotarget* 6 (16): 14572–83.

7. Ando, Kiyohiro, and Akira Nakagawara. 2021. “Acceleration or Brakes: Which Is Rational for Cell Cycle-Targeting Neuroblastoma Therapy?” *Biomolecules* 11 (5): 750. https://doi.org/10.3390/biom11050750.

8. Araki, Keigo, Keiko Kawauchi, Wataru Sugimoto, Daisuke Tsuda, Hiroya Oda, Ryosuke Yoshida, and Kiyoshi Ohtani. 2019. “Mitochondrial Protein E2F3d, a Distinctive E2F3 Product, Mediates Hypoxia-Induced Mitophagy in Cancer Cells.” *Communications Biology* 2 (1): 1–12. https://doi.org/10.1038/s42003-018-0246-9.

9. Armstrong, Barbara C., and Geoffrey W. Krystal. 1992. *Isolation and Characterization of Complementary DNA for N-Cym, a Gene Encoded by the DNA Strand Opposite to N-Myc. Cell Growth Differ*.

10. Aygun, Nevim. 2018. “Biological and Genetic Features of Neuroblastoma and Their Clinical Importance.” *Current Pediatric Reviews* 14 (2): 73–90. https://doi.org/10.2174/1573396314666180129101627.

11. B, Geoerger, Bourdeaut F, DuBois Sg, Fischer M, Geller Ji, Gottardo Ng, Marabelle A, et al. 2017. “A Phase I Study of the CDK4/6 Inhibitor Ribociclib (LEE011) in Pediatric Patients with Malignant Rhabdoid Tumors, Neuroblastoma, and Other Solid

Tumors." *Clinical Cancer Research : An Official Journal of the American Association for Cancer Research* 23 (10). https://doi.org/10.1158/1078-0432.CCR-16-2898.

12. Bahmad, Hisham F., Farah Chamaa, Sahar Assi, Reda M. Chalhoub, Tamara Abou-Antoun, and Wassim Abou-Kheir. 2019. "Cancer Stem Cells in Neuroblastoma: Expanding the Therapeutic Frontier." *Frontiers in Molecular Neuroscience* 12. https://www.frontiersin.org/articles/10.3389/fnmol.2019.00131.

13. Bahram, Fuad, Natalie von der Lehr, Cihan Cetinkaya, and Lars-Gunnar Larsson. 2000. "C-Myc Hot Spot Mutations in Lymphomas Result in Inefficient Ubiquitination and Decreased Proteasome-Mediated Turnover." *Blood* 95 (6): 2104–10. https://doi.org/10.1182/blood.V95.6.2104.

14. Baluapuri, Apoorva, Elmar Wolf, and Martin Eilers. 2020. "Target-Gene Independent Functions of MYC Oncogenes." *Nature Reviews. Molecular Cell Biology* 21 (5): 255–67. https://doi.org/10.1038/s41580-020-0215-2.

15. Banerjee, S. A., P. Hoppe, M. Brilliant, and D. M. Chikaraishi. 1992. "5' Flanking Sequences of the Rat Tyrosine Hydroxylase Gene Target Accurate Tissue-Specific, Developmental, and Transsynaptic Expression in Transgenic Mice." *Journal of Neuroscience* 12 (11): 4460–67. https://doi.org/10.1523/JNEUROSCI.12-11-04460.1992.

16. Bell, Emma, John Lunec, and Deborah Tweddle. 2007. "Cell Cycle Regulation Targets of MYCN Identified by Gene Expression Microarrays." *Cell Cycle* 6 (10): 1249–56. https://doi.org/10.4161/cc.6.10.4222.

17. Berg, Thorsten, Steven B. Cohen, Joel Desharnais, Corinna Sonderegger, Daniel J. Maslyar, Joel Goldberg, Dale L. Boger, and Peter K. Vogt. 2002. "Small-Molecule Antagonists of Myc/Max Dimerization Inhibit Myc-Induced Transformation of Chicken Embryo Fibroblasts." *Proceedings of the National Academy of Sciences* 99 (6): 3830–35. https://doi.org/10.1073/pnas.062036999.

18. Berkowitz, Steven A., and Loren A. Day. 1976. "Mass, Length, Composition and Structure of the Filamentous Bacterial Virus Fd." *Journal of Molecular Biology* 102 (3): 531–47. https://doi.org/10.1016/0022-2836(76)90332-6.

19. Berry, Teeara, William Luther, Namrata Bhatnagar, Yann Jamin, Evon Poon, Takaomi Sanda, Desheng Pei, et al. 2012. "The ALK(F1174L) Mutation Potentiates the Oncogenic Activity of MYCN in Neuroblastoma." *Cancer Cell* 22 (1): 117–30. https://doi.org/10.1016/j.ccr.2012.06.001.

20. Betters, Erin, Ying Liu, Anders Kjaeldgaard, Erik Sundström, and Martín I. García-Castro. 2010. "Analysis of Early Human Neural Crest Development." *Developmental Biology* 344 (2): 578–92. https://doi.org/10.1016/j.ydbio.2010.05.012.

21. Bijgaart, Renske J. E. van den, Michiel Kroesen, Melissa Wassink, Ingrid C. Brok, Esther D. Kers-Rebel, Louis Boon, Torben Heise, et al. 2019. "Combined Sialic Acid and Histone Deacetylase (HDAC) Inhibitor Treatment up-Regulates the Neuroblastoma Antigen GD2." *Journal of Biological Chemistry* 294 (12): 4437–49. https://doi.org/10.1074/jbc.RA118.002763.

22. Blavier, Laurence, Ren-Ming Yang, and Yves A. DeClerck. 2020. "The Tumor Microenvironment in Neuroblastoma: New Players, New Mechanisms of Interaction and

New Perspectives." *Cancers* 12 (10): E2912. https://doi.org/10.3390/cancers12102912.

23. Boeva, Valentina, Caroline Louis-Brennetot, Agathe Peltier, Simon Durand, Cécile Pierre-Eugène, Virginie Raynal, Heather C. Etchevers, et al. 2017. "Heterogeneity of Neuroblastoma Cell Identity Defined by Transcriptional Circuitries." *Nature Genetics* 49 (9): 1408–13. https://doi.org/10.1038/ng.3921.

24. Bortot, Barbara, Maura Apollonio, Gabriele Baj, Laura Andolfi, Luisa Zupin, Sergio Crovella, Matteo di Giosia, et al. 2022. "Advanced Photodynamic Therapy with an Engineered M13 Phage Targeting EGFR: Mitochondrial Localization and Autophagy Induction in Ovarian Cancer Cell Lines." *Free Radical Biology and Medicine* 179 (February): 242–51. https://doi.org/10.1016/j.freeradbiomed.2021.11.019.

25. Bouchard, C., K. Thieke, A. Maier, R. Saffrich, J. Hanley-Hyde, W. Ansorge, S. Reed, P. Sicinski, J. Bartek, and M. Eilers. 1999. "Direct Induction of Cyclin D2 by Myc Contributes to Cell Cycle Progression and Sequestration of P27." *The EMBO Journal* 18 (19): 5321–33. https://doi.org/10.1093/emboj/18.19.5321.

26. Bouchard, Caroline, Oliver Dittrich, Astrid Kiermaier, Karen Dohmann, Annette Menkel, Martin Eilers, and Bernhard Lüscher. 2001. "Regulation of Cyclin D2 Gene Expression by the Myc/Max/Mad Network: Myc-Dependent TRRAP Recruitment and Histone Acetylation at the Cyclin D2 Promoter." *Genes & Development* 15 (16): 2042–47. https://doi.org/10.1101/gad.907901.

27. Braal, C. Louwrens, Elisabeth M. Jongbloed, Saskia M. Wilting, Ron H. J. Mathijssen, Stijn L. W. Koolen, and Agnes Jager. 2021. "Inhibiting CDK4/6 in Breast Cancer with Palbociclib, Ribociclib, and Abemaciclib: Similarities and Differences." *Drugs* 81 (3): 317–31. https://doi.org/10.1007/s40265-020-01461-2.

28. Bracken, Adrian P., Marco Ciro, Andrea Cocito, and Kristian Helin. 2004. "E2F Target Genes: Unraveling the Biology." *Trends in Biochemical Sciences* 29 (8): 409–17. https://doi.org/10.1016/j.tibs.2004.06.006.

29. Brägelmann, Johannes, Stefanie Böhm, Matthew R. Guthrie, Gurkan Mollaoglu, Trudy G. Oliver, and Martin L. Sos. 2017. "Family Matters: How MYC Family Oncogenes Impact Small Cell Lung Cancer." *Cell Cycle* 16 (16): 1489–98. https://doi.org/10.1080/15384101.2017.1339849.

30. Bresler, Scott C., Daniel A. Weiser, Peter J. Huwe, Jin H. Park, Kateryna Krytska, Hannah Ryles, Marci Laudenslager, et al. 2014. "ALK Mutations Confer Differential Oncogenic Activation and Sensitivity to ALK Inhibition Therapy in Neuroblastoma." *Cancer Cell* 26 (5): 682–94. https://doi.org/10.1016/j.ccell.2014.09.019.

31. Bretones, Gabriel, M. Dolores Delgado, and Javier León. 2015. "Myc and Cell Cycle Control." *Biochimica et Biophysica Acta (BBA) - Gene Regulatory Mechanisms*, Myc proteins in cell biology and pathology, 1849 (5): 506–16. https://doi.org/10.1016/j.bbagrm.2014.03.013.

32. Brodeur, G. M., R. C. Seeger, A. Barrett, F. Berthold, R. P. Castleberry, G. D'Angio, B. De Bernardi, A. E. Evans, M. Favrot, and A. I. Freeman. 2016. "International Criteria for Diagnosis, Staging, and Response to Treatment in Patients with Neuroblasto-

ma." *Journal of Clinical Oncology*, September. https://doi.org/10.1200/JCO.1988.6.12.1874.

33. Brodeur, Garrett M. 2003. "Neuroblastoma: Biological Insights into a Clinical Enigma." *Nature Reviews Cancer* 3 (3): 203. https://doi.org/10.1038/nrc1014.

34. Burke, Jason R., Alison J. Deshong, Jeffrey G. Pelton, and Seth M. Rubin. 2010. "Phosphorylation-Induced Conformational Changes in the Retinoblastoma Protein Inhibit E2F Transactivation Domain Binding *." *Journal of Biological Chemistry* 285 (21): 16286–93. https://doi.org/10.1074/jbc.M110.108167.

35. Calao, M., E. O. Sekyere, H. J. Cui, B. B. Cheung, W. D. Thomas, J. Keating, J. B. Chen, et al. 2013. "Direct Effects of Bmi1 on P53 Protein Stability Inactivates Oncoprotein Stress Responses in Embryonal Cancer Precursor Cells at Tumor Initiation." *Oncogene* 32 (31): 3616–26. https://doi.org/10.1038/onc.2012.368.

36. Cantelli, Andrea, Marco Malferrari, Alice Soldà, Giorgia Simonetti, Sonny Forni, Edoardo Toscanella, Edoardo J. Mattioli, et al. 2021. "Human Serum Albumin-Oligothiophene Bioconjugate: A Phototheranostic Platform for Localized Killing of Cancer Cells by Precise Light Activation." *JACS Au* 1 (7): 925–35. https://doi.org/10.1021/jacsau.1c00061.

37. Casero, Robert A., and Laurence J. Marton. 2007. "Targeting Polyamine Metabolism and Function in Cancer and Other Hyperproliferative Diseases." *Nature Reviews. Drug Discovery* 6 (5): 373–90. https://doi.org/10.1038/nrd2243.

38. Cheever, Martin A., James P. Allison, Andrea S. Ferris, Olivera J. Finn, Benjamin M. Hastings, Toby T. Hecht, Ira Mellman, et al. 2009. "The Prioritization of Cancer Antigens: A National Cancer Institute Pilot Project for the Acceleration of Translational Research." *Clinical Cancer Research: An Official Journal of the American Association for Cancer Research* 15 (17): 5323–37. https://doi.org/10.1158/1078-0432.CCR-09-0737.

39. Chen, Lindi, Nunzio Iraci, Samuele Gherardi, Laura D. Gamble, Katrina M. Wood, Giovanni Perini, John Lunec, and Deborah A. Tweddle. 2010. "P53 Is a Direct Transcriptional Target of MYCN in Neuroblastoma." *Cancer Research* 70 (4): 1377–88. https://doi.org/10.1158/0008-5472.CAN-09-2598.

40. Chen, Ye, Liang Xu, Ruby Yu-Tong Lin, Markus Müschen, and H. Phillip Koeffler. 2020. "Core Transcriptional Regulatory Circuitries in Cancer." *Oncogene* 39 (43): 6633–46. https://doi.org/10.1038/s41388-020-01459-w.

41. Chen, Zhenghu, Zhenyu Wang, Jonathan C. Pang, Yang Yu, Shayahati Bieerkehazhi, Jiaxiong Lu, Ting Hu, et al. 2016. "Multiple CDK Inhibitor Dinaciclib Suppresses Neuroblastoma Growth via Inhibiting CDK2 and CDK9 Activity." *Scientific Reports* 6 (1): 29090. https://doi.org/10.1038/srep29090.

42. Cheung, Irene Y., Brian H. Kushner, Shakeel Modak, Ellen M. Basu, Stephen S. Roberts, and Nai-Kong V. Cheung. 2017. "Phase I Trial of Anti-GD2 Monoclonal Antibody Hu3F8 plus GM-CSF: Impact of Body Weight, Immunogenicity and Anti-GD2 Response on Pharmacokinetics and Survival." *Oncoimmunology* 6 (11): e1358331. https://doi.org/10.1080/2162402X.2017.1358331.

43. Cheung, N. K., H. Lazarus, F. D. Miraldi, C. R. Abramowsky, S. Kallick, U. M. Saarinen, T. Spitzer, S. E. Strandjord, P. F. Coccia, and N. A. Berger. 1987. "Ganglioside GD2 Specific Monoclonal Antibody 3F8: A Phase I Study in Patients with Neuroblastoma and Malignant Melanoma." *Journal of Clinical Oncology: Official Journal of the American Society of Clinical Oncology* 5 (9): 1430–40. https://doi.org/10.1200/JCO.1987.5.9.1430.

44. Ciaccio, Roberto, Piergiuseppe De Rosa, Sara Aloisi, Marta Viggiano, Leonardo Cimadom, Suleman Khan Zadran, Giovanni Perini, and Giorgio Milazzo. 2021. "Targeting Oncogenic Transcriptional Networks in Neuroblastoma: From N-Myc to Epigenetic Drugs." *International Journal of Molecular Sciences* 22 (23): 12883. https://doi.org/10.3390/ijms222312883.

45. Ciemerych, Maria A., and Peter Sicinski. 2005. "Cell Cycle in Mouse Development." *Oncogene* 24 (17): 2877–98. https://doi.org/10.1038/sj.onc.1208608.

46. Cole, Kristina A., Jonathan Huggins, Michael Laquaglia, Chase E. Hulderman, Mike R. Russell, Kristopher Bosse, Sharon J. Diskin, et al. 2011. "RNAi Screen of the Protein Kinome Identifies Checkpoint Kinase 1 (CHK1) as a Therapeutic Target in Neuroblastoma." *Proceedings of the National Academy of Sciences of the United States of America* 108 (8): 3336–41. https://doi.org/10.1073/pnas.1012351108.

47. Davis, A. C., M. Wims, G. D. Spotts, S. R. Hann, and A. Bradley. 1993. "A Null C-Myc Mutation Causes Lethality before 10.5 Days of Gestation in Homozygotes and Reduced Fertility in Heterozygous Female Mice." *Genes & Development* 7 (4): 671–82. https://doi.org/10.1101/gad.7.4.671.

48. Davis, J. Nathan, Laura McGhee, and Shari Meyers. 2003. "The ETO (MTG8) Gene Family." *Gene* 303 (January): 1–10. https://doi.org/10.1016/S0378-1119(02)01172-1.

49. De Bernardi, Bruno, Brigitte Nicolas, Luca Boni, Paolo Indolfi, Modesto Carli, Luca Cordero di Montezemolo, Alberto Donfrancesco, et al. 2003. "Disseminated Neuroblastoma in Children Older Than One Year at Diagnosis: Comparable Results With Three Consecutive High-Dose Protocols Adopted by the Italian Co-Operative Group for Neuroblastoma." *Journal of Clinical Oncology* 21 (8): 1592–1601. https://doi.org/10.1200/JCO.2003.05.191.

50. DeGregori, J., G. Leone, A. Miron, L. Jakoi, and J. R. Nevins. 1997. "Distinct Roles for E2F Proteins in Cell Growth Control and Apoptosis." *Proceedings of the National Academy of Sciences of the United States of America* 94 (14): 7245–50. https://doi.org/10.1073/pnas.94.14.7245.

51. DeGregori, James, and David G. Johnson. 2006. "Distinct and Overlapping Roles for E2F Family Members in Transcription, Proliferation and Apoptosis." *Current Molecular Medicine* 6 (7): 739–48. https://doi.org/10.2174/1566524010606070739.

52. Dhanasekaran, Renumathy, Anja Deutzmann, Wadie D. Mahauad-Fernandez, Aida S. Hansen, Arvin M. Gouw, and Dean W. Felsher. 2022. "The MYC Oncogene — the Grand Orchestrator of Cancer Growth and Immune Evasion." *Nature Reviews Clinical Oncology* 19 (1): 23–36. https://doi.org/10.1038/s41571-021-00549-2.

53. Dhillon, Sohita. 2015. "Dinutuximab: First Global Approval." *Drugs* 75 (8): 923–27. https://doi.org/10.1007/s40265-015-0399-5.

54. D'Oto, Alexandra, Jie Fang, Hongjian Jin, Beisi Xu, Shivendra Singh, Anoushka Mullasseril, Victoria Jones, et al. 2021. "KDM6B Promotes Activation of the Oncogenic CDK4/6-PRB-E2F Pathway by Maintaining Enhancer Activity in MYCN-Amplified Neuroblastoma." *Nature Communications* 12 (December): 7204. https://doi.org/10.1038/s41467-021-27502-2.

55. Dowdy, Steven F., Philip W. Hinds, Kenway Louie, Steven I. Reed, Andrew Arnold, and Robert A. Weinberg. 1993. "Physical Interaction of the Retinoblastoma Protein with Human D Cyclins." *Cell* 73 (3): 499–511. https://doi.org/10.1016/0092-8674(93)90137-F.

56. Downing, James R. 1999. "The Aml1-Eto Chimaeric Transcription Factor in Acute Myeloid Leukaemia: Biology and Clinical Significance." *British Journal of Haematology* 106 (2): 296–308. https://doi.org/10.1046/j.1365-2141.1999.01377.x.

57. Durbin, Adam D., Tingjian Wang, Virangika K. Wimalasena, Mark W. Zimmerman, Deyao Li, Neekesh V. Dharia, Luca Mariani, et al. 2022. "EP300 Selectively Controls the Enhancer Landscape of MYCN-Amplified Neuroblastoma." *Cancer Discovery* 12 (3): 730–51. https://doi.org/10.1158/2159-8290.CD-21-0385.

58. Durbin, Adam D., Mark W. Zimmerman, Neekesh V. Dharia, Brian J. Abraham, Amanda Balboni Iniguez, Nina Weichert-Leahey, Shuning He, et al. 2018a. "Selective Gene Dependencies in MYCN -Amplified Neuroblastoma Include the Core Transcriptional Regulatory Circuitry." *Nature Genetics* 50 (9): 1240–46. https://doi.org/10.1038/s41588-018-0191-z.

59. ———. 2018b. "Selective Gene Dependencies in MYCN-Amplified Neuroblastoma Include the Core Transcriptional Regulatory Circuitry." *Nature Genetics* 50 (9): 1240–46. https://doi.org/10.1038/s41588-018-0191-z.

60. Dyson, Nicholas J. 2016. "RB1: A Prototype Tumor Suppressor and an Enigma." *Genes & Development* 30 (13): 1492–1502. https://doi.org/10.1101/gad.282145.116.

61. Ewens, Kathryn G., Tricia R. Bhatti, Kimberly A. Moran, Jennifer Richards-Yutz, Carol L. Shields, Ralph C. Eagle, and Arupa Ganguly. 2017. "Phosphorylation of PRb: Mechanism for RB Pathway Inactivation in MYCN-Amplified Retinoblastoma." *Cancer Medicine* 6 (3): 619–30. https://doi.org/10.1002/cam4.1010.

62. Ferrucci, Francesca, Roberto Ciaccio, Sara Monticelli, Paolo Pigini, Simone di Giacomo, Stefania Purgato, Daniela Erriquez, et al. 2018. "MAX to MYCN Intracellular Ratio Drives the Aggressive Phenotype and Clinical Outcome of High Risk Neuroblastoma." *Biochimica et Biophysica Acta (BBA) - Gene Regulatory Mechanisms* 1861 (3): 235–45. https://doi.org/10.1016/j.bbagrm.2018.01.007.

63. Frolov, Maxim V., and Nicholas J. Dyson. 2004. "Molecular Mechanisms of E2F-Dependent Activation and PRB-Mediated Repression." *Journal of Cell Science* 117 (11): 2173–81. https://doi.org/10.1242/jcs.01227.

64. Gamble, L. D., U. R. Kees, D. A. Tweddle, and J. Lunec. 2012. "MYCN Sensitizes Neuroblastoma to the MDM2-P53 Antagonists Nutlin-3 and MI-63." *Oncogene* 31 (6): 752–63. https://doi.org/10.1038/onc.2011.270.

65. García-Gutiérrez, Lucía, María Dolores Delgado, and Javier León. 2019. "MYC Oncogene Contributions to Release of Cell Cycle Brakes." *Genes* 10 (3): 244. https://doi.org/10.3390/genes10030244.

66. Gartlgruber, Moritz, Ashwini Kumar Sharma, Andrés Quintero, Daniel Dreidax, Selina Jansky, Young-Gyu Park, Sina Kreth, et al. 2021. "Super Enhancers Define Regulatory Subtypes and Cell Identity in Neuroblastoma." *Nature Cancer* 2 (1): 114–28. https://doi.org/10.1038/s43018-020-00145-w.

67. Gelmetti, Vania, Jinsong Zhang, Mirco Fanelli, Saverio Minucci, Pier Giuseppe Pelicci, and Mitchell A. Lazar. 1998. "Aberrant Recruitment of the Nuclear Receptor Corepressor-Histone Deacetylase Complex by the Acute Myeloid Leukemia Fusion Partner ETO." *Molecular and Cellular Biology* 18 (12): 7185–91. https://doi.org/10.1128/MCB.18.12.7185.

68. Gilbert, Scott F. 2000. "The Neural Crest." *Developmental Biology. 6th Edition*. https://www.ncbi.nlm.nih.gov/books/NBK10065/.

69. Groningen, Tim van, Jan Koster, Linda J. Valentijn, Danny A. Zwijnenburg, Nurdan Akogul, Nancy E. Hasselt, Marloes Broekmans, et al. 2017. "Neuroblastoma Is Composed of Two Super-Enhancer-Associated Differentiation States." *Nature Genetics* 49 (8): 1261–66. https://doi.org/10.1038/ng.3899.

70. Groves, Andrew K., and Carole LaBonne. 2014. "Setting Appropriate Boundaries: Fate, Patterning and Competence at the Neural Plate Border." *Developmental Biology* 389 (1): 2–12. https://doi.org/10.1016/j.ydbio.2013.11.027.

71. Gubern, Albert, Manel Joaquin, Miriam Marquès, Pedro Maseres, Javier Garcia-Garcia, Ramon Amat, Daniel González-Nuñez, et al. 2016. "The N-Terminal Phosphorylation of RB by P38 Bypasses Its Inactivation by CDKs and Prevents Proliferation in Cancer Cells." *Molecular Cell* 64 (1): 25–36. https://doi.org/10.1016/j.molcel.2016.08.015.

72. Harenza, Jo Lynne, Maura A. Diamond, Rebecca N. Adams, Michael M. Song, Heather L. Davidson, Lori S. Hart, Maiah H. Dent, Paolo Fortina, C. Patrick Reynolds, and John M. Maris. 2017. "Transcriptomic Profiling of 39 Commonly-Used Neuroblastoma Cell Lines." *Scientific Data* 4 (March): 170033. https://doi.org/10.1038/sdata.2017.33.

73. Hassler, Markus, Shradha Singh, Wyatt W. Yue, Maciej Luczynski, Rachid Lakbir, Francisco Sanchez-Sanchez, Thomas Bader, Laurence H. Pearl, and Sibylle Mittnacht. 2007. "Crystal Structure of the Retinoblastoma Protein N Domain Provides Insight into Tumor Suppression, Ligand Interaction, and Holoprotein Architecture." *Molecular Cell* 28 (3): 371–85. https://doi.org/10.1016/j.molcel.2007.08.023.

74. Hatton, K. S., K. Mahon, L. Chin, F. C. Chiu, H. W. Lee, D. Peng, S. D. Morgenbesser, J. Horner, and R. A. DePinho. 1996. "Expression and Activity of L-Myc in Normal Mouse Development." *Molecular and Cellular Biology* 16 (4): 1794–1804. https://doi.org/10.1128/MCB.16.4.1794.

75. Hemann, Michael T., Anka Bric, Julie Teruya-Feldstein, Andreas Herbst, Jonas A. Nilsson, Carlos Cordon-Cardo, John L. Cleveland, William P. Tansey, and Scott W.

Lowe. 2005. “Evasion of the P53 Tumour Surveillance Network by Tumour-Derived MYC Mutants.” *Nature* 436 (7052): 807–11. https://doi.org/10.1038/nature03845.

76. Hendershot, Tyler J., Hongbin Liu, David E. Clouthier, Iain T. Shepherd, Eva Coppola, Michèle Studer, Anthony B. Firulli, Douglas L. Pittman, and Marthe J. Howard. 2008. “Conditional Deletion of Hand2 Reveals Critical Functions in Neurogenesis and Cell Type-Specific Gene Expression for Development of Neural Crest-Derived Noradrenergic Sympathetic Ganglion Neurons.” *Developmental Biology* 319 (2): 179–91. https://doi.org/10.1016/j.ydbio.2008.03.036.

77. Herranz, Daniel, Alberto Ambesi-Impiombato, Teresa Palomero, Stephanie A. Schnell, Laura Belver, Agnieszka A. Wendorff, Luyao Xu, et al. 2014. “A NOTCH1-Driven MYC Enhancer Promotes T Cell Development, Transformation and Acute Lymphoblastic Leukemia.” *Nature Medicine* 20 (10): 1130–37. https://doi.org/10.1038/nm.3665.

78. Hinds, P W, S F Dowdy, E N Eaton, A Arnold, and R A Weinberg. 1994a. “Function of a Human Cyclin Gene as an Oncogene.” *Proceedings of the National Academy of Sciences* 91 (2): 709–13. https://doi.org/10.1073/pnas.91.2.709.

79. ———. 1994b. “Function of a Human Cyclin Gene as an Oncogene.” *Proceedings of the National Academy of Sciences* 91 (2): 709–13. https://doi.org/10.1073/pnas.91.2.709.

80. Hogarty, Michael D., Murray D. Norris, Kimberly Davis, Xueyuan Liu, Nicholas F. Evageliou, Candace S. Hayes, Bruce Pawel, et al. 2008. “ODC1 Is a Critical Determinant of MYCN Oncogenesis and a Therapeutic Target in Neuroblastoma.” *Cancer Research* 68 (23): 9735–45. https://doi.org/10.1158/0008-5472.CAN-07-6866.

81. Hoogenboom, Hennie R, Adriaan P de Bruïne, Simon E Hufton, René M Hoet, Jan-Willem Arends, and Rob C Roovers. 1998. “Antibody Phage Display Technology and Its Applications.” *Immunotechnology* 4 (1): 1–20. https://doi.org/10.1016/S1380-2933(98)00007-4.

82. Horwacik, Irena, Przemyslaw Golik, Przemyslaw Grudnik, Michal Kolinski, Michal Zdzalik, Hanna Rokita, and Grzegorz Dubin. 2015. “Structural Basis of GD2 Ganglioside and Mimetic Peptide Recognition by 14G2a Antibody.” *Molecular & Cellular Proteomics : MCP* 14 (10): 2577–90. https://doi.org/10.1074/mcp.M115.052720.

83. Hu, Nan, Linqing Zou, Cheng Wang, and Guoqi Song. 2022. “RUNX1T1 Function in Cell Fate.” *Stem Cell Research & Therapy* 13 (July): 369. https://doi.org/10.1186/s13287-022-03074-w.

84. Huang, Miller, and William A. Weiss. 2013. “Neuroblastoma and MYCN.” *Cold Spring Harbor Perspectives in Medicine* 3 (10): a014415. https://doi.org/10.1101/cshperspect.a014415.

85. Huber, Katrin. 2006. “The Sympathoadrenal Cell Lineage: Specification, Diversification, and New Perspectives.” *Developmental Biology* 298 (2): 335–43. https://doi.org/10.1016/j.ydbio.2006.07.010.

86. Hurst, C. D., D. C. Tomlinson, S. V. Williams, F. M. Platt, and M. A. Knowles. 2008. “Inactivation of the Rb Pathway and Overexpression of Both Isoforms of E2F3 Are

Obligate Events in Bladder Tumours with 6p22 Amplification." *Oncogene* 27 (19): 2716–27. https://doi.org/10.1038/sj.onc.1210934.

87. Jansky, Selina, Ashwini Kumar Sharma, Verena Körber, Andrés Quintero, Umut H. Toprak, Elisa M. Wecht, Moritz Gartlgruber, et al. 2021. "Single-Cell Transcriptomic Analyses Provide Insights into the Developmental Origins of Neuroblastoma." *Nature Genetics* 53 (5): 683–93. https://doi.org/10.1038/s41588-021-00806-1.

88. Joshi, Shweta. 2020. "Targeting the Tumor Microenvironment in Neuroblastoma: Recent Advances and Future Directions." *Cancers* 12 (8): E2057. https://doi.org/10.3390/cancers12082057.

89. Kalinovsky, Daniel V, Alexey V Kibardin, Irina V Kholodenko, Elena V Svirshchevskaya, Igor I Doronin, Mariya V Konovalova, Maria V Grechikhina, et al. 2022. "Therapeutic Efficacy of Antibody-Drug Conjugates Targeting GD2-Positive Tumors." *Journal for Immunotherapy of Cancer* 10 (6): e004646. https://doi.org/10.1136/jitc-2022-004646.

90. Kalkat, Manpreet, Diana Resetca, Corey Lourenco, Pak-Kei Chan, Yong Wei, Yu-Jia Shiah, Natasha Vitkin, et al. 2018. "MYC Protein Interactome Profiling Reveals Functionally Distinct Regions That Cooperate to Drive Tumorigenesis." *Molecular Cell* 72 (5): 836-848.e7. https://doi.org/10.1016/j.molcel.2018.09.031.

91. Kent, Lindsey N., and Gustavo Leone. 2019. "The Broken Cycle: E2F Dysfunction in Cancer." *Nature Reviews. Cancer* 19 (6): 326–38. https://doi.org/10.1038/s41568-019-0143-7.

92. Keyel, Michelle E, and C Patrick Reynolds. 2018. "Spotlight on Dinutuximab in the Treatment of High-Risk Neuroblastoma: Development and Place in Therapy." *Biologics : Targets & Therapy* 13 (December): 1–12. https://doi.org/10.2147/BTT.S114530.

93. Kim, H. Y., B. Y. Ahn, and Y. Cho. 2001. "Structural Basis for the Inactivation of Retinoblastoma Tumor Suppressor by SV40 Large T Antigen." *The EMBO Journal* 20 (1–2): 295–304. https://doi.org/10.1093/emboj/20.1.295.

94. Klutz, Stephan, Laura Holtmann, Martin Lobedann, and Gerhard Schembecker. 2016. "Cost Evaluation of Antibody Production Processes in Different Operation Modes." *Chemical Engineering Science* 141 (February): 63–74. https://doi.org/10.1016/j.ces.2015.10.029.

95. Knudsen, E S, and J Y Wang. 1997. "Dual Mechanisms for the Inhibition of E2F Binding to RB by Cyclin-Dependent Kinase-Mediated RB Phosphorylation." *Molecular and Cellular Biology* 17 (10): 5771–83. https://doi.org/10.1128/MCB.17.10.5771.

96. Knudsen, Erik S., and Karen E. Knudsen. 2008. "Tailoring to RB: Tumour Suppressor Status and Therapeutic Response." *Nature Reviews. Cancer* 8 (9): 714–24. https://doi.org/10.1038/nrc2401.

97. Knudson, Alfred G. 1971. "Mutation and Cancer: Statistical Study of Retinoblastoma." *Proceedings of the National Academy of Sciences of the United States of America* 68 (4): 820–23.

98. Kocak, H., S. Ackermann, B. Hero, Y. Kahlert, A. Oberthuer, D. Juraeva, F. Roels, et al. 2013. “Hox-C9 Activates the Intrinsic Pathway of Apoptosis and Is Associated with Spontaneous Regression in Neuroblastoma.” *Cell Death & Disease* 4 (April): e586. https://doi.org/10.1038/cddis.2013.84.

99. Kolupaeva, Victoria, and Veerle Janssens. 2013. “PP1 and PP2A Phosphatases--Cooperating Partners in Modulating Retinoblastoma Protein Activation.” *The FEBS Journal* 280 (2): 627–43. https://doi.org/10.1111/j.1742-4658.2012.08511.x.

100. Kovesdi, Imre, Ronald Reichel, and Joseph R. Nevins. 1986. “Identification of a Cellular Transcription Factor Involved in E1A Trans-Activation.” *Cell* 45 (2): 219–28. https://doi.org/10.1016/0092-8674(86)90386-7.

101. Krengel, Ute, and Paula A. Bousquet. 2014. “Molecular Recognition of Gangliosides and Their Potential for Cancer Immunotherapies.” *Frontiers in Immunology* 5 (July): 325. https://doi.org/10.3389/fimmu.2014.00325.

102. Kroesen, Michiel, Christian Büll, Paul R. Gielen, Ingrid C. Brok, Inna Armandari, Melissa Wassink, Maaike W. G. Looman, et al. 2016. “Anti-GD2 MAb and Vorinostat Synergize in the Treatment of Neuroblastoma.” *OncoImmunology* 5 (6): e1164919. https://doi.org/10.1080/2162402X.2016.1164919.

103. Kwon, Jungeun Sarah, Nicholas J. Everetts, Xia Wang, Weikang Wang, Kimiko Della Croce, Jianhua Xing, and Guang Yao. 2017. “Controlling Depth of Cellular Quiescence by an Rb-E2F Network Switch.” *Cell Reports* 20 (13): 3223–35. https://doi.org/10.1016/j.celrep.2017.09.007.

104. Lammie, G., N. Cheung, W. Gerald, M. Rosenblum, and C. Cordoncardo. 1993. “Ganglioside Gd(2) Expression in the Human Nervous-System and in Neuroblastomas - an Immunohistochemical Study.” *International Journal of Oncology* 3 (5): 909–15. https://doi.org/10.3892/ijo.3.5.909.

105. Ledsgaard, Line, Mogens Kilstrup, Aneesh Karatt-Vellatt, John McCafferty, and Andreas H. Laustsen. 2018. “Basics of Antibody Phage Display Technology.” *Toxins* 10 (6): 236. https://doi.org/10.3390/toxins10060236.

106. Lee, Changwook, Jeong Ho Chang, Hyun Sook Lee, and Yunje Cho. 2002. “Structural Basis for the Recognition of the E2F Transactivation Domain by the Retinoblastoma Tumor Suppressor.” *Genes & Development* 16 (24): 3199–3212. https://doi.org/10.1101/gad.1046102.

107. Lentine, Brandon, Lisa Antonucci, Ray Hunce, Justina Edwards, Valerie Marallano, and Nancy A. Krucher. 2012. “Dephosphorylation of Threonine-821 of the Retinoblastoma Tumor Suppressor Protein (Rb) Is Required for Apoptosis Induced by UV and Cdk Inhibition.” *Cell Cycle* 11 (17): 3324–30. https://doi.org/10.4161/cc.21693.

108. Lewis, Elizabeth C., Jacqueline M. Kraveka, William Ferguson, Don Eslin, Valerie I. Brown, Genevieve Bergendahl, William Roberts, et al. 2020. “A Subset Analysis of a Phase II Trial Evaluating the Use of DFMO as Maintenance Therapy for High-Risk Neuroblastoma.” *International Journal of Cancer* 147 (11): 3152–59. https://doi.org/10.1002/ijc.33044.

109. Liban, Tyler J., Edgar M. Medina, Sarvind Tripathi, Satyaki Sengupta, R. William Henry, Nicolas E. Buchler, and Seth M. Rubin. 2017. “Conservation and Divergence of C-Terminal Domain Structure in the Retinoblastoma Protein Family.” *Proceedings of the National Academy of Sciences* 114 (19): 4942–47. https://doi.org/10.1073/pnas.1619170114.

110. Liban, Tyler J., Michael J. Thwaites, Frederick A. Dick, and Seth M. Rubin. 2016. “Structural Conservation and E2F Binding Specificity within the Retinoblastoma Pocket Protein Family.” *Journal of Molecular Biology* 428 (20): 3960–71. https://doi.org/10.1016/j.jmb.2016.08.017.

111. Liu, Yizhou, Wei Chen, Justin Gaudet, Matthew D. Cheney, Liya Roudaia, Tomasz Cierpicki, Rachel C. Klet, et al. 2007. “Structural Basis for Recognition of SMRT/N-CoR by the MYND Domain and Its Contribution to AML1/ETO’s Activity.” *Cancer Cell* 11 (6): 483–97. https://doi.org/10.1016/j.ccr.2007.04.010.

112. Liu, Yizhou, Matthew D. Cheney, Justin J. Gaudet, Maksymilian Chruszcz, Stephen M. Lukasik, Daisuke Sugiyama, Jeff Lary, et al. 2006. “The Tetramer Structure of the Nervy Homology Two Domain, NHR2, Is Critical for AML1/ETO’s Activity.” *Cancer Cell* 9 (4): 249–60. https://doi.org/10.1016/j.ccr.2006.03.012.

113. Lourenco, Corey, Diana Resetca, Cornelia Redel, Peter Lin, Alannah S. MacDonald, Roberto Ciaccio, Tristan M. G. Kenney, et al. 2021. “MYC Protein Interactors in Gene Transcription and Cancer.” *Nature Reviews Cancer* 21 (9): 579–91. https://doi.org/10.1038/s41568-021-00367-9.

114. Lüscher, Bernhard, and Jörg Vervoorts. 2012. “Regulation of Gene Transcription by the Oncoprotein MYC.” *Gene* 494 (2): 145–60. https://doi.org/10.1016/j.gene.2011.12.027.

115. Malynn, B. A., I. M. de Alboran, R. C. O’Hagan, R. Bronson, L. Davidson, R. A. DePinho, and F. W. Alt. 2000. “N-Myc Can Functionally Replace c-Myc in Murine Development, Cellular Growth, and Differentiation.” *Genes & Development* 14 (11): 1390–99.

116. Maris, John M. 2010. “Recent Advances in Neuroblastoma.” *New England Journal of Medicine* 362 (23): 2202–11. https://doi.org/10.1056/NEJMra0804577.

117. Marshall, Glenn M., Daniel R. Carter, Belamy B. Cheung, Tao Liu, Marion K. Mateos, Justin G. Meyerowitz, and William A. Weiss. 2014. “The Prenatal Origins of Cancer.” *Nature Reviews Cancer* 14 (4): 277–89. https://doi.org/10.1038/nrc3679.

118. Massó-Vallés, Daniel, and Laura Soucek. 2020. “Blocking Myc to Treat Cancer: Reflecting on Two Decades of Omomyc.” *Cells* 9 (4): 883. https://doi.org/10.3390/cells9040883.

119. Matthay, Katherine K., John M. Maris, Gudrun Schleiermacher, Akira Nakagawara, Crystal L. Mackall, Lisa Diller, and William A. Weiss. 2016. “Neuroblastoma.” *Nature Reviews Disease Primers* 2 (November): 16078. https://doi.org/10.1038/nrdp.2016.78.

120. McCafferty, John, Andrew D. Griffiths, Greg Winter, and David J. Chiswell. 1990. “Phage Antibodies: Filamentous Phage Displaying Antibody Variable Domains.” *Nature* 348 (6301): 552–54. https://doi.org/10.1038/348552a0.

121. Merkestein, Myrte, Samantha Laber, Fiona McMurray, Daniel Andrew, Gregor Sachse, Jeremy Sanderson, Mengdi Li, et al. 2015. “FTO Influences Adipogenesis by Regulating Mitotic Clonal Expansion.” *Nature Communications* 6 (April): 6792. https://doi.org/10.1038/ncomms7792.

122. Messing, Joachim. 2016. “Phage M13 for the Treatment of Alzheimer and Parkinson Disease.” *Gene* 583 (2): 85–89. https://doi.org/10.1016/j.gene.2016.02.005.

123. Milazzo, G., D. Mercatelli, G. Di Muzio, L. Triboli, P. De Rosa, G. Perini, and F.M. Giorgi. 2020. “Histone Deacetylases (HDACs): Evolution, Specificity, Role in Transcriptional Complexes, and Pharmacological Actionability.” *Genes* 11 (5). https://doi.org/10.3390/genes11050556.

124. Mishra, Suresh, Gerry Melino, and Liam J. Murphy. 2007. “Transglutaminase 2 Kinase Activity Facilitates Protein Kinase A-Induced Phosphorylation of Retinoblastoma Protein *.” *Journal of Biological Chemistry* 282 (25): 18108–15. https://doi.org/10.1074/jbc.M607413200.

125. Moghimi, Babak, Sakunthala Muthugounder, Samy Jambon, Rachelle Tibbetts, Long Hung, Hamid Bassiri, Michael D. Hogarty, David M. Barrett, Hiroyuki Shimada, and Shahab Asgharzadeh. 2021. “Preclinical Assessment of the Efficacy and Specificity of GD2-B7H3 SynNotch CAR-T in Metastatic Neuroblastoma.” *Nature Communications* 12 (January). https://doi.org/10.1038/s41467-020-20785-x.

126. Molenaar, Jan J., Marli E. Ebus, Dirk Geerts, Jan Koster, Fieke Lamers, Linda J. Valentijn, Ellen M. Westerhout, Rogier Versteeg, and Huib N. Caron. 2009. “Inactivation of CDK2 Is Synthetically Lethal to MYCN Over-Expressing Cancer Cells.” *Proceedings of the National Academy of Sciences of the United States of America* 106 (31): 12968–73. https://doi.org/10.1073/pnas.0901418106.

127. Molenaar, Jan J., Marli E. Ebus, Jan Koster, Peter van Sluis, Carel J.M. van Noesel, Rogier Versteeg, and Huib N. Caron. 2008. “Cyclin D1 and CDK4 Activity Contribute to the Undifferentiated Phenotype in Neuroblastoma.” *Cancer Research* 68 (8): 2599–2609. https://doi.org/10.1158/0008-5472.CAN-07-5032.

128. Morandi, Fabio, Federica Sabatini, Marina Podestà, and Irma Airoldi. 2021. “Immunotherapeutic Strategies for Neuroblastoma: Present, Past and Future.” *Vaccines* 9 (1): 43. https://doi.org/10.3390/vaccines9010043.

129. Mosse, Yael P., Sharon J. Diskin, Nora Wasserman, Katherine Rinaldi, Edward F. Attiyeh, Kristina Cole, Jayanti Jagannathan, Karishma Bhambhani, Cynthia Winter, and John M. Maris. 2007. “Neuroblastomas Have Distinct Genomic DNA Profiles That Predict Clinical Phenotype and Regional Gene Expression.” *Genes, Chromosomes and Cancer* 46 (10): 936–49. https://doi.org/10.1002/gcc.20477.

130. Mosse, Yael P., Marci Laudenslager, Deepa Khazi, Alex J. Carlisle, Cynthia L. Winter, Eric Rappaport, and John M. Maris. 2004. “Germline PHOX2B Mutation in Hereditary Neuroblastoma.” *The American Journal of Human Genetics* 75 (4): 727–30. https://doi.org/10.1086/424530.

131. Mossé, Yaël P., Marci Laudenslager, Luca Longo, Kristina A. Cole, Andrew Wood, Edward F. Attiyeh, Michael J. Laquaglia, et al. 2008. “Identification of *ALK* as a Major Familial Neuroblastoma Predisposition Gene.” *Nature* 455 (7215): 930–35. https://doi.org/10.1038/nature07261.

132. Murphy, Daniel J., Melissa R. Junttila, Laurent Pouyet, Anthony Karnezis, Ksenya Shchors, Duyen A. Bui, Lamorna Brown-Swigart, Leisa Johnson, and Gerard I. Evan. 2008. “Distinct Thresholds Govern Myc’s Biological Output In Vivo.” *Cancer Cell* 14 (6): 447–57. https://doi.org/10.1016/j.ccr.2008.10.018.

133. Muth, Daniel, Seda Ghazaryan, Isabella Eckerle, Emily Beckett, Christina Pöhler, Julia Batzler, Claudia Beisel, et al. 2010. “Transcriptional Repression of SKP2 Is Impaired in MYCN-Amplified Neuroblastoma.” *Cancer Research* 70 (9): 3791–3802. https://doi.org/10.1158/0008-5472.CAN-09-1245.

134. Narasimha, Anil M., Manuel Kaulich, Gary S. Shapiro, Yoon J. Choi, Piotr Sicinski, and Steven F. Dowdy. 2014. “Cyclin D Activates the Rb Tumor Suppressor by Mono-Phosphorylation.” *ELife* 3 (June). https://doi.org/10.7554/eLife.02872.

135. Nazha, Bassel, Cengiz Inal, and Taofeek K. Owonikoko. 2020. “Disialoganglioside GD2 Expression in Solid Tumors and Role as a Target for Cancer Therapy.” *Frontiers in Oncology* 10 (July). https://doi.org/10.3389/fonc.2020.01000.

136. Negroni, A., S. Scarpa, A. Romeo, S. Ferrari, A. Modesti, and G. Raschellà. 1991. “Decrease of Proliferation Rate and Induction of Differentiation by a MYCN Antisense DNA Oligomer in a Human Neuroblastoma Cell Line.” *Cell Growth & Differentiation: The Molecular Biology Journal of the American Association for Cancer Research* 2 (10): 511–18.

137. O’Callaghan, R., R. Bradley, and W. Paranchych. 1973. “The Effect of M13 Phage Infection upon the F Pili of E. Coli.” *Virology* 54 (1): 220–29. https://doi.org/10.1016/0042-6822(73)90131-1.

138. Oeggerli, Martin, Sanja Tomovska, Peter Schraml, Daniele Calvano-Forte, Salome Schafroth, Ronald Simon, Thomas Gasser, Michael J. Mihatsch, and Guido Sauter. 2004. “E2F3 Amplification and Overexpression Is Associated with Invasive Tumor Growth and Rapid Tumor Cell Proliferation in Urinary Bladder Cancer.” *Oncogene* 23 (33): 5616–23. https://doi.org/10.1038/sj.onc.1207749.

139. Ohtani, K., J. DeGregori, and J. R. Nevins. 1995. “Regulation of the Cyclin E Gene by Transcription Factor E2F1.” *Proceedings of the National Academy of Sciences of the United States of America* 92 (26): 12146–50. https://doi.org/10.1073/pnas.92.26.12146.

140. Ohtsubo, M., A. M. Theodoras, J. Schumacher, J. M. Roberts, and M. Pagano. 1995. “Human Cyclin E, a Nuclear Protein Essential for the G1-to-S Phase Transition.” *Molecular and Cellular Biology* 15 (5): 2612–24. https://doi.org/10.1128/MCB.15.5.2612.

141. Olsson, A. Y., A. Feber, S. Edwards, R. te Poele, I. Giddings, S. Merson, and C. S. Cooper. 2007. “Role of E2F3 Expression in Modulating Cellular Proliferation Rate in Human Bladder and Prostate Cancer Cells.” *Oncogene* 26 (7): 1028–37. https://doi.org/10.1038/sj.onc.1209854.

142. Parodi, Stefano, Marzia Ognibene, Riccardo Haupt, and Annalisa Pezzolo. 2020. “The Over-Expression of E2F3 Might Serve as Prognostic Marker for Neuroblastoma Patients with Stage 4S Disease.” *Diagnostics (Basel, Switzerland)* 10 (5): E315. https://doi.org/10.3390/diagnostics10050315.

143. Passaretti, Paolo, Inam Khan, Timothy R. Dafforn, and Pola Goldberg Oppenheimer. 2020. “Improvements in the Production of Purified M13 Bacteriophage Bio-Nanoparticle.” *Scientific Reports* 10 (1): 18538. https://doi.org/10.1038/s41598-020-75205-3.

144. Pearson, Andrew D. J., C. Ross Pinkerton, Ian J. Lewis, John Imeson, Caroline Ellershaw, David Machin, European Neuroblastoma Study Group, and Children’s Cancer and Leukaemia Group (CCLG formerly United Kingdom Children’s Cancer Study Group). 2008. “High-Dose Rapid and Standard Induction Chemotherapy for Patients Aged over 1 Year with Stage 4 Neuroblastoma: A Randomised Trial.” *The Lancet. Oncology* 9 (3): 247–56. https://doi.org/10.1016/S1470-2045(08)70069-X.

145. Pearson, Andrew DJ, C Ross Pinkerton, Ian J Lewis, John Imeson, Caroline Ellershaw, and David Machin. 2008. “High-Dose Rapid and Standard Induction Chemotherapy for Patients Aged over 1 Year with Stage 4 Neuroblastoma: A Randomised Trial.” *The Lancet Oncology* 9 (3): 247–56. https://doi.org/10.1016/S1470-2045(08)70069-X.

146. Peifer, Martin, Falk Hertwig, Frederik Roels, Daniel Dreidax, Moritz Gartlgruber, Roopika Menon, Andrea Krämer, et al. 2015. “Telomerase Activation by Genomic Rearrangements in High-Risk Neuroblastoma.” *Nature* 526 (7575): 700–704. https://doi.org/10.1038/nature14980.

147. Pugh, Trevor J., Olena Morozova, Edward F. Attiyeh, Shahab Asgharzadeh, Jun S. Wei, Daniel Auclair, Scott L. Carter, et al. 2013. “The Genetic Landscape of High-Risk Neuroblastoma.” *Nature Genetics* 45 (3): 279–84. https://doi.org/10.1038/ng.2529.

148. Puissant, Alexandre, Stacey M. Frumm, Gabriela Alexe, Christopher F. Bassil, Jun Qi, Yvan H. Chanthery, Erin A. Nekritz, et al. 2013. “Targeting MYCN in Neuroblastoma by BET Bromodomain Inhibition.” *Cancer Discovery* 3 (3): 308–23. https://doi.org/10.1158/2159-8290.CD-12-0418.

149. Rader, JulieAnn, Mike R. Russell, Lori S. Hart, Michael S. Nakazawa, Lili T. Belcastro, Daniel Martinez, Yimei Li, et al. 2013. “Dual CDK4/CDK6 Inhibition Induces Cell Cycle Arrest and Senescence in Neuroblastoma.” *Clinical Cancer Research : An Official Journal of the American Association for Cancer Research* 19 (22). https://doi.org/10.1158/1078-0432.CCR-13-1675.

150. Rader, Julieann, Mike R. Russell, Lori S. Hart, Michael S. Nakazawa, Lili T. Belcastro, Daniel Martinez, Yimei Li, et al. 2013. “Dual CDK4/CDK6 Inhibition Induces Cell-Cycle Arrest and Senescence in Neuroblastoma.” *Clinical Cancer Research: An Official Journal of the American Association for Cancer Research* 19 (22): 6173–82. https://doi.org/10.1158/1078-0432.CCR-13-1675.

151. Rasched, I., and E. Oberer. 1986. “Ff Coliphages: Structural and Functional Relationships.” *Microbiological Reviews* 50 (4): 401–27. https://doi.org/10.1128/mr.50.4.401-427.1986.

152. Richman, Sarah A., Selene Nunez-Cruz, Babak Moghimi, Lucy Z. Li, Zachary T. Gershenson, Zissimos Mourelatos, David M. Barrett, Stephan A. Grupp, and Michael C. Milone. 2018. "High-Affinity GD2-Specific CAR T Cells Induce Fatal Encephalitis in a Preclinical Neuroblastoma Model." *Cancer Immunology Research* 6 (1): 36–46. https://doi.org/10.1158/2326-6066.CIR-17-0211.

153. Rihani, Ali, Jo Vandesompele, Frank Speleman, and Tom Van Maerken. 2015. "Inhibition of CDK4/6 as a Novel Therapeutic Option for Neuroblastoma." *Cancer Cell International* 15 (1): 1–8. https://doi.org/10.1186/s12935-015-0224-y.

154. Rossetti, Stefano, André T Hoogeveen, and Nicoletta Sacchi. 2004. "The MTG Proteins: Chromatin Repression Players with a Passion for Networking." *Genomics* 84 (1): 1–9. https://doi.org/10.1016/j.ygeno.2004.02.011.

155. Rowley, J. D. 1973. "Identificaton of a Translocation with Quinacrine Fluorescence in a Patient with Acute Leukemia." *Annales De Genetique* 16 (2): 109–12.

156. Rubin, Seth M. 2013. "Deciphering the Rb Phosphorylation Code." *Trends in Biochemical Sciences* 38 (1): 12–19. https://doi.org/10.1016/j.tibs.2012.10.007.

157. Rubin, Seth M., Anne-Laure Gall, Ning Zheng, and Nikola P. Pavletich. 2005. "Structure of the Rb C-Terminal Domain Bound to E2F1-DP1: A Mechanism for Phosphorylation-Induced E2F Release." *Cell* 123 (6): 1093–1106. https://doi.org/10.1016/j.cell.2005.09.044.

158. Rubin, Seth M., Julien Sage, and Jan M. Skotheim. 2020. "Integrating Old and New Paradigms of G1/S Control." *Molecular Cell* 80 (2): 183–92. https://doi.org/10.1016/j.molcel.2020.08.020.

159. Rushlow, Diane E., Berber M. Mol, Jennifer Y. Kennett, Stephanie Yee, Sanja Pajovic, Brigitte L. Thériault, Nadia L. Prigoda-Lee, et al. 2013a. "Characterisation of Retinoblastomas without RB1 Mutations: Genomic, Gene Expression, and Clinical Studies." *The Lancet. Oncology* 14 (4): 327–34. https://doi.org/10.1016/S1470-2045(13)70045-7.

160. Rushlow, Diane E, Berber M Mol, Jennifer Y Kennett, Stephanie Yee, Sanja Pajovic, Brigitte L Thériault, Nadia L Prigoda-Lee, et al. 2013b. "Characterisation of Retinoblastomas without RB1 Mutations: Genomic, Gene Expression, and Clinical Studies." *The Lancet Oncology* 14 (4): 327–34. https://doi.org/10.1016/S1470-2045(13)70045-7.

161. Ryl, Tatsiana, Erika E. Kuchen, Emma Bell, Chunxuan Shao, Andrés F. Flórez, Gregor Mönke, Sina Gogolin, et al. 2017. "Cell-Cycle Position of Single MYC-Driven Cancer Cells Dictates Their Susceptibility to a Chemotherapeutic Drug." *Cell Systems* 5 (3): 237-250.e8. https://doi.org/10.1016/j.cels.2017.07.005.

162. Sanidas, Ioannis, Robert Morris, Katerina A. Fella, Purva H. Rumde, Myriam Boukhali, Eric C. Tai, David T. Ting, Michael S. Lawrence, Wilhelm Haas, and Nicholas J. Dyson. 2019. "A Code of Mono-Phosphorylation Modulates the Function of RB." *Molecular Cell* 73 (5): 985-1000.e6. https://doi.org/10.1016/j.molcel.2019.01.004.

163. Sariola, Hannu, TerÄvÄ Harri, Juhani Rapola, and Ulla M. Saarinen. 1991. "Cell-Surface Ganglioside GD2 in the Immunohistochemical Detection and Differential Diagnosis of Neuroblastoma." *American Journal of Clinical Pathology* 96 (2): 248–52. https://doi.org/10.1093/ajcp/96.2.248.

164. Sawai, S., A. Shimono, Y. Wakamatsu, C. Palmes, K. Hanaoka, and H. Kondoh. 1993. "Defects of Embryonic Organogenesis Resulting from Targeted Disruption of the N-Myc Gene in the Mouse." *Development (Cambridge, England)* 117 (4): 1445–55. https://doi.org/10.1242/dev.117.4.1445.

165. Schaub, Franz X., Varsha Dhankani, Ashton C. Berger, Mihir Trivedi, Anne B. Richardson, Reid Shaw, Wei Zhao, et al. 2018. "Pan-Cancer Alterations of the MYC Oncogene and Its Proximal Network across the Cancer Genome Atlas." *Cell Systems* 6 (3): 282-300.e2. https://doi.org/10.1016/j.cels.2018.03.003.

166. Schengrund, Cara-Lynne. 2020. "Gangliosides and Neuroblastomas." *International Journal of Molecular Sciences* 21 (15): 5313. https://doi.org/10.3390/ijms21155313.

167. Schulte, Johannes H., Soyoung Lim, Alexander Schramm, Nicolaus Friedrichs, Jan Koster, Rogier Versteeg, Ingrid Ora, et al. 2009. "Lysine-Specific Demethylase 1 Is Strongly Expressed in Poorly Differentiated Neuroblastoma: Implications for Therapy." *Cancer Research* 69 (5): 2065–71. https://doi.org/10.1158/0008-5472.CAN-08-1735.

168. Schumacher-Kuckelkorn, Roswitha, Ruth Volland, Anke Gradehandt, Barbara Hero, Thorsten Simon, and Frank Berthold. 2017. "Lack of Immunocytological GD2 Expression on Neuroblastoma Cells in Bone Marrow at Diagnosis, during Treatment, and at Recurrence*." *Pediatric Blood & Cancer* 64 (1): 46–56. https://doi.org/10.1002/pbc.26184.

169. Schweigerer, L., S. Breit, A. Wenzel, K. Tsunamoto, R. Ludwig, and M. Schwab. 1990. "Augmented MYCN Expression Advances the Malignant Phenotype of Human Neuroblastoma Cells: Evidence for Induction of Autocrine Growth Factor Activity." *Cancer Research* 50 (14): 4411–16.

170. Sears, R., K. Ohtani, and J. R. Nevins. 1997. "Identification of Positively and Negatively Acting Elements Regulating Expression of the E2F2 Gene in Response to Cell Growth Signals." *Molecular and Cellular Biology* 17 (9): 5227–35. https://doi.org/10.1128/MCB.17.9.5227.

171. Shendy, Noha A.M., Mark W. Zimmerman, Brian J. Abraham, and Adam D. Durbin. 2022. "Intrinsic Transcriptional Heterogeneity in Neuroblastoma Guides Mechanistic and Therapeutic Insights." *Cell Reports Medicine* 3 (5): 100632. https://doi.org/10.1016/j.xcrm.2022.100632.

172. Sherr, Charles J. 1996. "Cancer Cell Cycles." *Science* 274 (5293): 1672–77. https://doi.org/10.1126/science.274.5293.1672.

173. Simões-Costa, Marcos, and Marianne E. Bronner. 2015. "Establishing Neural Crest Identity: A Gene Regulatory Recipe." *Development (Cambridge, England)* 142 (2): 242–57. https://doi.org/10.1242/dev.105445.

174. Singh, Hardeep P., Dominic W. H. Shayler, G. Esteban Fernandez, Matthew E. Thornton, Cheryl Mae Craft, Brendan H. Grubbs, and David Cobrinik. 2022. "An Immature, Dedifferentiated, and Lineage-Deconstrained Cone Precursor Origin of N-Myc–Initiated Retinoblastoma." *Proceedings of the National Academy of Sciences* 119 (28): e2200721119. https://doi.org/10.1073/pnas.2200721119.

175. Sm, Rubin, Gall Al, Zheng N, and Pavletich Np. 2005. "Structure of the Rb C-Terminal Domain Bound to E2F1-DP1: A Mechanism for Phosphorylation-Induced E2F Release." *Cell* 123 (6). https://doi.org/10.1016/j.cell.2005.09.044.

176. Strieder, Verena, and Werner Lutz. 2003. "E2F Proteins Regulate MYCN Expression in Neuroblastomas." *The Journal of Biological Chemistry* 278 (5): 2983–89. https://doi.org/10.1074/jbc.M207596200.

177. Sur, Inderpreet Kaur, Outi Hallikas, Anna Vähärautio, Jian Yan, Mikko Turunen, Martin Enge, Minna Taipale, Auli Karhu, Lauri A. Aaltonen, and Jussi Taipale. 2012. "Mice Lacking a Myc Enhancer That Includes Human SNP Rs6983267 Are Resistant to Intestinal Tumors." *Science* 338 (6112): 1360–63. https://doi.org/10.1126/science.1228606.

178. Thomas*, T., and T. J. Thomas. 2001. "Polyamines in Cell Growth and Cell Death: Molecular Mechanisms and Therapeutic Applications." *Cellular and Molecular Life Sciences CMLS* 58 (2): 244–58. https://doi.org/10.1007/PL00000852.

179. Topacio, Benjamin R., Evgeny Zatulovskiy, Sandra Cristea, Shicong Xie, Carrie S. Tambo, Seth M. Rubin, Julien Sage, Mardo Kõivomägi, and Jan M. Skotheim. 2019. "Cyclin D-Cdk4,6 Drives Cell-Cycle Progression via the Retinoblastoma Protein's C-Terminal Helix." *Molecular Cell* 74 (4): 758-770.e4. https://doi.org/10.1016/j.molcel.2019.03.020.

180. Torres-Acosta, Mario, Alejandro González-Mora, Federico Ruiz-Ruiz, Marco Rito-Palomares, and Jorge Benavides. 2020. "Economic Evaluation of M13 Bacteriophage Production at Large-Scale for Therapeutic Applications Using Aqueous Two-Phase Systems." *Journal of Chemical Technology & Biotechnology* 95 (11): 2822–33. https://doi.org/10.1002/jctb.6526.

181. Trochet, Delphine, Franck Bourdeaut, Isabelle Janoueix-Lerosey, Anne Deville, Loïc de Pontual, Gudrun Schleiermacher, Carole Coze, et al. 2004. "Germline Mutations of the Paired–Like Homeobox 2B (PHOX2B) Gene in Neuroblastoma." *The American Journal of Human Genetics* 74 (4): 761–64. https://doi.org/10.1086/383253.

182. Ulfo, Luca, Andrea Cantelli, Annapaola Petrosino, Paolo Emidio Costantini, Michela Nigro, Francesco Starinieri, Eleonora Turrini, et al. 2022. "Orthogonal Nanoarchitectonics of M13 Phage for Receptor Targeted Anticancer Photodynamic Therapy." *Nanoscale* 14 (3): 632–41. https://doi.org/10.1039/d1nr06053h.

183. Ulfo, Luca, Paolo Emidio Costantini, Matteo Di Giosia, Alberto Danielli, and Matteo Calvaresi. 2022. "EGFR-Targeted Photodynamic Therapy." *Pharmaceutics* 14 (2): 241. https://doi.org/10.3390/pharmaceutics14020241.

184. Valentijn, Linda J., Jan Koster, Danny A. Zwijnenburg, Nancy E. Hasselt, Peter van Sluis, Richard Volckmann, Max M. van Noesel, et al. 2015. "*TERT* Rear-

rangements Are Frequent in Neuroblastoma and Identify Aggressive Tumors." *Nature Genetics* 47 (12): 1411–14. https://doi.org/10.1038/ng.3438.

185. Wang, Haiwei, Xinrui Wang, Liangpu Xu, and Ji Zhang. 2022. "Prognostic Analysis of E2F Transcription Factors E2F1 and E2F3 in Four Independent Pediatric Neuroblastoma Cohorts." *BMC Pediatrics* 22 (1): 376. https://doi.org/10.1186/s12887-022-03424-w.

186. Wang, Liyuan, Chan Chen, Zemin Song, Honghong Wang, Minghui Ye, Donghai Wang, Wenqian Kang, Hudan Liu, and Guoliang Qing. 2022. "EZH2 Depletion Potentiates MYC Degradation Inhibiting Neuroblastoma and Small Cell Carcinoma Tumor Formation." *Nature Communications* 13 (January): 12. https://doi.org/10.1038/s41467-021-27609-6.

187. Wang, Lu, Tze King Tan, Adam D. Durbin, Mark W. Zimmerman, Brian J. Abraham, Shi Hao Tan, Phuong Cao Thi Ngoc, et al. 2019. "ASCL1 Is a MYCN- and LMO1-Dependent Member of the Adrenergic Neuroblastoma Core Regulatory Circuitry." *Nature Communications* 10 (1): 5622. https://doi.org/10.1038/s41467-019-13515-5.

188. Weiss, William A., Ken Aldape, Gayatry Mohapatra, Burt G. Feuerstein, and J. Michael Bishop. 1997. "Targeted Expression of MYCN Causes Neuroblastoma in Transgenic Mice." *The EMBO Journal* 16 (11): 2985–95. https://doi.org/10.1093/emboj/16.11.2985.

189. Wezenbeek, Peter M. G. F. van, Theo J. M. Hulsebos, and John G. G. Schoenmakers. 1980. "Nucleotide Sequence of the Filamentous Bacteriophage M13 DNA Genome: Comparison with Phage Fd." *Gene* 11 (1): 129–48. https://doi.org/10.1016/0378-1119(80)90093-1.

190. Woo, Chan-Wook, Fei Tan, Hope Cassano, JungHwa Lee, Kwang Chul Lee, and Carol J. Thiele. 2008. "Use of RNA Interference to Elucidate the Effect of MYCN on Cell Cycle in Neuroblastoma." *Pediatric Blood & Cancer* 50 (2): 208–12. https://doi.org/10.1002/pbc.21195.

191. Wu, Nan, Deshui Jia, Breanna Bates, Ryan Basom, Charles G. Eberhart, and David MacPherson. 2017. "A Mouse Model of MYCN-Driven Retinoblastoma Reveals MYCN-Independent Tumor Reemergence." *The Journal of Clinical Investigation* 127 (3): 888–98. https://doi.org/10.1172/JCI88508.

192. Wu, Zi-Liang, Eileen Schwartz, Robert Seeger, and Stephan Ladisch. 1986. "Expression of GD2 Ganglioside by Untreated Primary Human Neuroblastomas1." *Cancer Research* 46 (1): 440–43.

193. Xiao, Bing, James Spencer, Adrienne Clements, Nadeem Ali-Khan, Sibylle Mittnacht, Cristina Broceño, Manfred Burghammer, Anastassis Perrakis, Ronen Marmorstein, and Steven J. Gamblin. 2003. "Crystal Structure of the Retinoblastoma Tumor Suppressor Protein Bound to E2F and the Molecular Basis of Its Regulation." *Proceedings of the National Academy of Sciences of the United States of America* 100 (5): 2363–68. https://doi.org/10.1073/pnas.0436813100.

194. Yamane, Brett H., Jacquelyn A. Hank, Mark R. Albertini, and Paul M. Sondel. 2009. "The Development of Antibody-IL-2 Based Immunotherapy with Hu14.18-IL2

(EMD-273063) in Melanoma and Neuroblastoma." *Expert Opinion on Investigational Drugs* 18 (7): 991–1000. https://doi.org/10.1517/13543780903048911.

195. Yao, Guang, Tae Jun Lee, Seiichi Mori, Joseph R. Nevins, and Lingchong You. 2008. "A Bistable Rb–E2F Switch Underlies the Restriction Point." *Nature Cell Biology* 10 (4): 476–82. https://doi.org/10.1038/ncb1711.

196. Yeo, Nan Cher, Alejandro Chavez, Alissa Lance-Byrne, Yingleong Chan, David Menn, Denitsa Milanova, Chih-Chung Kuo, et al. 2018. "An Enhanced CRISPR Repressor for Targeted Mammalian Gene Regulation." *Nature Methods* 15 (8): 611–16. https://doi.org/10.1038/s41592-018-0048-5.

197. Yuan, Junying, and Bruce A. Yankner. 2000. "Apoptosis in the Nervous System." *Nature* 407 (6805): 802–9. https://doi.org/10.1038/35037739.

198. Zhao, Xu, Ying Yang, Bao-Fa Sun, Yue Shi, Xin Yang, Wen Xiao, Ya-Juan Hao, et al. 2014. "FTO-Dependent Demethylation of N6-Methyladenosine Regulates MRNA Splicing and Is Required for Adipogenesis." *Cell Research* 24 (12): 1403–19. https://doi.org/10.1038/cr.2014.151.

199. Zheng, Ning, Brenda A. Schulman, Langzhou Song, Julie J. Miller, Philip D. Jeffrey, Ping Wang, Claire Chu, et al. 2002. "Structure of the Cul1–Rbx1–Skp1–F BoxSkp2 SCF Ubiquitin Ligase Complex." *Nature* 416 (6882): 703–9. https://doi.org/10.1038/416703a.

200. Zhong, Xiaodan, Yutong Zhang, Linyu Wang, Hao Zhang, Haiming Liu, and Yuanning Liu. 2019. "Cellular Components in Tumor Microenvironment of Neuroblastoma and the Prognostic Value." *PeerJ* 7 (December): e8017. https://doi.org/10.7717/peerj.8017.

201. Zimmerman, Kathryn A., George D. Yancopoulos, Robert G. Collum, Russell K. Smith, Nancy E. Kohl, Kathleen A. Denis, Marion M. Nau, et al. 1986. "Differential Expression of Myc Family Genes during Murine Development." *Nature* 319 (6056): 780. https://doi.org/10.1038/319780a0.

202. Zugbi, Santiago, Daiana Ganiewich, Arpita Bhattacharyya, Rosario Aschero, Daniela Ottaviani, Claudia Sampor, Eduardo G. Cafferata, et al. 2020. "Clinical, Genomic, and Pharmacological Study of MYCN-Amplified RB1 Wild-Type Metastatic Retinoblastoma." *Cancers* 12 (9): 2714. https://doi.org/10.3390/cancers12092714.